# ATLAS+CMS DARK MATTER FORUM RECOMMENDATIONS

Author/contributor list to be added as document is finalized.

May 14, 2015

# Contents

# 1
# Introduction

This document presents recommendations for the Monte Carlo (MC) production and parameter scans for various theoretical models of Dark Matter production at hadron colliders. In particular, the document is intended to be a reference for dataset generation of Dark Matter models for the early stages of Run-2 at the LHC.

What is the motivation for this report?

First, the physics is compelling. Measurements at the energy frontier can make quantitative statements about dark matter.

Second, in Run-1 at the LHC, there was confusion in the community over the interpretation of the data.

Third, there are reasons to strive for uniformity in interpretation in the different experiments. This will ultimately aid in the combination of data, but also facilitates cross checks of results.

What is the format of this report?

First, it describes the signatures and models of interest for dark matter searches during Run-2 at the LHC.

Secondly, it provides information on the tools to be used to simulate signals and related uncertainties.

Finally, it makes a recommendation on a scan of parameters within those models based on supporting material.

# 2

# *Overall choices for simplified models*

Many Run-1 results of dark matter searches were interpreted in the context of Effective Field Theory (EFT). There were several reasons for this. First, the presentation is model independent. Secondly, the approach is economical, requiring only a few simulated datasets. Finally, at the time, there was no catalogue of alternative interpretations of the data. The downside of the EFT approach is that many of the implicit limitations were not widely understood.

Since then, there has arisen a consensus on a handful of simple models of dark matter production that have a hope of mapping into a more complete theory. This document describes them. Also, in some cases, there is no good alternative to using EFT. Even in the case of simplified models, we recommend showing the EFT limit.

Assumptions and simplifications made in this report:

- choice of Dark Matter type: Dirac (unless specified otherwise) and what we might be missing
- Minimal Flavor Violation (MFV) – new physics appears only through Yukawa couplings – and what we might be missing
- minimal width for mediators
- minimal particle content

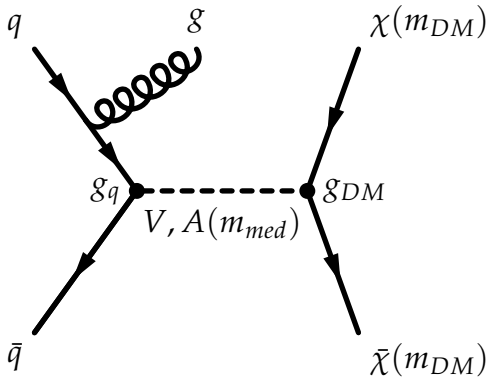


Figure 3.1: Representative Feynman diagram showing the pair production of dark matter particles in association with a parton from the initial state via a vector or axial-vector mediator. The cross section and kinematics depend upon the mediator and dark matter masses, and the mediator couplings to dark matter and quarks respectively: ($M_{med}$, $m_{\mathrm{DM}}$, $g_{\mathrm{DM}}$, $g_q$).

# 3
# Recommended models for all MET+X analyses

## 3.1 Vector and axial vector mediator, s-channel exchange

A simple extension of the Standard Model (SM) is an additional $U(1)$ gauge symmetry, where a dark matter (DM) candidate particle has charges only under this new group. Assuming that some SM particles are also charged under this group, then a new vector boson can mediate interactions between the SM and DM.

We consider the case of a DM particle that is a Dirac fermion and where the production proceeds via the exchange of a spin-1 mediator in the $s$-channel. We consider vector and axial-vector couplings between the spin-1 mediator and SM and DM fields, with the corresponding interaction Lagrangians:

$$\mathcal{L}_{\mathrm{vector}} = g_q \sum_{q=udscbt} Z'_\mu \bar{q}\gamma^\mu q + g_{\mathrm{DM}} Z'_\mu \bar{\chi}\gamma^\mu \chi \tag{3.1}$$

$$\mathcal{L}_{\mathrm{axial-vector}} = g_q \sum_{q=udscbt} Z'_\mu \bar{q}\gamma^\mu\gamma^5 q + g_{\mathrm{DM}} Z'_\mu \bar{\chi}\gamma^\mu\gamma^5 \chi. \tag{3.2}$$

The universal coupling $g_q$ is assumed for quarks. It is also possible to consider another model in which mixed vector and axial-vector couplings are considered, for instance the couplings to the quarks are vector whereas those to DM are axial-vector. As a starting point, we consider only the models with the vector couplings only and axial vector couplings only.

We assume that no additional visible or invisible decays contribute to the width of the mediator. This is referred to as the minimal width and it is defined as follows for the vector and axial-

vector models:

$$\Gamma^{V/A}_{\text{min}} = \Gamma^{V/A}_{\bar{\chi}\chi} + \sum_{q} \Gamma^{V/A}_{\bar{q}q}. \tag{3.3}$$

The leading order expressions for the partial widths are:

$$\Gamma^{\text{V}}_{\bar{\chi}\chi} = \frac{g^2_{\text{DM}} M_{med}}{12\pi} \left(1 + \frac{2m^2_{\text{DM}}}{M^2_{med}}\right) \beta_{DM} \theta(M_{med} - 2m_{\text{DM}}) \tag{3.4}$$

$$\Gamma^{\text{V}}_{\bar{q}q} = \frac{3g^2_q M_{med}}{12\pi} \left(1 + \frac{2m^2_q}{M^2_{med}}\right) \beta_q \theta(M_{med} - 2m_q) \tag{3.5}$$

$$\Gamma^{\text{A}}_{\bar{\chi}\chi} = \frac{g^2_{\text{DM}} M_{med}}{12\pi} \beta^{3/2}_{DM} \theta(M_{med} - 2m_{\text{DM}}) \tag{3.6}$$

$$\Gamma^{\text{A}}_{\bar{q}q} = \frac{3g^2_q M_{med}}{12\pi} \beta^{3/2}_q \theta(M_{med} - 2m_q)\,, \tag{3.7}$$

$\theta(x)$ denotes the Heaviside step function, and $\beta_f = \sqrt{1 - \frac{4m^2_f}{M^2_{med}}}$ is the velocity of the fermion $f$ in the mediator rest frame. Note the color factor 3 in the quark terms. Figure 3.2 shows the minimal width as a function of mediator mass for both vector and axial-vector mediators assuming $g_q$ =$g_{\text{DM}}$ =1. With this choice of the couplings, the dominant contribution to the minimal width comes from the quarks due to the color factor enhancement and the large number of them.

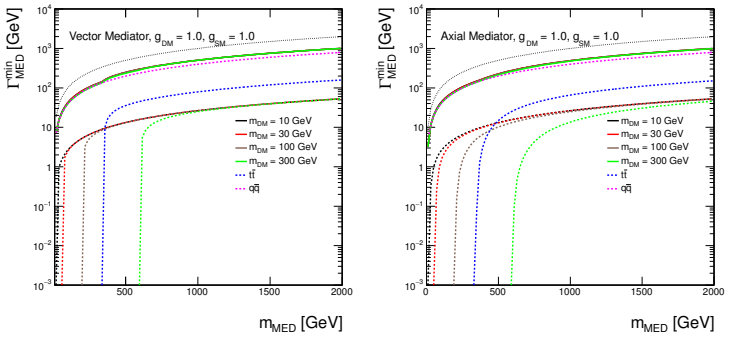


Figure 3.2: Minimal width as a function of mediator mass for vector and axial-vector mediator assuming couplings of 1. The total width is shown as solid lines for Dark Matter masses of 10 GeV, 30 GeV, 100 GeV and 300 GeV in black, red, brown and green, respectively. The individual contributions from Dark Matter are indicated by dotted lines with the same colors. The contribution from all quarks but top is shown as magenta dotted line and the contribution from top quarks only is illustrated by the dotted blue line. The dotted black line shows the extreme case $\Gamma_{\text{min}} = M_{med}$.

The simplified models described here have four free parameters: mediator mass $M_{med}$, Dark Matter mass $m_{\text{DM}}$, coupling of the mediator to quarks $g_q$ and coupling of the mediator to Dark Matter $g_{\text{DM}}$. In order to determine an optimal choice of the parameter grid for presentation of the early Run-2 results, dependencies of the kinematic quantities and cross sections on the individual parameters need to be studied. The following paragraphs list the main observations from the scans over the parameters that support the final proposal for the parameter grid.

*Scan over the couplings* Figure 3.3 reveals there are no differences in the shape of the $\not{E}_T$ distribution among the samples where the pair of $m_{\text{DM}}$ =10 GeV Dark Matter particles are produced on-shell from the mediator of $M_{med}$ =1 TeV, generated with different choices of the

coupling strength. This a generator-level prediction with no kinematic selections or detector simulation. The considered coupling values range from 0.1 to 1.45, where the latter value approximates the maximum allowed coupling value, holding $g_q = g_{\mathrm{DM}}$, such that $\Gamma_{\mathrm{min}} < M_{med}$. Based on similar plots for different choices of $M_{med}$ and $m_{\mathrm{DM}}$, we conclude that the shapes of kinematic distributions are not altered either for the on-shell Dark Matter production where $M_{med} > 2m_{\mathrm{DM}}$, or for the off-shell Dark Matter production where $M_{med} < 2m_{\mathrm{DM}}$. Only the cross sections change. Differences in kinematic distributions are expected only close to the transition region where both on-shell and off-shell decays occur.

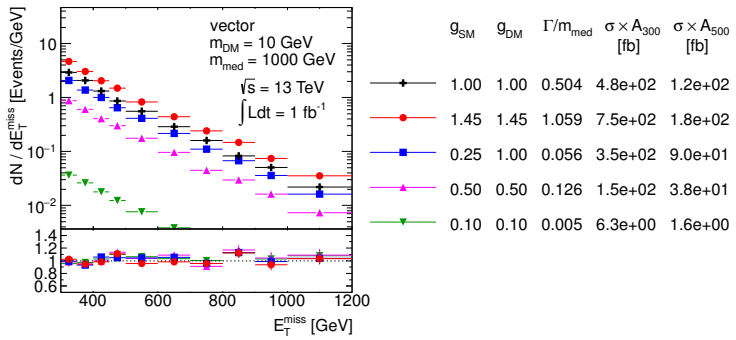


Figure 3.3: Scan over couplings. The $\not{E}_T$ distribution is compared for the vector mediator models using the parameters as indicated. Ratios of the normalized distributions with respect to the first one are shown. $A_{300}$ and $A_{500}$ in the table denote the acceptance of the $\not{E}_T > 300\,\mathrm{GeV}$ and $\not{E}_T > 500\,\mathrm{GeV}$ cut, respectively.

The only situation requiring a more careful treatment is the case of extremely heavy and narrow mediators, which can arise for small coupling strengths. Upon close examination, it was determined that this case is not peculiar. However, the complete story is a cautionary tale about understanding the details of the generator tools. Figure 3.4 suggests a change in the shape of the $\not{E}_T$ distribution for a $M_{med}$ =5 TeV mediator once $\Gamma_{\mathrm{min}}/M_{med}$ is of the order of a percent or lower. This, however, does not come from physics, but is an artifact of the generator implementation, where a cutoff for the regions far away from the mediator mass is sometimes used. This is illustrated in Fig. 3.5 showing the invariant mass of the Dark Matter pair in the samples generated for a $M_{med}$ =7 TeV mediator with different coupling strengths. In all cases, it is expected to observe a peak around the mediator mass with a tail extending to $m_{\bar{\chi}\chi} \to 0$, significantly enhanced by parton distribution functions at low Bjorken $x$. For coupling strength 1 and 3, the massive enhancement at $m_{\bar{\chi}\chi} \to 0$ implies that resonant production at $m_{\bar{\chi}\chi} = 7\,\mathrm{TeV}$ is statistically suppressed such that barely any events are generated there. However, for narrower mediators with couplings below 1, the peak around 7 TeV is clearly visible in the generated sample and the dominant tail at $m_{\bar{\chi}\chi} \to 0$ is artificially cut off, leading to unphysical cross section predictions and kinematic shapes. This explains why the sample with the narrowest mediator in Fig. 3.4 is heavily suppressed in terms of production cross section and also gives different $\not{E}_T$ shape. In general, for such extreme parameter choices the EFT model should give the correct answer. **[TODO: add results of ongoing study.]**

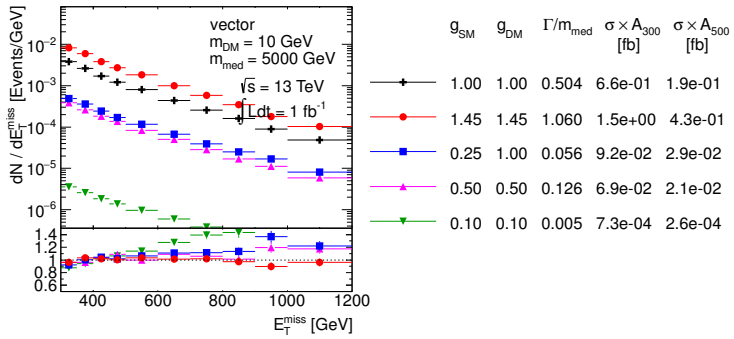


Figure 3.4: Scan over couplings. The $\not{E}_T$ distribution is compared for the vector mediator models using the parameters as indicated. Ratios of the normalized distributions with respect to the first one are shown. $A_{300}$ and $A_{500}$ in the table denote the acceptance of the $\not{E}_T > 300\,\text{GeV}$ and $\not{E}_T > 500\,\text{GeV}$ cut, respectively.

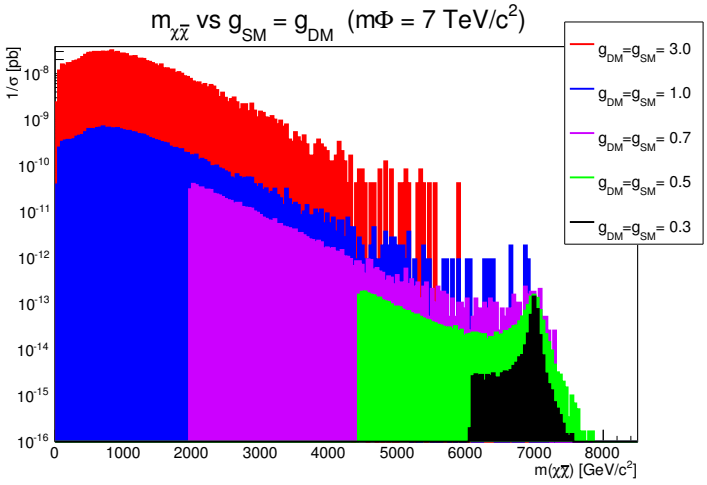


Figure 3.5: Invariant mass of the Dark Matter pair in the samples with $M_{med} = 7\,\text{TeV}$ and different coupling strengths.

The conclusion is that the choice $g_q = g_{\text{DM}}$ is a reasonable reduction in the parameter space since kinematic distributions are robust to changes in the specific values. There are no complications associated with small couplings, but, also, the early part of Run-1 will not be sensitive to them. We recommend a range of couplings that limit the calculated width of the mediator to be near or below $M_{med}$.

*Scan over the Dark Matter mass* For a fixed mediator mass $M_{med}$ and couplings, both the cross section and the kinematic distributions remain similar for different Dark Matter masses as long as $M_{med} > 2m_{\text{DM}}$. This simply reflects the fact that most mediators are produced on-shell, and the details of the invisible decay are unimportant. This is illustrated in Fig. 3.6 for an example of $M_{med} = 1\,\text{TeV}$ $10\,\text{GeV} < m_{\text{DM}} < 300\,\text{GeV}$. It is observed that the cross section decreases as the $m_{\text{DM}}$ approaches $M_{med}/2$. Once the Dark Matter pair is produced off-shell, the cross section of the simplified model is suppressed and the $\not{E}_T$ spectrum hardens, as demonstrated with the choice of $m_{\text{DM}} = 1\,\text{TeV}$ in the same plot. Figure 3.7 reveals the $\not{E}_T$ spectrum hardens further with increasing $m_{\text{DM}}$, accompanied by the gradual decrease of the cross section. From these observations one can conclude:

- A coarse binning along $m_{\text{DM}}$ is sufficient at $M_{med} \gg 2m_{\text{DM}}$.
- Finer binning is needed in order to capture the changes in the

cross section and kinematic quantities close to the production threshold on both sides around $M_{med} = 2m_{\mathrm{DM}}$.

- Due to the significant cross section suppression of the off-shell Dark Matter pair production, it is not necessary to populate the parameter space $M_{med} \ll 2m_{\mathrm{DM}}$ since the LHC is not going to be able to probe the models there.

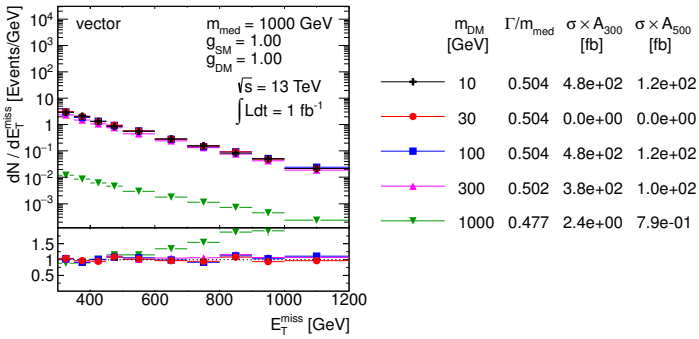


Figure 3.6: Scan over Dark Matter mass. The $\not{E}_T$ distribution is compared for the vector mediator models using the parameters as indicated. Ratios of the normalized distributions with respect to the first one are shown. $A_{300}$ and $A_{500}$ in the table denote the acceptance of the $\not{E}_T > 300\,\mathrm{GeV}$ and $\not{E}_T > 500\,\mathrm{GeV}$ cut, respectively.

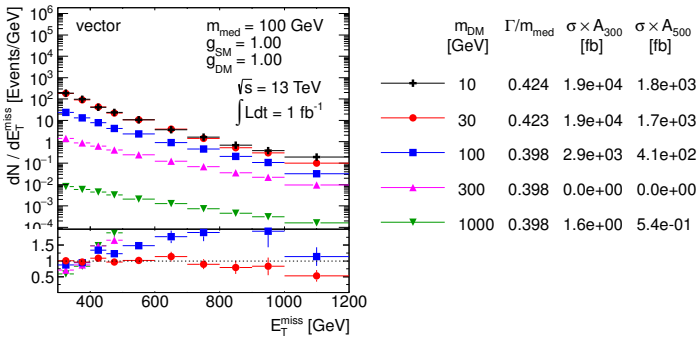


Figure 3.7: Scan over Dark Matter mass. The $\not{E}_T$ distribution is compared for the vector mediator models using the parameters as indicated. Ratios of the normalized distributions with respect to the first one are shown. $A_{300}$ and $A_{500}$ in the table denote the acceptance of the $\not{E}_T > 300\,\mathrm{GeV}$ and $\not{E}_T > 500\,\mathrm{GeV}$ cut, respectively.

*Scan over the mediator mass* Changing the mediator mass for fixed Dark Matter mass and couplings leads to significant differences in cross section and shapes of the kinematic variables for $M_{med} > 2m_{\mathrm{DM}}$ as shown in Fig. 3.8. As expected, higher mediator masses lead to harder $\not{E}_T$ spectra. On the other hand, the $\not{E}_T$ shapes are similar in the off-shell Dark Matter production regime. This is illustrated in Fig. 3.9. Therefore, a coarse binning in $m_{\mathrm{DM}}$ is sufficient at $M_{med} \ll 2m_{\mathrm{DM}}$.

*Proposed parameter grid* The final step in proposing a parameter grid is to evaluate the sensitivity of Run-2 LHC data with respect to rate and/or kinematics. The expected upper limit at 95% confidence level on the product of cross section, acceptance and efficiency, $\sigma \times A \times \epsilon$, in the final Run-1 ATLAS mono-jet analysis [A$^+$15] is 51 fb and 7.2 fb for $\not{E}_T > 300\,\mathrm{GeV}$ and $\not{E}_T > 500\,\mathrm{GeV}$, respectively. The ATLAS projections for 14 TeV [ATL14] predict a factor of two increase in sensitivity with the first $5\,\mathrm{fb}^{-1}$ of data already. Given the cross section for $V$+jets processes increases by

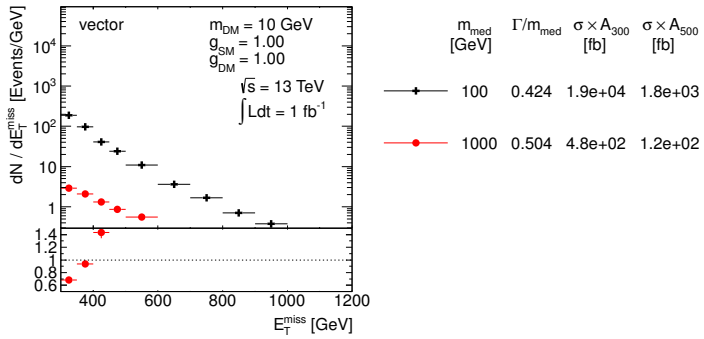


Figure 3.8: Scan over mediator mass. The $\not{E}_T$ distribution is compared for the vector mediator models using the parameters as indicated. Ratios of the normalized distributions with respect to the first one are shown. $A_{300}$ and $A_{500}$ in the table denote the acceptance of the $\not{E}_T > 300\,\text{GeV}$ and $\not{E}_T > 500\,\text{GeV}$ cut, respectively.

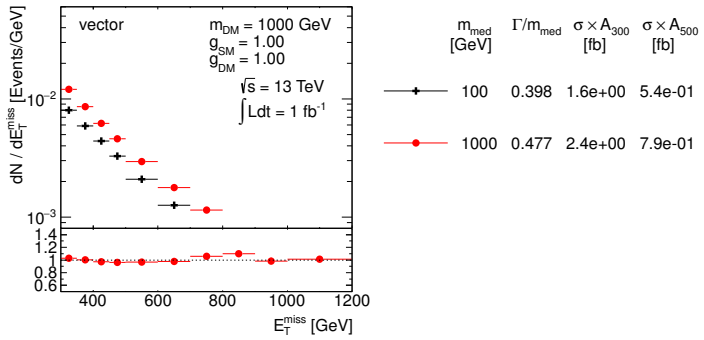


Figure 3.9: Scan over mediator mass. The $\not{E}_T$ distribution is compared for the vector mediator models using the parameters as indicated. Ratios of the normalized distributions with respect to the first one are shown. $A_{300}$ and $A_{500}$ in the table denote the acceptance of the $\not{E}_T > 300\,\text{GeV}$ and $\not{E}_T > 500\,\text{GeV}$ cut, respectively.

roughly a factor 2 when going from $\sqrt{s} = 8\,\text{TeV}$ to 13 TeV, similar fiducial cross section limits can be expected with the first Run-2 data as from the final Run-1 analysis. The generator level cross section times the acceptance at $\not{E}_T > 500\,\text{GeV}$ for the model with couplings $g_q = g_{\text{DM}} = 1$, light Dark Matter of $m_{\text{DM}}$ =10 GeV and a $M_{med}$ =1 TeV vector mediator is at the order of 100 fb, i.e. the early Run-2 mono-jet analysis is going to be sensitive to heavier mediators than this. The value of $\sigma \times A$ at $\not{E}_T > 500\,\text{GeV}$ for 5 TeV vector mediator is at the order of 0.1 fb, therefore this model probably lies beyond the reach of the LHC.

Based on these arguments, the following $M_{med}$ grid points are chosen, roughly equidistant in the logarithmic scale: 10 GeV, 20 GeV, 50 GeV, 100 GeV, 200 GeV, 300 GeV, 500 GeV, 1000 GeV and 2000 GeV. Given the fact that significant changes in cross section happen around the $M_{med} = 2m_{\text{DM}}$ threshold, the $m_{\text{DM}}$ grid points are taken at approximately $M_{med}/2$, namely: 10 GeV, 50 GeV, 150 GeV, 500 GeV and 1000 GeV. Points on the on-shell diagonal are always chosen to be 5 GeV away from the threshold, to avoid numerical instabilities in the event generation. The detailed studies of the impact of the parameter changes on the cross section and kinematic distributions presented earlier in this section support removing some of the grid points and rely on interpolation. The optimised grids proposed for the vector and axial-vector mediators are given in Table. 3.1, containing 29 mass points each. One point at very high mediator mass (5 TeV) is added for each of the DM masses scanned, to aid the reinterpretation of results in terms of contact interaction operators (EFTs).

| $m_{\mathrm{DM}}$/GeV | $m_{\mathrm{med}}$/GeV | | | | | | | | | |
|---|---|---|---|---|---|---|---|---|---|---|
| 1 | 10 | 20 | 50 | 100 | 200 | 300 | 500 | 1000 | 2000 | 5000 |
| 10 | 10 | 15 | 50 | 100 | ″ | ″ | ″ | ″ | ″ | ″ |
| 50 | 10 | | 50 | 95 | 200 | 300 | ″ | ″ | ″ | ″ |
| 150 | 10 | | | | 200 | 295 | 500 | ″ | ″ | ″ |
| 500 | 10 | | | | | | 500 | 995 | 2000 | ″ |
| 1000 | 10 | | | | | | | 1000 | 1995 | 5000 |

Table 3.1: Simplified model benchmarks for $s-$channel simplified models (spin-1 mediators decaying to Dirac DM fermions in the V and A case, taking the minimum width for $g_q$ = $g_{\mathrm{DM}}$ = 1)

The presentation of the results in the $g_q$–$g_{\mathrm{DM}}$ plane for fixed masses benefits from cross section scaling and is discussed in Section 3.3.

## 3.2 *Scalar and pseudoscalar mediator, s-channel exchange*

One of the simplest UV complete extensions of the effective field theory approach is the addition of a scalar/pseudoscalar mediator between DM and SM. A gauge singlet mediator can have tree-level interactions with a singlet DM particle that is either a Dirac or Majorana fermion, or DM that is a scalar itself. The spin-0 mediator can either be a real or complex scalar; a complex scalar contains both scalar and pseudoscalar particles, whereas the real field only contains the scalar particle. In this document we consider only two of the possible choices for this simplified model: one where the interaction with the SM is mediated by a real scalar, and the second where we consider only a light pseudoscalar, assuming that the associated scalar is decoupled from the low-energy spectrum.

Couplings to the SM fermions can be arranged by mixing with the SM Higgs. Such models have interesting connections with Higgs physics, and can be viewed as generalizations of the Higgs portal to DM. The most general scalar mediator models will have renormalizable interactions between the SM Higgs and the new scalar $\phi$ or pseudoscalar $a$, as well as $\phi/a$ interactions with electroweak gauge bosons. Such interactions are model dependent, often subject to constraints from electroweak precision tests, and would suggest specialized searches which cannot be generalized to a broad class of models (unlike, for instance, the $\not{E}_T$ + jets searches). As a result, for this class of minimal simplified models with spin-0 mediators, we will focus primarily on couplings to fermions and loop-induced couplings to gluons.

Working under the assumption of Minimal Flavor Violation (MFV) implies scalar couplings to fermions are proportional to the fermion mass. However, the overall normalization constant of this coupling can differ for for up- and down-type quarks and charged leptons. Assuming that DM is a fermion $\chi$ that couples to the SM only through a scalar $\phi$ or pseudoscalar $a$, the most general tree-level Lagrangians compatible with the MFV assumption are [CRTW14, ADR$^+$14]:

$$\mathcal{L}_\phi = g_\chi \phi \bar{\chi}\chi + \frac{\phi}{\sqrt{2}} \sum_i \left( g_u y_i^u \bar{u}_i u_i + g_d y_i^d \bar{d}_i d_i + g_\ell y_i^\ell \bar{\ell}_i \ell_i \right) , \quad (3.8)$$

$$\mathcal{L}_a = i g_\chi a \bar{\chi}\gamma_5\chi + \frac{ia}{\sqrt{2}} \sum_i \Big( g_u y_i^u \bar{u}_i \gamma_5 u_i + g_d y_i^d \bar{d}_i \gamma_5 d_i + g_\ell y_i^\ell \bar{\ell}_i \gamma_5 \ell_i \Big) . \quad (3.9)$$

Here, the sums run over the all SM generations; the Yukawa couplings $y_i^f$ are normalized to $y_i^f = \sqrt{2} m_i^f / v$ where $v \simeq 246\,\text{GeV}$ represents the Higgs vacuum expectation value (VEV). While the couplings $g_u, g_d, g_\ell$ to SM fermions are factors multiplying the SM Yukawa structure, we parametrise the DM-mediator coupling as $g_\chi$, without any additional Yukawa structure between the mediator and the dark sector.

As already stated we only choose a minimal set of interactions that do not include interactions with the SM Higgs field. For simplicity and ease of comparison, we assume universal SM-mediator couplings $g_v \equiv g_u = g_d = g_\ell$ in the remainder of this work. This allows the relative discovery and exclusion power of each search to be directly compared, though again we emphasize the importance of multiple search channels, not an exclusive focus on the single, most powerful channel under the assumption of universal couplings.

Given these simplifications, the minimal set of parameters under consideration is

$$\left\{ m_\chi,\ m_{\phi/a},\ g_\chi,\ g_v \right\} . \quad (3.10)$$

Despite our simplifying assumption, one should keep the more general possibility in mind, as even simple extensions of the mediating sector can result in $g_u \neq g_d \neq g_\ell$. A well-known realization of this would be the coupling of the pseudoscalar to up-type quarks (proportional to $m_u \cot\beta$) and down-type quarks and charged leptons (proportional to $m_{d/\ell} \tan\beta$) in two-Higgs doublet extensions of the SM. Here $\tan\beta$ denoting the ratio of VEVs of the two Higgs doublets. This possibility of non-equal couplings motivates searches in complementary channels which probe couplings to different flavors of quarks and leptons.

We choose the minimal mediator width given by

$$\Gamma^{S/P}_{\text{min}} = \Gamma^{S/P}_{\bar{\chi}\chi} + \sum_q \Gamma^{S/P}_{\bar{q}q} + \Gamma^{S/P}_{gg}, \quad (3.11)$$

with the following LO expressions for the partial widths:

$$\Gamma^{\mathrm{S}}_{\bar{\chi}\chi} = \frac{g^2_{\mathrm{DM}} M_{med}}{8\pi} \beta^{3/2}_{DM} \theta(M_{med} - 2m_{\mathrm{DM}}) \tag{3.12}$$

$$\Gamma^{\mathrm{S}}_{\bar{q}q} = \frac{3 g^2_q M_{med}}{8\pi} \frac{m^2_q}{v^2} \beta^{3/2}_q \theta(M_{med} - 2m_q) \tag{3.13}$$

$$\Gamma^{\mathrm{S}}_{gg} = \frac{g^2_q \alpha^2_s}{2\pi^3 v^2 M_{med}} \left| \sum_q m^2_q F_{\mathrm{S}} \left( \frac{4m^2_q}{M^2_{med}} \right) \right|^2 \tag{3.14}$$

$$\Gamma^{\mathrm{P}}_{\bar{\chi}\chi} = \frac{g^2_{\mathrm{DM}} M_{med}}{8\pi} \beta_{DM} \theta(M_{med} - 2m_{\mathrm{DM}}) \tag{3.15}$$

$$\Gamma^{\mathrm{P}}_{\bar{q}q} = \frac{3 g^2_q M_{med}}{8\pi} \frac{m^2_q}{v^2} \beta_q \theta(M_{med} - 2m_q) \tag{3.16}$$

$$\Gamma^{\mathrm{P}}_{gg} = \frac{g^2_q \alpha^2_s}{2\pi^3 v^2 M_{med}} \left| \sum_q m^2_q F_{\mathrm{P}} \left( \frac{4m^2_q}{M^2_{med}} \right) \right|^2 , \tag{3.17}$$

with the form factors defined as

$$F_{\mathrm{S}}(x) = 1 + (1 - x) \arctan^2 \left( \frac{1}{\sqrt{x - 1}} \right) \tag{3.18}$$

$$F_{\mathrm{P}}(x) = \arctan^2 \left( \frac{1}{\sqrt{x - 1}} \right) . \tag{3.19}$$

The minimal width for scalar and pseudo-scalar mediators with $g_q = g_{\mathrm{DM}} = 1$ are shown in Fig. 3.10, illustrating the effect of choosing the SM Higgs-like Yukawa couplings for the SM fermions. For the mediator mass above twice the top quark mass $m_t$, the minimal width receives the dominant contribution from the top quark. For lighter mediator masses, Dark Matter dominates as the couplings to lighter quarks are Yukawa suppressed.

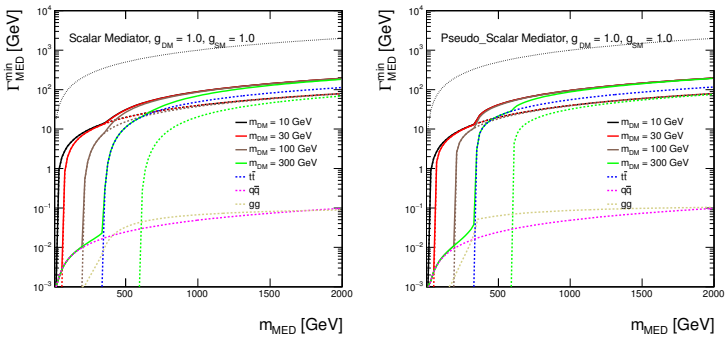


Figure 3.10: Minimal width as a function of mediator mass for scalar and pseudo-scalar mediator assuming couplings of 1. The total width is shown as solid lines for Dark Matter masses of $m_{\mathrm{DM}}$ =10 GeV, 30 GeV, 100 GeV and 300 GeV in black, red, brown and green, respectively. The individual contributions from Dark Matter are indicated by dotted lines with the same colors. The contribution from all quarks but top is shown as magenta dotted line and the contribution from top quarks only is illustrated by the dotted blue line. The dotted beige line shows the contribution fron the coupling to gluons. The dotted black line shows the extreme case $\Gamma_{\mathrm{min}} = M_{med}$.

Similarly as in the case of the vector and axial-vector couplings of spin-1 mediators, scans in the parameter space are performed also for the scalar and pseudo-scalar couplings of the spin-0 mediators in order to decide on the optimised parameter grid for the presentation of Run-2 results. Figures 3.11- 3.15 show the scans over the couplings, Dark Matter mass and mediator mass and the same conclusions apply as in Section 3.1.

Since the top quark gives the dominant contribution to the mediator width due to SM Higgs-like Yukawa couplings, the effect of the kinematic threshold at $M_{med} = 2m_t$ was studied in detail. A scan

over the mediator mass is shown in Fig. 3.15 where $M_{med}$ = 300 GeV and 500 GeV are chosen to be below and above $2m_t$. The off-shell Dark Matter production regime is assumed by taking $m_{\mathrm{DM}} = 1$ TeV in order to study solely the effects of the couplings to quarks. No differences in the kinematic distributions are observed and also the cross sections remain similar in this case. Therefore, it is concluded that no significant changes appear for mediator masses around the $2m_t$ threshold.

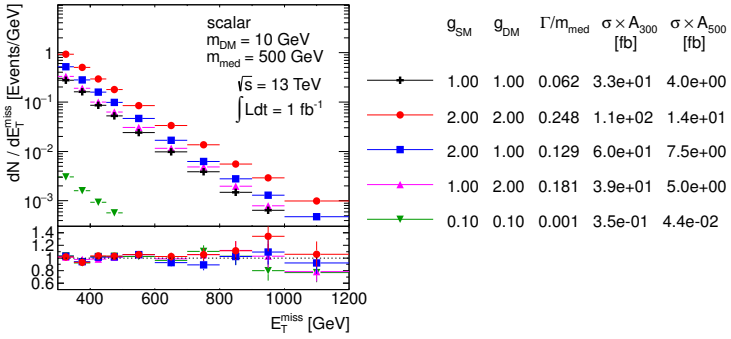


| $g_{SM}$ | $g_{DM}$ | $\Gamma/m_{med}$ | $\sigma \times A_{300}$ [fb] | $\sigma \times A_{500}$ [fb] |
|---|---|---|---|---|
| 1.00 | 1.00 | 0.062 | 3.3e+01 | 4.0e+00 |
| 2.00 | 2.00 | 0.248 | 1.1e+02 | 1.4e+01 |
| 2.00 | 1.00 | 0.129 | 6.0e+01 | 7.5e+00 |
| 1.00 | 2.00 | 0.181 | 3.9e+01 | 5.0e+00 |
| 0.10 | 0.10 | 0.001 | 3.5e-01 | 4.4e-02 |

Figure 3.11: Scan over couplings. The $\not{E}_T$ distribution is compared for the scalar mediator models using the parameters as indicated. Ratios of the normalized distributions with respect to the first one are shown. $A_{300}$ and $A_{500}$ in the table denote the acceptance of the $\not{E}_T > 300$ GeV and $\not{E}_T > 500$ GeV cut, respectively.

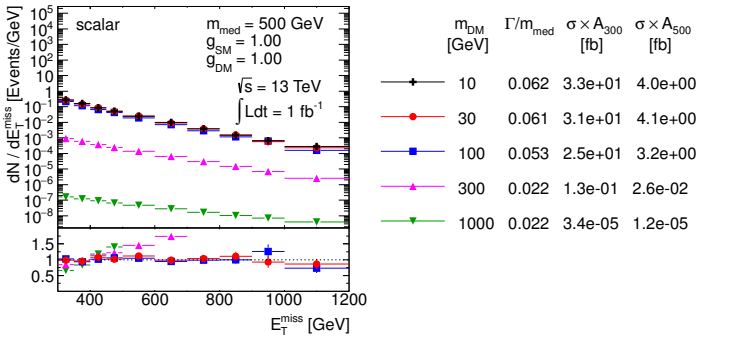


| $m_{DM}$ [GeV] | $\Gamma/m_{med}$ | $\sigma \times A_{300}$ [fb] | $\sigma \times A_{500}$ [fb] |
|---|---|---|---|
| 10 | 0.062 | 3.3e+01 | 4.0e+00 |
| 30 | 0.061 | 3.1e+01 | 4.1e+00 |
| 100 | 0.053 | 2.5e+01 | 3.2e+00 |
| 300 | 0.022 | 1.3e-01 | 2.6e-02 |
| 1000 | 0.022 | 3.4e-05 | 1.2e-05 |

Figure 3.12: Scan over Dark Matter mass. The $\not{E}_T$ distribution is compared for the scalar mediator models using the parameters as indicated. Ratios of the normalized distributions with respect to the first one are shown. $A_{300}$ and $A_{500}$ in the table denote the acceptance of the $\not{E}_T > 300$ GeV and $\not{E}_T > 500$ GeV cut, respectively.

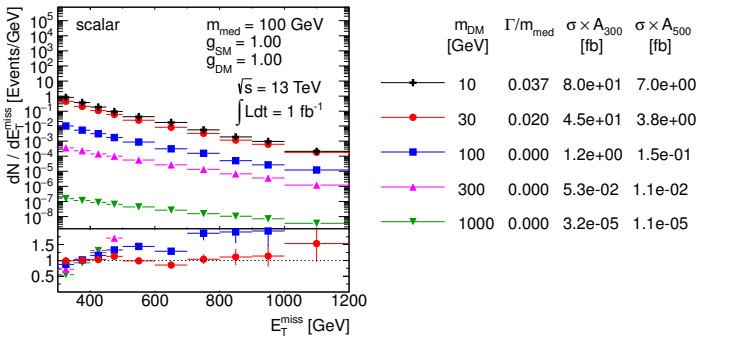


| $m_{DM}$ [GeV] | $\Gamma/m_{med}$ | $\sigma \times A_{300}$ [fb] | $\sigma \times A_{500}$ [fb] |
|---|---|---|---|
| 10 | 0.037 | 8.0e+01 | 7.0e+00 |
| 30 | 0.020 | 4.5e+01 | 3.8e+00 |
| 100 | 0.000 | 1.2e+00 | 1.5e-01 |
| 300 | 0.000 | 5.3e-02 | 1.1e-02 |
| 1000 | 0.000 | 3.2e-05 | 1.1e-05 |

Figure 3.13: Scan over Dark Matter mass. The $\not{E}_T$ distribution is compared for the scalar mediator models using the parameters as indicated. Ratios of the normalized distributions with respect to the first one are shown. $A_{300}$ and $A_{500}$ in the table denote the acceptance of the $\not{E}_T > 300$ GeV and $\not{E}_T > 500$ GeV cut, respectively.

The optimized parameter grid in the $M_{med}$–$m_{\mathrm{DM}}$ plane for scalar and pseudo-scalar mediators is motivated by similar arguments as in the previous section. Therefore, a similar pattern is followed here, taking again $g_q = g_{\mathrm{DM}} = 1$. Only the sensitivity to the highest mediator masses has to be revisited. The generator level cross section times the acceptance at $\not{E}_T > 500$ GeV for the model with couplings $g_q = g_{\mathrm{DM}} = 1$, light Dark Matter of $m_{\mathrm{DM}}$ =10 GeV and

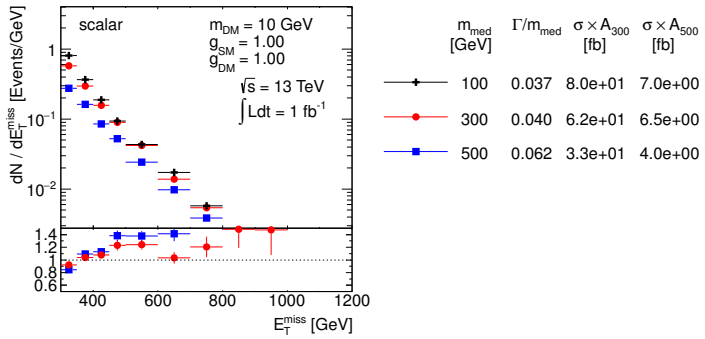


Figure 3.14: Scan over mediator mass. The $\not{E}_T$ distribution is compared for the scalar mediator models using the parameters as indicated. Ratios of the normalized distributions with respect to the first one are shown. $A_{300}$ and $A_{500}$ in the table denote the acceptance of the $\not{E}_T > 300\,\text{GeV}$ and $\not{E}_T > 500\,\text{GeV}$ cut, respectively.

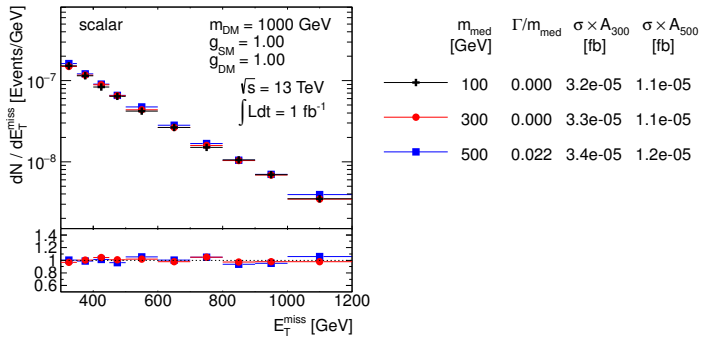


Figure 3.15: Scan over mediator mass. The $\not{E}_T$ distribution is compared for the scalar mediator models using the parameters as indicated. Ratios of the normalized distributions with respect to the first one are shown. $A_{300}$ and $A_{500}$ in the table denote the acceptance of the $\not{E}_T > 300\,\text{GeV}$ and $\not{E}_T > 500\,\text{GeV}$ cut, respectively.

a $M_{med}$ =500 GeV scalar mediator is at the order of 10 fb, i.e. just at the edge of the early Run-2 sensitivity. Increasing the mediator mass to 1 TeV pushes the product $\sigma \times A$ down to approximately 0.1 fb, below the LHC sensitivity. Therefore, we choose to remove the 2 TeV mediator mass from the grid and present the final grid with 26 mass points only in Fig. 3.2. One point at very high mediator mass (5 TeV) is added for each of the DM masses scanned, to aid the reinterpretation of results in terms of contact interaction operators (EFTs).

| $m_{\text{DM}}$ (GeV) | $m_{\text{med}}$ (GeV) | | | | | | | | |
|---|---|---|---|---|---|---|---|---|---|
| 1 | 10 | 20 | 50 | 100 | 200 | 300 | 500 | 1000 | 5000 |
| 10 | 10 | 15 | 50 | 100 | | | | | 5000 |
| 50 | 10 | | 50 | 95 | 200 | 300 | | | 5000 |
| 150 | 10 | | | | 200 | 295 | 500 | | 5000 |
| 500 | 10 | | | | | | 500 | 995 | 5000 |
| 1000 | 10 | | | | | | | 1000 | 5000 |

Table 3.2: Simplified model benchmarks for $s-$channel simplified models (spin-0 mediators decaying to Dirac DM fermions in the scalar and pseudoscalar case, taking the minimum width for $g_q = g_{\text{DM}} = 1$)

The proposal for the scan in the $g_q$–$g_{\text{DM}}$ plane is described in the following section.

## 3.3 *Cross section scaling*

The aim of the parameter grid optimization is to find out whether certain parts of the parameter space can be omitted and one can rely on the neighboring grid points in order to populate the missing parts. There are two ways of doing this:

- Interpolation is used in-between the grid points that are close enough such that finer granularity is not needed for the presentation purposes, or between the points where smooth or no changes of the results are expected. The latter argument is exactly the one that motivates the reduction of the grid points in the $M_{med}$–$m_{\mathrm{DM}}$ plane.

- Recalculation of the results can be used when the dependencies with respect to the neighboring grid points are known.

The results of the scan over the couplings presented in the previous sections indicate there are no changes in kinematic distributions for different choices of the coupling strengths. This means that the acceptance remains the same in the whole $g_q$–$g_{\mathrm{DM}}$ plane and it is sufficient to perform the detector simulation only for one single choice of $g_q, g_{\mathrm{DM}}$. The resulting truth-level selection acceptance and the detector reconstruction efficiency can then be applied to all remaining grid points in the $g_q$–$g_{\mathrm{DM}}$ plane where only the generator-level cross section needs to be known. This significantly reduces the computing time as the detector response is by far the most expensive part of the Monte Carlo sample production. However, the number of generated samples can be reduced even further if a parameterization of the cross section dependence from one grid point to another exists.

Let us now elaborate on a cross section scaling procedure. The propagator on the s-channel exchange is written in a Breit-Wigner form as $\frac{1}{q^2-M_{med}^2+iM_{med}\Gamma}$, where $q$ is the momentum transfer calculated from the two partons entering the hard process after the initial state radiation, which is equivalent to the invariant mass of the Dark Matter pair. The size of the momenum transfer with respect to the mediator mass allows to classify the production in the following way:

- off-shell production when $q^2 \gg M_{med}$ leading to suppressed cross sections,

- on-shell production when $q^2 \sim M_{med}$ leading to enhanced cross sections,

- effective field theory (EFT) limit when $q^2 \ll M_{med}$.

All three categories can be distinguished in Fig. 3.16 showing the upper limit on the interaction scale $M^* \equiv M_{med}/\sqrt{g_q g_{\mathrm{DM}}}$ for vector mediator. In the case of the off-shell production and the EFT limit, the first term in the propagator dominates which reduces the dependence on the mediator width. Therefore, in these cases one can approximate the cross section as

$$\sigma \propto g_q^2 g_{\mathrm{DM}}^2. \tag{3.20}$$

The on-shell production regime is the most interesting one as it gives the best chances for a discovery at the LHC given the cross section enhancement. The propagator term with the width cannot

be neglected in this case and, in the narrow width approximation which requires $\Gamma \ll M_{med}$, one can integrate

$$\int \frac{ds}{(s - M_{med}^2)^2 + M_{med}^2\Gamma^2} = \frac{\pi}{M_{med}\Gamma} \tag{3.21}$$

which further implies the cross section scaling

$$\sigma \propto \frac{g_q^2 g_{\mathrm{DM}}^2}{\Gamma}. \tag{3.22}$$

The narrow with approximation is important here as it ensures an integration over parton distribution functions (PDFs) can be neglected. In other words, it is assumed the integrant in Eq. 3.21 is non-zero only for a small region of $s$, such that the PDFs can be taken to be constant in this range. Since $\Gamma \sim g_q^2 + g_{\mathrm{DM}}^2$, one can simplify this rule in the extreme cases as follows

$$\sigma \propto \frac{g_q^2 g_{\mathrm{DM}}^2}{g_q^2 + g_{\mathrm{DM}}^2} \xrightarrow{g_q \ll g_{\mathrm{DM}}} g_q^2 \tag{3.23}$$

$$\sigma \propto \frac{g_q^2 g_{\mathrm{DM}}^2}{g_q^2 + g_{\mathrm{DM}}^2} \xrightarrow{g_q \gg g_{\mathrm{DM}}} g_{\mathrm{DM}}^2 \,. \tag{3.24}$$

However, it is important to keep in mind that there is no simple scaling rule for how the cross section changes with the Dark Matter mass and the mediator mass, or for mediators with a large width, because PDFs matter in such cases as well. Therefore, the scaling procedure outlined above is expected to work only for fixed masses and fixed mediator width, assuming the narrow width approximation applies.

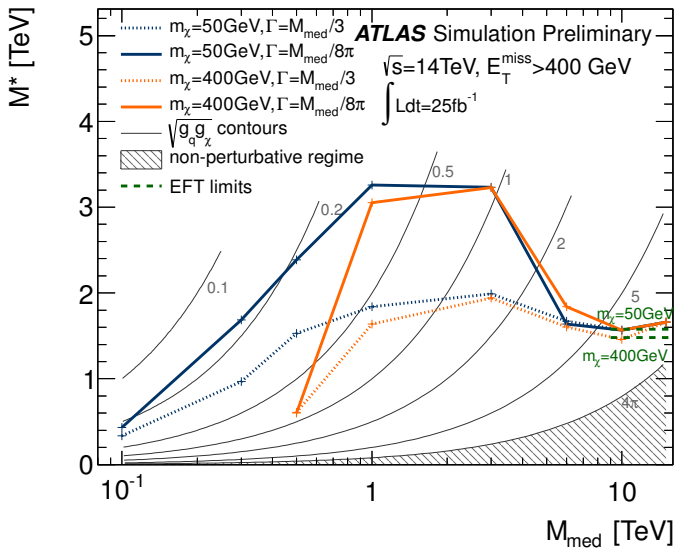


Figure 3.16: Comparison of the 95% CL lower limits on the scale of the interaction of a $Z'$-like simplified model at 14 TeV, in terms of the mediator mass. Corresponding limits from EFT models are shown on the same plot as green dashed lines to show equivalence between the two models for high mediator masses. Taken from Ref. [ATL14].

Figures 3.17 and 3.18 show the minimal width in the $g_q$–$g_{\mathrm{DM}}$ plane for all vector, axial-vector, scalar and pseudo-scalar mediators for $M_{med} = 100\,\mathrm{GeV}$ and 1000 GeV, respectively, taking $m_{\mathrm{DM}} = 10\,\mathrm{GeV}$. The individual colors indicate the lines of constant width

along which the cross section scaling works. For vector and axial-vector mediators, the minimal width is predominantly defined by $g_q$ due to the number of quark flavors and the color factor. On the contrary, both the Standard Model and Dark Matter partial width have comparable contributions in case of scalar and pseudo-scalar mediators if the top quark channel is open ($M_{med} > 2m_t$). However, mostly $g_{\mathrm{DM}}$ defines the minimal width for $M_{med} < 2m_t$ due to the Yukawa-suppressed light quark couplings.

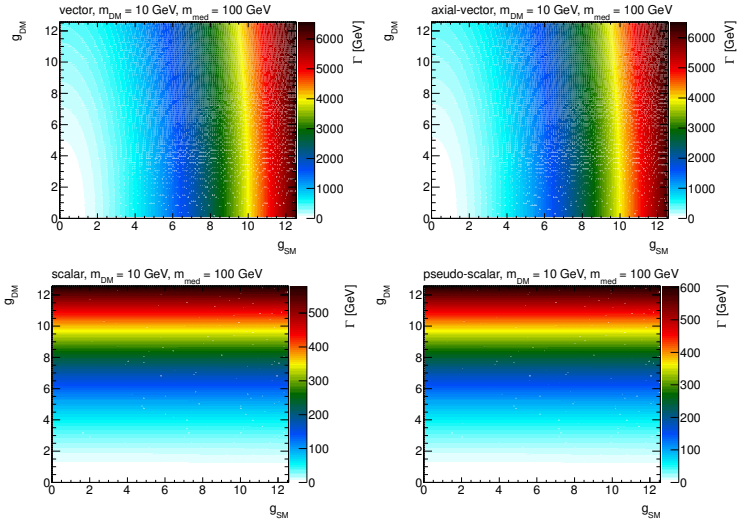


Figure 3.17: Minimal width for vector, axial-vector, scalar and pseudo-scalar mediators as a function of the individual couplings $g_q$ and $g_{\mathrm{DM}}$, assuming $M_{med} = 100\,\mathrm{GeV}$ and $m_{\mathrm{DM}} = 10\,\mathrm{GeV}$.

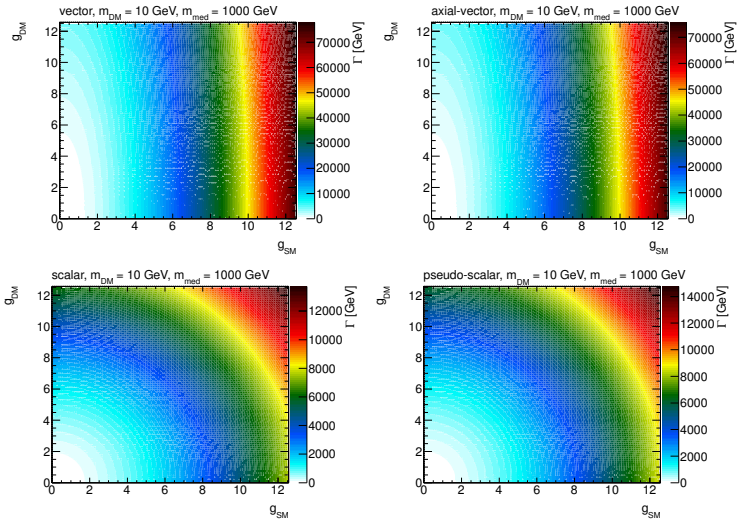


Figure 3.18: Minimal width for vector, axial-vector, scalar and pseudo-scalar mediators as a function of the individual couplings $g_q$ and $g_{\mathrm{DM}}$, assuming $M_{med} = 1\,\mathrm{TeV}$ and $m_{\mathrm{DM}} = 10\,\mathrm{GeV}$.

The performance of the cross section scaling is demonstrated in Fig. 3.19 where two mass points $M_{med} = 100\,\mathrm{GeV}$ and 1 TeV with $m_{\mathrm{DM}} = 10\,\mathrm{GeV}$ are chosen and rescaled from the starting point $g_q = g_{\mathrm{DM}} = 1$ according to Eq. 3.22 to populate the whole $g_q$–$g_{\mathrm{DM}}$ plane. This means the width is not kept constant in this test and this is done in purpose in order to point out deviations from the scaling when the width is altered. For each mass point, the rescaled cross section is compared to the generator cross section and the ratio of the two is plotted. For the given choice of the mass points,

the scaling seems to work approximately with the precision of $\sim 20\%$ in the region where $\Gamma_{\text{min}} < M_{med}$. Constant colors indicate the lines along which the cross section scaling works precisely and there is a remarkable resemblance of the patterns shown in the plots of the mediator width. To prove the scaling along the lines of constant width works, one such line is chosen in Fig. 3.20 for a scalar mediator, defined by $M_{med} = 300\,\text{GeV}$, $m_{\text{DM}} = 100\,\text{GeV}$, $g_q = g_{\text{DM}} = 1$, and the rescaled and generated cross sections are found to agree within 3%.

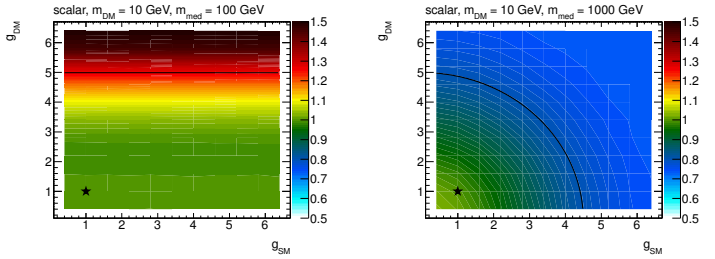


Figure 3.19: Ratio of the rescaled and generated cross sections in the $g_q$–$g_{\text{DM}}$ plane. The point at $g_q = g_{\text{DM}} = 1$, taken as a reference for the rescaling, is denoted by a star symbol. Scalar model with $M_{med} = 100\,\text{GeV}$ (left) and 1 TeV (right) is plotted for $m_{\text{DM}} = 10\,\text{GeV}$. The limiting case $\Gamma_{\text{min}} = M_{med}$ is shown as a black line.

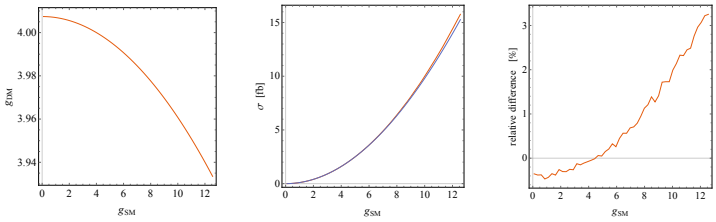


Figure 3.20: Scaling along the lines of constant width. The line of constant width for $M_{med} = 300\,\text{GeV}$ and $m_{\text{DM}} = 100\,\text{GeV}$, intercepting $g_q = g_{\text{DM}} = 4$ is shown on left. The generated and rescaled cross sections are compared in the middle, the corresponding ratio is shown on right.

*Proposed parameter grid* We propose to present the results in the $g_q$–$g_{\text{DM}}$ plane using the following prescription:

- Since the shapes of kinematic quantities do not change for different couplings, use the acceptance and efficiency for the available $m_{\text{DM}} = 50\,\text{GeV}$, $M_{med} = 300\,\text{GeV}$, $g_q = g_{\text{DM}} = 1$ grid point from the $M_{med}$–$m_{\text{DM}}$ plane for the scalar and pseudo-scalar mediator. In case of the vector and axial-vector mediator, use the grid point $m_{\text{DM}} = 50\,\text{GeV}$, $M_{med} = 1\,\text{TeV}$, $g_q = g_{\text{DM}} = 1$.
- Generate additional samples in order to get generator cross sections only. For scalar and pseudo-scalar mediator, choose $m_{\text{DM}} = 50\,\text{GeV}$, $M_{med} = 300\,\text{GeV}$ with the following values for $g_q = g_{\text{DM}}$: 0.1, 2, 3, 4, 5, 6. For vector and axial vector mediator, choose $m_{\text{DM}} = 50\,\text{GeV}$, $M_{med} = 1\,\text{TeV}$ with the following values for $g_q = g_{\text{DM}}$: 0.1, 0.25, 0.5, 0.75, 1.25, 1.5. The upper values are defined by the minimal width reaching the mediator mass.
- Rescale the generator cross sections along the lines of constant width in order to populate the whole $g_q$–$g_{\text{DM}}$ plane.

*Rescaling to different mediator width* In general there may be an interest to consider larger mediator masses than $\Gamma_{\text{min}}$ in order to accommodate further couplings of the mediator. The cross section

scaling method described above can be used to reinterpret the results presented for the minimal width, since multiplying the width by factor $n$ is equivalent to changing the coupling strength by factor $\sqrt{n}$, i.e.

$$\sigma(g_q, g_{\mathrm{DM}}, n\Gamma_{\mathrm{min}}(g_q, g_{\mathrm{DM}})) \propto \frac{g_q^2 g_{\mathrm{DM}}^2}{\Gamma_{\mathrm{min}}(\sqrt{n}g_q, \sqrt{n}g_{\mathrm{DM}})} \,. \tag{3.25}$$

The cross section for the sample with couplings $g_q$ and $g_{\mathrm{DM}}$ and modified mediator width $\Gamma = n\Gamma_{\mathrm{min}}$ can therefore be rescaled from a sample generated with the minimal width corresponding to the couplings scaled by $\sqrt{n}$ as described in the following formula.

$$\sigma(g_q, g_{\mathrm{DM}}, n\Gamma_{\mathrm{min}}(g_q, g_{\mathrm{DM}})) = \frac{1}{n^2}\sigma(\sqrt{n}g_q, \sqrt{n}g_{\mathrm{DM}}, \Gamma_{\mathrm{min}}(\sqrt{n}g_q, \sqrt{n}g_{\mathrm{DM}})) \tag{3.26}$$

Here, it is again assumed the narrow width approximation applies. The advantage of doing this is in the fact that no event selection and detector response needs to be simulated since the changes in couplings do not have an effect on the shapes of kinematic distributions.

## 3.4 *Colored scalar mediator, t-channel exchange*

The preceding sections address models with a Dirac fermion coupled to the SM through exchange of a neutral spin-0 or spin-1 in an $s$-channel process. A $t$-channel process may couple the SM and DM directly, leading to a different phenomenology. Here, we examine a model where $\chi$ is a Standard Model (SM) singlet, the mediating particle, labeled $\phi$, is charged and coloured, and the SM particle is a quark. Following the example of Ref. [PVZ14], the interaction Lagrangian is written as

$$\mathcal{L}_{\mathrm{int}} = g \sum_{i=1,2,3} (\phi_L^i \bar{Q}_L^i + \phi_{uR}^i \bar{u}_R^i + \phi_{dR}^i \bar{d}_R^i)\chi \tag{3.27}$$

To do (**??**)

where $Q_L^i$, $u_R^i$ and $d_R^i$ are the SM quarks and $\phi_L^i$, $\phi_{uR}^i$ and $\phi_{dR}^i$ are the corresponding mediators, which (unlike the $s$-channel mediators) must be heavier than $\chi$. These mediators have SM gauge representations under $(SU(3), SU(2))_Y$ of $(3,2)_{-1/6}$, $(3,1)_{2/3}$ and $(3,1)_{-1/3}$ respectively. Variations of the model previously studied include coupling to the left-handed quarks only [CEHL14, BDSJ$^+$14], to the $\phi_{uR}^i$ [DNRT13] or $\phi_{dR}^i$ [PVZ14, A$^+$14b], or some combination [BB13, AWZ14].

As for the $s$-channel models, we assume Minimal Flavour Violation (MFV), setting the mediator masses for each flavour; the same logic also applies to the couplings $g$. The available parameters are then

$$\{m_\chi,\, M_\phi,\, g\}. \tag{3.28}$$

In practice, the third mediator mass and coupling could be separated from the other two, if higher order corrections to the MFV prediction arise due to the large top Yukawa coupling — a common variation is then to define this split between the first two generations and the third, so the parameters are extended to

$$\{m_\chi,\, M_{\phi_{1,2}},\, M_{\phi_3},\, g_{1,2},\, g_3\}. \tag{3.29}$$

For the purposes of the rest of this section, we will assume the universal variant $M_{\phi_{1,2}} = M_{\phi_3}$, $g_{1,2} = g_3$.

The minimal width of each mediator is expressed, using the example of decay to an up quark, as

$$\begin{aligned}\Gamma(\phi_i \to \bar{u}_i\chi) = \frac{g_i^2}{16\pi M_{\phi_i}^3}(M_{\phi_i}^2 - m_{u_i}^2 - m_\chi^2) \\ \times \sqrt{M_{\phi_i}^4 + m_{u_i}^4 + m_\chi^4 - 2M_{\phi_i}^2 m_{u_i}^2 - 2M_{\phi_i}^2 m_\chi^2 - 2m_{u_i}^2 m_\chi^2}\,,\end{aligned} \tag{3.30}$$

which reduces to

$$\frac{g_i^2 M_{\phi_i}}{16\pi}\left(1 - \frac{m_\chi^2}{M_{\phi_i}^2}\right)^2 \tag{3.31}$$

in the limit $M_{\phi_i}, m_\chi \gg m_{u_i}$.

The leading-order processes involved in MET+jet production are shown in Fig. 3.21. Note that the generation index for $\phi$ is linked to the incoming fermion(s). Thus, mono-jet production via $\phi_u^3$ is not possible at this order, while production through $\phi_d^3$ is suppressed by the $b$ parton PDF. This model can also give a signal in the di-jet + MET channel when, for example, the $\chi$ is exchanged in the $t$-channel and the resulting $\phi$ pair each decay to a jet + $\chi$. Fig. **??** shows the leading order diagrams. Except for the $gg$ induced process, di-jet production through $\phi_u^3$ is not possible, and production through $\phi_d^3$ is again suppressed. The diagram involving the t-channel exchange of $\chi$ is strongly dependent upon the Dirac fermion assumption. For a Majorana fermion, $q\bar{q}, \bar{q}\bar{q}$, and $qq$ production would be possible with the latter having a pronounced enhancement at the LHC.

This model is similar to the MSSM with only light squarks and a neutralino, except for two distinct points: the $\chi$ is a Dirac fermion and the coupling $g$ is not limited to be weak scale. In the MSSM, most of these processes are sub-dominant, even if resonantly enhanced, because the production is proportional to weak couplings. In the more general theories considered here, $g$ is free to take on large values of order 1 or more, and thus diagrams neglected in MSSM simulation can occur at a much higher rate here. While constraints from SUSY jets+MET analyses on these models should be

translated to this model, LHC experiments should also test their sensitivity to them.

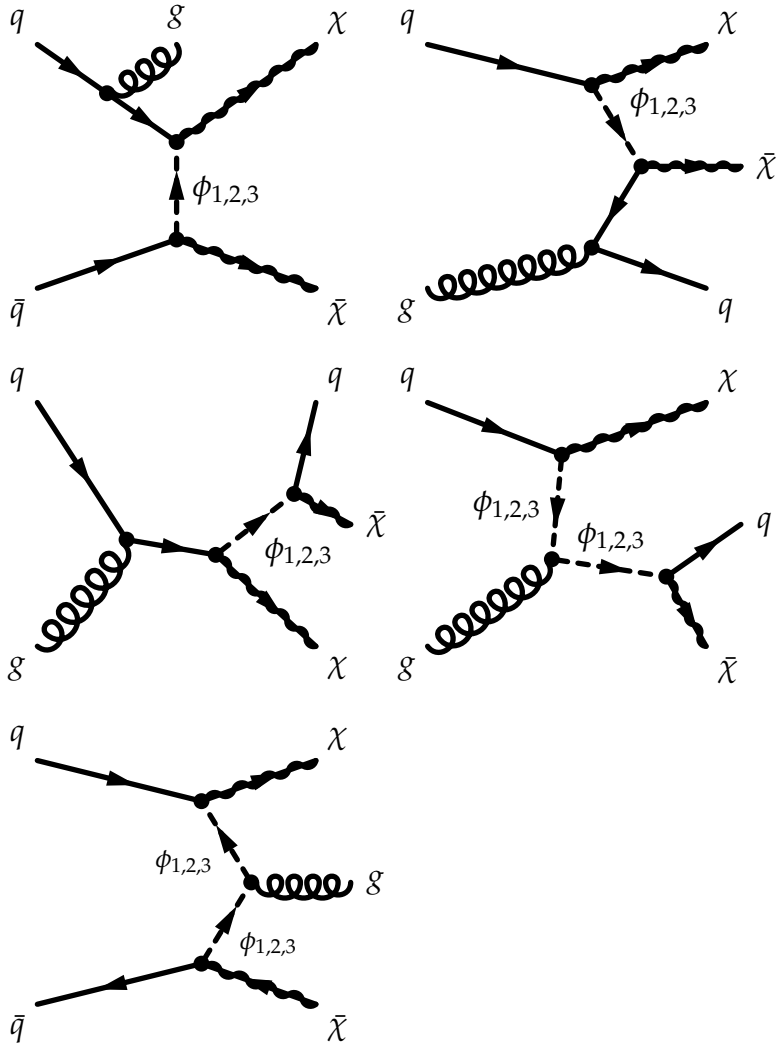


Figure 3.21: Leading order mono-jet $t$-channel processes, adapted from [**?** ]Papucci:2014.

### Parameter scans

Ref. [**?** ] studies the parameter space and obtains bounds on this model from LHC Run 1 mono-jet and dijets+MET data.

As in the $s$-channel models, scans should be performed over $m_\chi$ and $m_\phi$. The viable ranges of both parameters nearly coincide with the scan proposed for the $s$-channel; for simplicity we recommend adopting the $s$-channel mono-jet grid.

The rates of the first three diagrams of Fig. 3.21 scale as one with the coupling $g$. In the heavy mediator limit, then, the kinematic distributions depend only indirectly on the coupling through the effect on the minimal mediator width. In contrast with the $s$-channel case, however, the bounds one obtains from X+MET searches depends strongly on the width of the mediator, as is visible in Figs. 5 and 6 of Ref. [**?** ], except in the heavy mediator limit ($M_\phi \approx 2\,\text{TeV}$). A scan over the width was not available for this report; thus we recommend scanning a range of possible widths as discussed in a more-limited way for the $s$-channel mono-jet, spanning from the minimal width to a value approaching the particle limit (for exam-

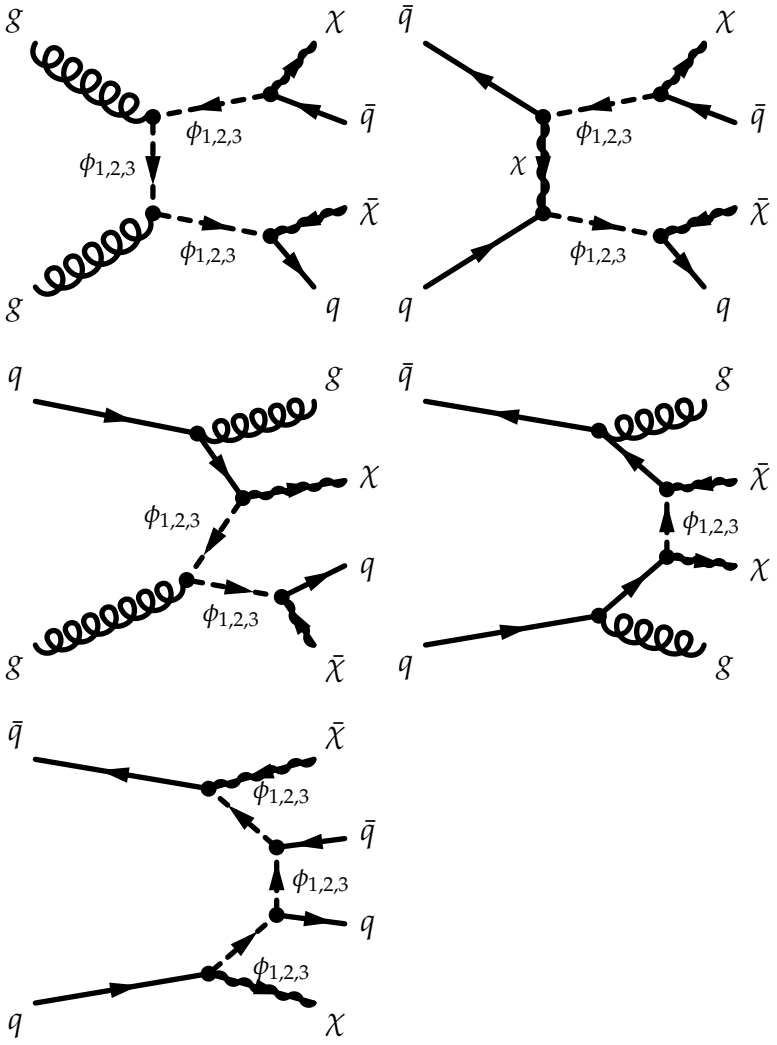


Figure 3.22: Leading order two-jet $t$-channel processes, adapted from [**?** ]Papucci:2014.

ple, $\Gamma \approx M_\phi/3$ in Ref. [**?** ]).

## Implementation

The MadGraph implementation of the Ref. [**?** ] is available from the Forum repository , following the matching and merging prescription described in its Section II and Appendix A.

To do (**??**)

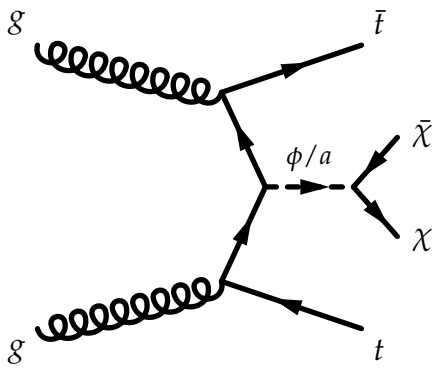


Figure 4.1: Representative Feynman diagram showing the pair production of dark matter particles in association with $t\bar{t}$.

# 4
# Specific models for signatures with heavy flavor quarks

## 4.1 $t\bar{t}$+MET models

As described in Section 3.2, a model with a scalar/pseudoscalar particle mediating the DM-SM interactions is one of the simplest UV completions of our EFT models. With the MFV assumption, the top quark plays a primary role in the phenomenology. The model predicts not only the monojet process described earlier, but also production of dark matter in association with top pairs, as illustrated in Fig. 4.1.

### 4.1.1 Parameter scan

As discussed in Sec. **??**, the MFV and universal coupling assumptions for spin-0 mediators leads to quark mass dependent Yukawa couplings and therefore dominant couplings to top quarks.Therefore DM+$t\bar{t}$ searches are strongly physically motivated and it is important to establish benchmarks for collider searches following the assumptions described in Sec. **??**, in particular a Dirac fermion DM particle, universal couplings and minimum width, $\Gamma_{\phi,a}$.

The benchmark points scanning the model parameters have been selected to ensure that the kinematic features of the parameter space are sufficiently represented. Detailed studies were performed to identify points in the $m_{\mathrm{DM}}$, $m_{\phi,a}$, $g_{\mathrm{DM}}$, $g_q$ (and $\Gamma_{\phi,a}$) parameter space that differ significantly from each other in terms of expected detector acceptance. Because missing transverse momentum is the key observable for searches, the mediator $p_T$ spectra is taken to represent the main kinematics of a model. Another consideration in determining the set of benchmarks is to focus on the phase space

where we expect the searches to be sensitive during the 2015 LHC run. Based on a projected integrated luminosity of 30 fb$^{-1}$ expected for 2015, we disregard model points with a cross section times branching ratio smaller than 0.1 fb.

The kinematics is most dependent on the masses $m_{\mathrm{DM}}$ and $m_{\phi,a}$. Figure 4.2 and 4.3 show typical dependencies for scalar and pseudoscalar couplings respectively. Typically, the mediator $p_T$ spectra broadens with larger $m_{\phi,a}$. The kinematics are also quite different between on-shell and off-shell production. Furthermore, the kinematic differences between scalar and pseudoscalar are large with light mediator masses and are reduced for larger masses. It is therefore important to benchmark points covering on-shell and off-shell production with sufficient granularity.

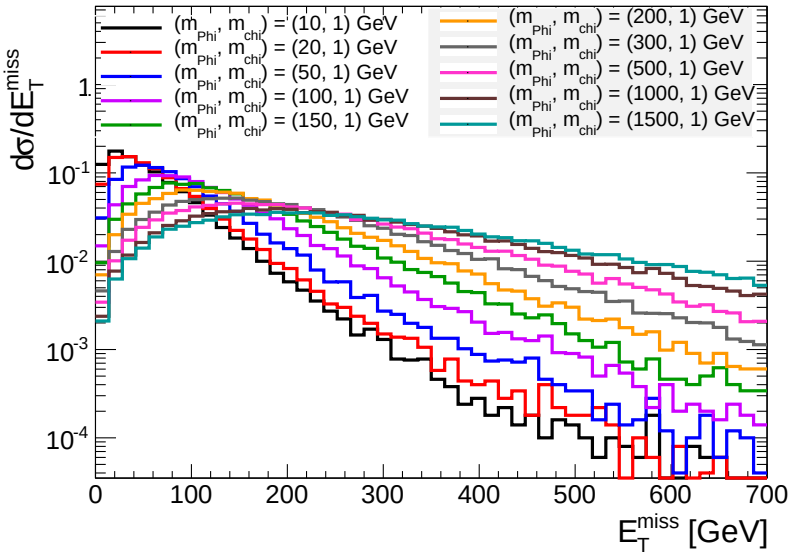


Figure 4.2: Example of the dependence of the kinematics on the scalar mediator mass. The Dark Matter mass is fixed to be 1GeV.

Typically only weak dependencies on width or equivalently couplings are observed (see Fig 4.5), except for large mediator masses of $\sim$ 1.5 TeV or for very small couplings of $\sim 10^{-2}$. These regimes where width effects are significant have production cross sections that are too small to be relevant for 30 fb$^{-1}$ and are not considered here. However, with the full Run-2 dataset, such models may be within reach. The weak dependence on the typical width values can be understood as the parton distribution function are the dominant effect on mediator production. In other words, for couplings $\sim O(1)$ the width is large enough that the $p_T$ of the mediator is determined mainly by the PDF.

Another case where the width can impact the kinematics is when $m_{\phi,a}$ is slightly larger than $2m_\chi$. Here, the width determines the relative contribution between on-shell and off-shell production. An example is given in Fig. 4.6. In our recommendations we propose to use for simplicity the minimal width, as this is represents the most

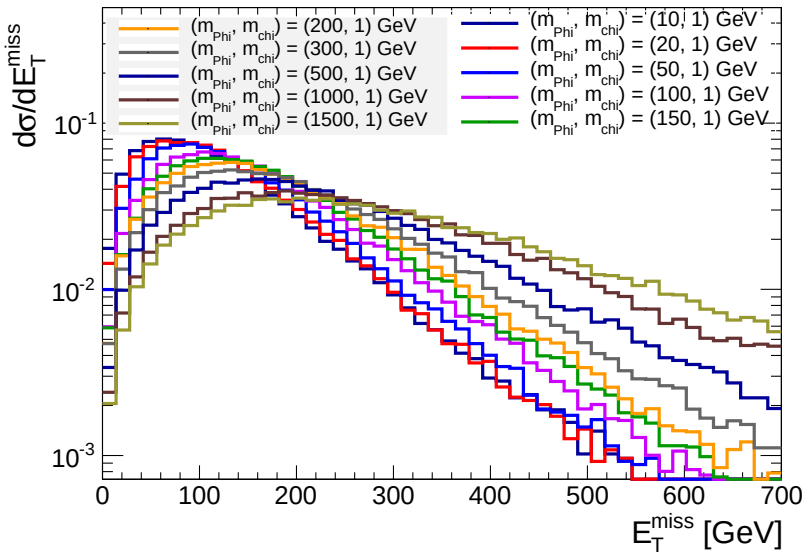


Figure 4.3: Example of the dependence of the kinematics on the pseudoscalar mediator mass. The Dark Matter mass is fixed to be 1GeV.

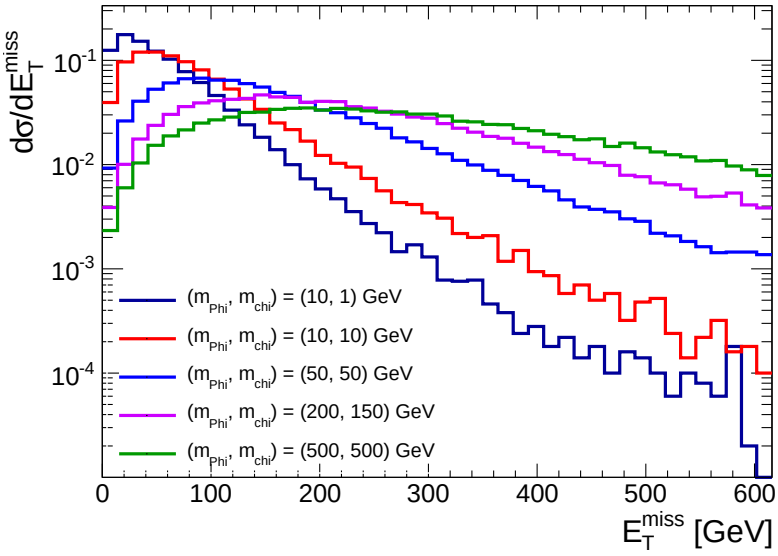


Figure 4.4: Example of the dependence of the kinematic for points of the grid proposed in Tab. 3.2 close to the $m_{\phi,a} \sim 2m_\chi$ limit.3

conservative choice to interpret the LHC results. **[TODO: mention larger widths too]**

Given that the kinematics are similar for all couplings $\sim O(1)$, we recommend to generate only samples with $g_{\mathrm{DM}} = g_q = 1$. It follows from this that these benchmark points should be a good approximation for non-unity couplings and for $g_{\mathrm{DM}} \neq g_q$, provided that the sample is rescaled to the appropriate cross section times branching ratio. While the simple scaling function $\sigma' * BR' = [\sigma * BR] * (g'_q/g_q)^2 * (g'_{\mathrm{DM}}/g_{\mathrm{DM}})^2 * (\Gamma/\Gamma')$ is sufficient for a limited range of coupling values (see Fig. 4.7 for example), we also choose

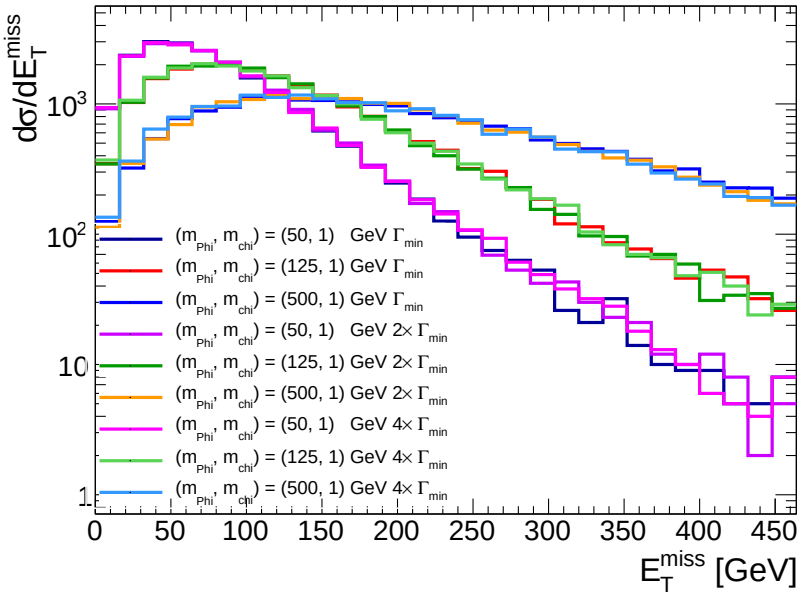


Figure 4.5: Study of the dependence of kinematics on the width of a scalar mediator. The width is increased up to four times the minimal width for each mediator and dark matter mass combination.

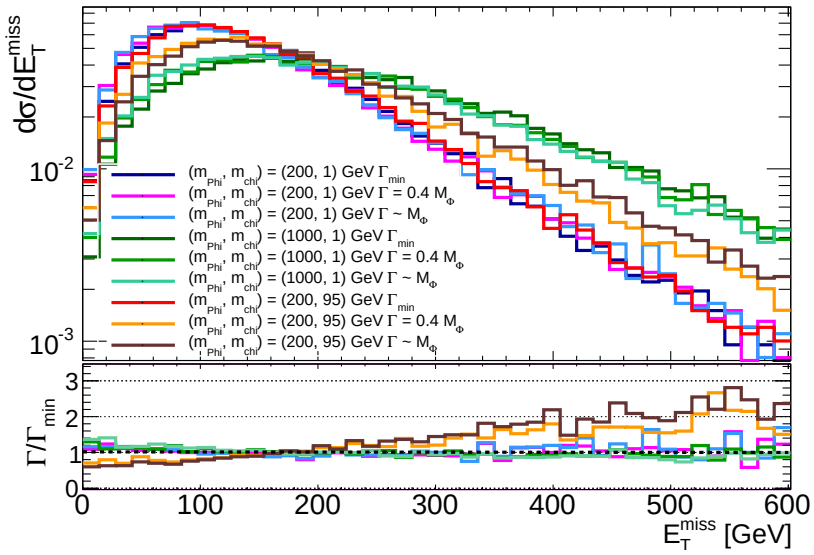


Figure 4.6: Dependence of the kinematics on the width of a scalar mediator. The width is increased up to the mediator mass. Choices of mediator and dark matter masses such that $m_{\phi,a}$ is slightly larger than $2m_\chi$ is the only case that shows a sizeable variation of the kinematics as a function of the width.

to provide instead a table of cross section times branching ratio values over a large range of couplings to support interpretation of search results (see the Appendix C). The table lists couplings from $g = 0.1$ to $g = 3.5$, where the upper limit is chosen to close to the perturbative limit.

The points for the parameter scan chosen for this model are listed in Table 3.2, chosen to be harmonized with those for other analyses employing the same scalar model as benchmark. Based on the sensitivity considerations above, DM masses are only simulated

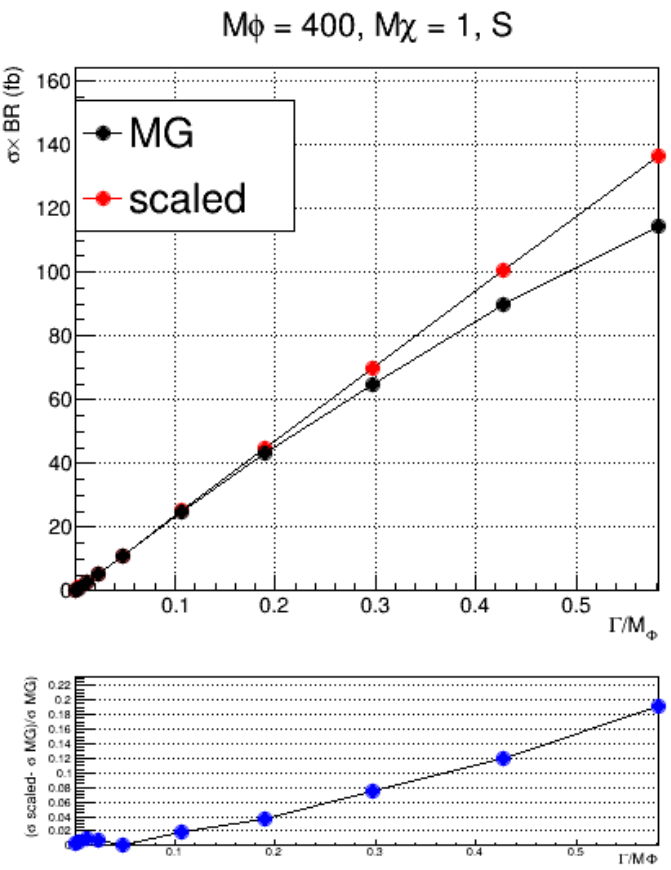


Figure 4.7: An example comparing a simple cross section scaling versus the computation from the generator, for a scalar model with $m_\phi = 400\,\text{GeV}$, $m_{\text{DM}} = 1\,\text{GeV}$ and all couplings set to unity. In this example, the scaling relationship holds for $\Gamma_\phi / m_\phi$ below 0.2, beyond which finite width effects become important and the simple scaling breaks down.

up to 500 GeV, leading to a total of 24 benchmark points.

In addition to the considerations discussed in the preceding subsections, very light DM fermions are included ($m_{\text{DM}} = 10\,\text{GeV}$) as this is a region where colliders have a complementary sensitivity to current direct detection experiments.

## 4.2 $b\bar{b}$+MET models

In some theoretically motivated scenario (e.g. for high $tan\beta$ in the pMSSM ), spin-0 mediators might couple more strongly to down generation quarks. This assumption strongly motivates the study of final states involving $b$-quarks, as a complementary search to the $t\bar{t}$+DM models presented in the previous section.

As in the $t\bar{t}$ case, detailed studies were performed, analyzing these models and their key features. It was found that they show the same weak dependence of the kinematics of the event on width variation, except in few corner cases. In addition, it was found that the same benchmark parameters of the $t\bar{t}$ case could be chosen.

In this particular model we recommend an additional care when

choosing the flavor scheme generation. It is found that the best modeling of two $b$-quarks final states is achieved using a 4-flavor scheme and a massive treatment of the $b$-quarks **[TODO: Add reference]**. In addition, we recommend to calculate the cross sections of these models in the 5-flavour scheme, and as in the *tbart* case we provide values for the suggested coupling scan in the appendix. The PDF used to calculate these cross section is NNPDF3.0 (lhaid 263000).

**[TODO: The following figures are placeholders for now and will be added later]**.

Figure 4.8: Comparison of the subleading jet $p_T$ and $b$-jet multiplicity for $bb$+DM scalar model generated in the 4-flavour (left) and 5-flavour (right) schemes, respectively

Figure 4.9: Example of the dependence of the kinematics on the scalar mediator mass. The Dark Matter mass is fixed to be 1GeV.

Figure 4.10: Example of the dependence of the kinematics on the pseudoscalar mediator mass. The Dark Matter mass is fixed to be 1GeV.

## 4.3 *Models with a single top−quark + MET*

Many different theories predict final states with a single top and associated missing transverse momentum (monotop), some of them including dark matter candidates. A simplified model encompassing the processes leading to this phenomenology is described in Refs. [AFM11, AAB$^+$14, BCDF15], and is adopted as one of the benchmarks for Run 2 LHC searches.

A dark matter candidate $\chi$ and a new particle $M$ (vector or scalar) are added to the SM, in a theory that respects the $\mathrm{SU}(2)_L \times \mathrm{U}(1)_Y$ symmetry and produces a single top quark in association with either the DM particle or a new particle decaying invisibly.

Within this model, two distinct processes can lead to monotop production:

- resonant production, as shown in the diagram of Fig. 4.11 (a), where a color triplet scalar (S in the figure, $\varphi$ in the following) or vector ($X$) field are exchanged in the s-channel, and decay into a spin 1/2 invisible new fermion (called $f_{met}$ in the figure) and a top quark;

- non-resonant production, as shown in the diagrams of Fig. 4.11 (b) and (c), where a flavor-changing interaction produces a top quark in association with a new colored scalar ($\Phi$) or vector ($V$). The new colored particles, called $v_{met}$ in the figure, decay invisibly, e.g. to a pair of DM particles. $v_{met}$ can also decay into a top quark and an up quark, leading to a same-sign top quark final state; a detailed study of the complementarity of this signature is beyond the scope of this Forum report.

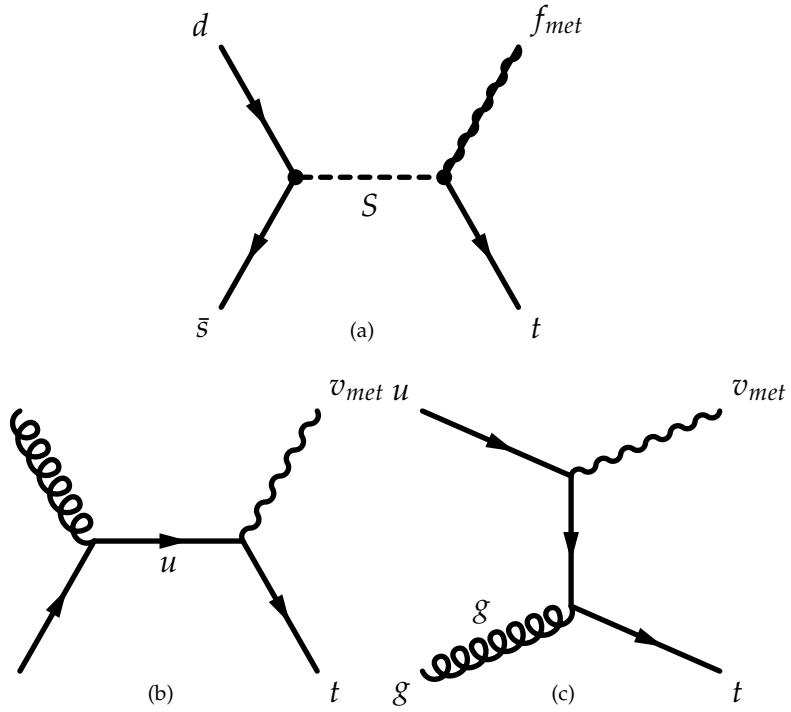


Figure 4.11: Feynman diagram of leading order processes leading to monotop events: production of a coloured scalar resonance $S$ decaying into a top quark and a spin-1/2 fermion $f_{met}$ (a), $s-$ (b) and $t$-channel (c) non resonant production of a top quark in association with a spin-1 boson $v_{met}$.

In the following, resonant and non-resonant production are treated independently as separate benchmarks. Only the simpler case of a scalar resonance is considered as an early benchmark for the resonant model, while the case of vector resonances can be studied in the future.

### Resonant production

In this case, a colored 2/3-charged scalar ($\varphi$) is produced and decays into a top quark and a spin-1/2 invisible particle, $\chi$. The dynamics of the new sector is described by the following Lagrangian:

$$\begin{aligned}\mathcal{L} = \Bigg[ & \varphi \bar{d}^c \left[ a^q_{SR} + b^q_{SR}\gamma_5 \right] d + \varphi \bar{u} \left[ a^{1/2}_{SR} + b^{1/2}_{SR}\gamma_5 \right] \chi \\ & + X_\mu \bar{d}^c \gamma^\mu \left[ a^q_{VR} + b^q_{VR}\gamma_5 \right] d + X_\mu \bar{u} \gamma^\mu \left[ a^{1/2}_{VR} + b^{1/2}_{VR}\gamma_5 \right] \chi + \text{h.c.} \Bigg]\end{aligned} \tag{4.1}$$

where $u$ ($d$) stands for any $up$-quark ($down$-quark), the index $S$ ($V$) stands for scalar (vector) field, and the index $q$ runs over the three quark generations, and the color indices are not shown.

In the notation of [AAB+14], the couplings of the new colored fields to down-type quarks are embedded into the $3 \times 3$ antisymmetric matrices $a^q_{\{S,V\}R}$ (scalar/vector couplings) and $b^q_{\{S,V\}R}$ (pseudoscalar/axial vector couplings) while those to the new fermion $\chi$ and one single up-type quarks are given by the three-component vectors $a^{1/2}_{\{S,V\}R}$ and $b^{1/2}_{\{S,V\}R}$ in flavor space.

In the following, we only consider the model with a new colored scalar, as the requirement of invariance under $SU(2)_L \times U(1)_Y$ would require the introduction of further particles in the case of a new colored vector [BCDF15]. Note that the resulting model can be likened to the MSSM with an RPV coupling between a top squark

and fermions and an RPC coupling between a top squark–top–neutralino.

### Non-Resonant production

For the non-resonant production, the top quark is produced in association with the new particle: either a new scalar ($\phi$) or a new vector ($V$). For simplicity, we only consider the case of a vector new particle, as the scalar case would involve a mixing with the SM Higgs boson and therefore a larger number of free parameters. The Lagrangian describing the dynamics of the non-resonant case is:

$$\mathcal{L} = \left[\phi\bar{u}\left[a^0_{FC}+b^0_{FC}\gamma_5\right]u+V_\mu\bar{u}\gamma^\mu\left[a^1_{FC}+b^1_{FC}\gamma_5\right]u+\text{h.c.}\right] \qquad (4.2)$$

The strength of the interactions among these two states and a pair of up-type quarks is modeled via two $3\times3$ symmetric matrices in flavor space $a^{\{0,1\}}_{FC}$ for the scalar/vector couplings and $b^{\{0,1\}}_{FC}$ for the pseudoscalar/axial vector couplings.

### Model parameters and assumptions

The models considered as benchmarks for the first LHC searches contain further assumptions in terms of the flavour and chiral structure of the model with respect to the full Lagrangians of equations (4.1) and (4.2). These assumptions are qualitatively discussed below.

*Assumptions in the flavour and chiral structure of the models* We only consider right-handed quark components, in order to simplify the model phenomenology. The representation of the left-handed components under the $\mathrm{SU}(2)_L$ symmetry would lead to a coupling to *down*-type quarks, since the effective theory is invariant under $\mathrm{SU}(2)_L\times\mathrm{U}(1)_Y$ gauge symmetry. This implies the vector to be an SU(2)L singlet, hence in turn setting the vector and axial vector matrices to have elements of equal values.

Furthermore, in order to be visible at the LHC in the monotop final state, these models must include a strong coupling between the new particle $\phi$ and $t\chi$. The same kind of assumption exists for the non-resonant production. This means that only the couplings between the new scalar resonance and light quarks ($a_{VR}, a_{SR}$), and the couplings between the new vector, the top quark and light quarks ($a_{FC}$), are set to non-zero values

$$(a^q_{SR})_{11} = (a^{1/2}_{SR})_3 = a \qquad (4.3)$$

### Implementation

This Section describes the notations used in the MadGraph model convention, in term of the ones introduced in the previous Section.

The Madgraph model [Fuk] used for these benchmarks corresponds to the Lagrangian from [AFM11]. Each coupling constant of

this model can be set via the parameter card and the blocks which are relevant for the two models used for the experimental searches are described below. The relevant parameters in the MadGraph parameter cards, also expressed in the notation introduced in the previous Section, are as follows for the two models considered.

1. Resonant scalar model described by the Lagrangian (4.1)
   - `AQS` and `BQS`: $3 \times 3$ matrices (flavour space) fixing the coupling of the scalar $\phi$ ($S$ stands for scalar) and *down*-type quarks ($Q$ stands for quarks), previously called $a^q/b^q_{SR}$.
   - `A12S` and `B12S`: $3 \times 1$ matrices (flavour space) fixing the coupling of the new fermion $\chi$ (where 12 stands for spin-1/2 fermion) and $up$-type quarks, previously called $a^{1/2}_{VR}$.
   - particle names: the scalar $\phi$ is labeled $S$ and the fermion $\chi$ is $f_{met}$
2. Non-resonant vectorial model described by the Lagrangian (4.2)
   - `A1FC` and `B1FC`: $3 \times 3$ matrices (flavour space) fixing the coupling of the vector $V$ (1 stands for vector) and $up$-type quarks, previously called $a^1_{FC}$.
   - particle name: the vector $V$ is labelled $v_{met}$, while the dark matter candidate $\chi$ is not implemented (as this model assumes $\mathrm{BR}(V \to \chi\chi) = 100\%$)

The width of the scalar resonance and of the new vector are set to all allowed decays in the ATLAS implementation, while the only allowed decay in the CMS implementation to the new fermion and a top quark for the resonant model. **[TODO: Can we reach a consensus between ATLAS and CMS?]**

### Parameter scan

The relevant parameters for the resonant model are:

- The mass of the new scalar $\phi$;
- The mass of the new fermion $\chi$;
- The coupling of the new scalar to the new fermion and top quark $a$, related to the width of the scalar in the minimal width assumption;

The relevant parameters for the non-resonant model are:

- The mass of the new vector $V$;
- The coupling of the new vector to the up and top quark $a$, related to the width of the scalar in the minimal width assumption;
- The coupling of the new vector to the new fermion $\chi$, related to the branching fraction of the vector into invisible and visible particle, and as a consequence to the width of the vector.

In the case of the non-resonant model, the current implementation of the model does not allow changing the DM mass directly as the new vector is treated as a particle that always decays invisibly.

It has been checked for the non-resonant model that the relevant kinematics does not change when changing the width of the resonance, for widths up to 10% of the resonance mass. Figures 4.12 and 4.13 show the $V$ mass distribution, the transverse momentum for $V$ in the case of the $V \to t\bar{u}$ decay, for different $V$ masses and widths. Since they only show kinematic quantities related to the mediator, these figures are relevant independently of the $V$ decay mode (be it visible or invisible).

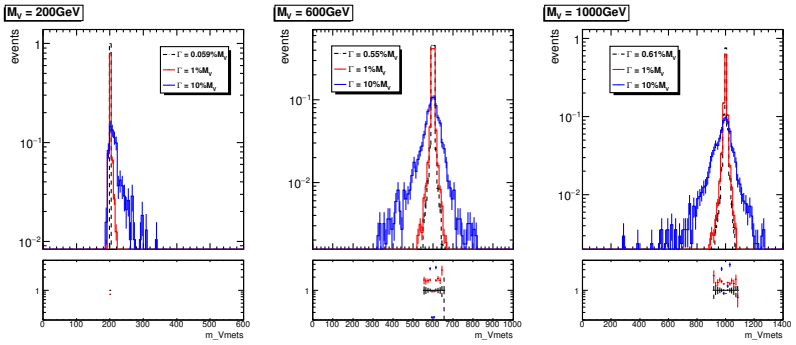


Figure 4.12: Distribution of $V$ invariant mass for the $gu \to tV(\to t\bar{u})$ (on-shell V) for $m_V$ = 200, 600, 1000 GeV (from left to right) and for three different visible decay width (computed from Madgraph directly according to the allowed decays and their couplings, 1% and 10%).

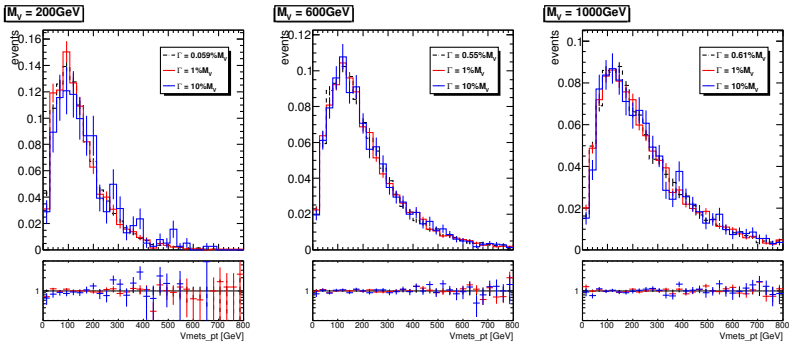


Figure 4.13: Distribution of the $V$ $p_T$ for the $gu \to tV(\to t\bar{u})$ (on-shell V) for $m_V$ = 200, 600, 1000 GeV (from left to right) and for three different visible decay width (computed from Madgraph directly, 1% and 10%).

The limited timescale allowed to reach a consensus for the recommendations contained in this document has not allowed further studies on the parameter scan of these models. The two Collaborations have however agreed to continue studying these models and agree on a common parameter scan, following the same path as for other models described in this document.

## 4.4 *Models with a single b−quark + MET*

A model of bottom-flavored Dark Matter ($b$-FDM) has been proposed in Ref. [ABHL14] to explain the Galactic Center (GC) gamma-ray excess observed in data collected by the Fermi-LAT collaboration [**?** ].

The increase from 8 to 13 TeV will lead to large cross section improvements, as shown in Appendix C.2. The increase in the center of mass energy leads to a cross-section increase that is a function of $m_\Phi$, with a smaller dependency for $m_{\mathrm{DM}}$. Therefore, the sensitivity to this model will increase in early 13 TeV data compared to the 8 TeV searches [**?** ].

The model contains a Dirac fermion transforming as a flavor triplet. The third component of the triplet $\chi_b$ comprises the cosmological DM. A flavor singlet, color triplet scalar field $\Phi$ mediates the interactions between the DM and the Standard Model quarks.The model is similar to the MSSM with a light bottom squark and neutralino, and is thus a flavor-specific example of a $t$-channel model.

The Lagrangian considered is given by

$$-\mathcal{L} \supset g\Phi^* \chi_b b_R + \mathrm{h.c.} \tag{4.4}$$

Within the framework of minimal flavor violation, the other fermions in the flavor triplet can be made sufficiently heavy and weakly-coupled that they can be neglected in the analysis.

An annihilation cross section consistent with the gamma-ray excess can be achieved for perturbative values of the couplings while being consistent with LHC constraints on the colored mediator. For parameters capable of explaining the anomalous gamma-ray signal in terms of Dark Matter coupling preferentially to $b-$ quarks, the model predicts a direct detection cross section that is consistent with current constraints, but within the near future reach of Direct Detection experiments. The model will be decisively tested with data from the upcoming high-energy run at the LHC.

## *4.5 Parameter scan*

The nature of the model doesn't allow to derive a simple scaling behaviour which would allow us reduce the number of points to be simulated. This is because of the interference of diagrams with QCD production of the mediator (which scale as $g^0$) with diagrams that scale with $g$.

To do (**??**)

The coupling can be chosen as a discrete set of values $g = 0.5, 1, 2, 3...$ for each mass point, which would allow a bound on $g$ to be determined. The coupling could also be chosen to fullfill constraints from the relic density (see Appendix C.1, with corresponding cross sections in Tables C.3-**??**). A sizable, $O(1)$ coupling benchmark such as $g = 1$ should be considered for each mass point since this would be a distinctive feature of this benchmark from SUSY models with sbottom squarks.

In light of these considerations, we recommend to produce the following benchmark points in the parameter space for this model:

- $m_{\mathrm{DM}} = 10 - 500$ GeV with a binning of 50 GeV for $m_{\mathrm{DM}} < 100$ and 100 GeV otherwise
- $m_\Phi = 10 - 1300$ with a binning of 100 GeV.

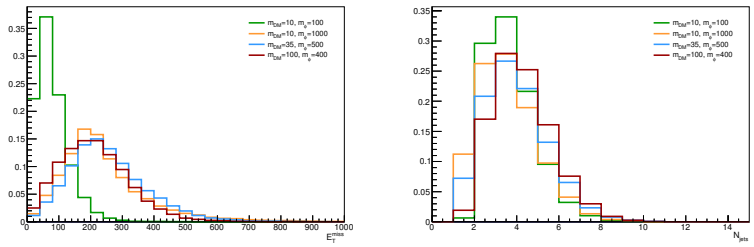

Figure 4.14: MET (left) and jet multiplicity (right) for various DM and mediator masses and couplings normalised to the relic density observed in the early universe.

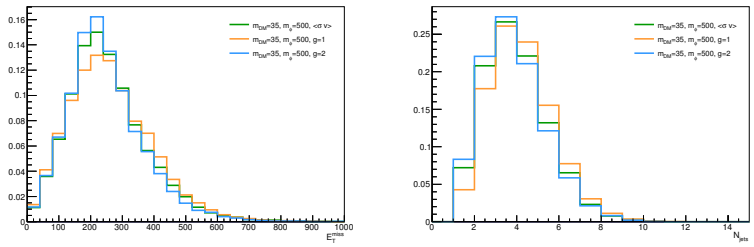

Figure 4.15: MET (left) and jet multiplicity (right) for $m_{\mathrm{DM}} = 35$ GeV and $m_{\Phi} = 500$ GeV for couplings corresponding to relic density weights and also $g = 1, 2$

- $m_{\Phi} > m_{DM} + m_b$ .

To do why this? May be trivial... (**??**)

-

Cross-sections for unity couplings can be found in Appendix C.2.

To do What about the coupling scan? (**??**)

## *4.6 Model implementation*

We simulate the model using the `MG5_aMC` v2.2.3. The corresponding card files can be found on the Forum SVN repository **??**.

To do (**??**)

A possible production configuration is:

```
set group\_subprocesses Auto\\
set ignore\_six\_quark\_processes False\\
set gauge unitary\\
set complex\_mass\_scheme False\\
import model DM\_Bflavored --modelname\\
define p = g u c d s u~ c~ d~ s~ b b~\\
define j = g u c d s u~ c~ d~ s~\\
define l+ = e+ mu+\\
define l- = e- mu-\\
define vl = ve vm vt\\
define vl~ = ve~ vm~ vt~\\
generate p p > n1 n1~ b b~\\
add process p p > n1 n1~ b\\
add process p p > n1 n1~ b~\\
\\
output bFDM\\
launch\\
set MX 200\\
set Mphix 1000\\
set gx 1\\
set maxjetflavor 5\\
set pdlabel cteq6l1\\
```

168;2015-05-14 17:58:52 +0200 (Thu, 14 May 2015);doglioni

```
set ebeam1 6500\\
set ebeam2 6500\\
set nevents 20000\\
set htjmin 180\\
set wphix auto\\
```

# 5
# Specific models for signatures with EW bosons

In this Section, we consider models with a photon, a W boson, a Z boson or a Higgs boson in the final state, accompanied by Dark Matter particles that either couple directly to the boson or are mediated by a new particle. The experimental signature is identified as *V+MET*.

These models are interesting both as some are demanded by gauge coupling relations in models where the gluon provides the experimentally detectable signature, and also as stand-alone models with final states that cannot be generated by the models in Section 3.

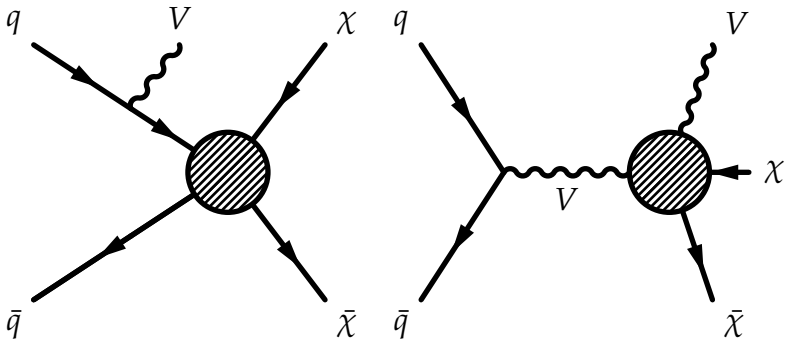


Figure 5.1: Sketch of benchmark models including a contact interaction for V+MET searches, adapted from [NCC+14].

The models considered can be divided into four categories:

*Models including a contact operator, where the boson is radiated from the initial state*
As depicted in the left diagram of Figure 5.1, these models follow the nomenclature and theory for the EFT benchmarks commonly used by MET+X searches [GIR+10]. These models have been used in past experimental searches [Kha14, Aad14b, K+14, Aad14b, A+14a, Aad14a], and they will not be described here.

*Simplified models with a boson radiated either from the initial state or from the mediator*
These models follow those already described in Section 3, replacing the gluon with a boson.

*Models including a contact operator, where the boson is directly coupled to DM*
Shown on the right-hand side of Figure 5.1, these models allow for a contact interaction vertex that directly couples the boson to Dark Matter.

*V-specific simplified models* These models postulate direct couplings of new mediators to bosons, e.g. they couple the Higgs boson to a new vector or to a new scalar [CDM+14, BLW14].

The following Sections describe the models within these categories, the parameters for each of the benchmark models chosen, the studies towards the choices of the parameters to be scanned, and finally point to the location of their Matrix Element implementation.

## 5.1 Simplified models with boson radiation

Monojet searches are generally more sensitive with respect to final states including bosons, due to the much larger rates of signal events featuring quark or gluon radiation with respect to radiation of bosons [ZBW13], in combination with the low branching ratios if leptons from boson decays are required in the final state. The rates for the Higgs boson radiation is too low for these models to be considered a viable benchmark [CDM+14]. However, the presence of photons, leptons from W and Z decays, and W or Z bosons decaying hadronically allow backgrounds to be rejected more effectively, making Z/gamma/W+MET searches still worth comparing with searches in the jet+MET final state.

### 5.1.1 Vector mediator exchanged in the s-channel

An example Feynman diagam for these processes can be constructed by taking Fig. 3.1 and replacing the gluon with $\gamma, W$ or $Z$. The interest for searches with W bosons in the final state has been elevated by the increased cross section for certain choices of couplings for a spin-1 mediator [BT13]. Run-1 searches have considered three sample cases for the product of up and down quark couplings to the mediator $\xi$:

- No couplings between mediator and either up or down quarks ($\xi = 0$);
- Same coupling between mediator and each of the quark types ($\xi = 1$);
- Coupling of opposite sign between mediator and each of the quark types ($\xi = -1$).

The $\xi = -1$ case leads to a large increase in the cross-section of the process, and modifies the spectrum of missing transverse energy or transverse mass used for the searches. The sensitivity of the W+MET search for this benchmark in this case surpasses that of the jet+MET search. However, as shown in Ref. [BCD+15], the cross-section increase is due to the production of longitudinally polarized W bosons, as a consequence of a violation of electroweak gauge symmetries. Unless further particles are introduced (in a

fashion similar to the Higgs boson in the Standard Model), choosing a value of $\xi = -1$ for this simplified model will lead to a manifest violation of unitarity at LHC energies. The simplified model with a vector mediator exchanged in the s-channel model can still be considered as a benchmark for searches with a W boson if $\xi = 1$. We leave the study of further models with cross-section enhancements due to different couplings to up and down quarks for studies beyond the early LHC searches covered in this document. An example of such model is the case of both DM and SM Higgs charged under a new U(1)', with a a small mass mixing between SM Z-boson and the new $Z'$. This leads to different effective DM couplings to $u_L$ and $d_L$, proportional to their coupling to the Z boson, detailed in Appendix B.

The scan in the parameters that characterize this simplified model for EW boson + MET searches follow what is already detailed in Section 3.

As in the case of the jet+MET models, the width does not have a significant impact on the kinematic distributions relevant for those searches. An example of the particle-level analysis acceptance using the generator-level cuts from Ref. [Aad15] for the photon+MET analysis, but raising the photon $p_T$ cut to 150 GeV is shown in Figure 5.2, comparing a width that is set to $\Gamma = M_{med}/3$ to the minimal width (the ratio between the two widths ranges from 1.05 to 1.5 with increasing mediator masses).

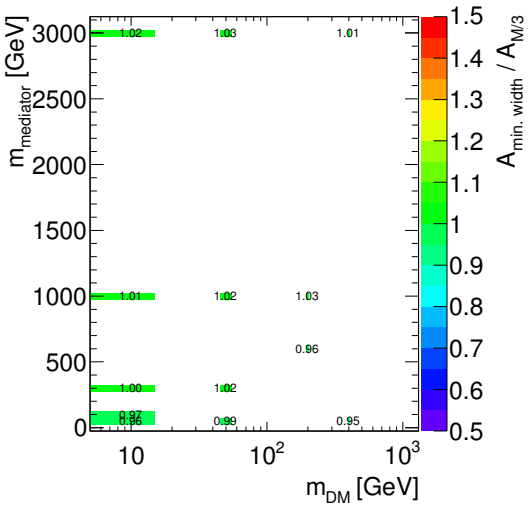


Figure 5.2: Analysis acceptance for the photon+MET analysis when varying the mediator width, in the case of a vector mediator exchanged in the $s-$channel

Examples of relevant kinematic distributions for selected benchmark points are shown in Fig. 5.3. leading-order cross-sections for the chosen benchmark points are shown in Appendix B.

### 5.1.2 *Colored scalar mediator exchanged in the t-channel*

The model parameters with emission of an EW boson generally follow those in Section 3, even though fewer diagrams are involved. A representative Feynman diagram can be constructed by replacing a gluon in Fig. 3.21 with a $\gamma, W, Z$ boson.

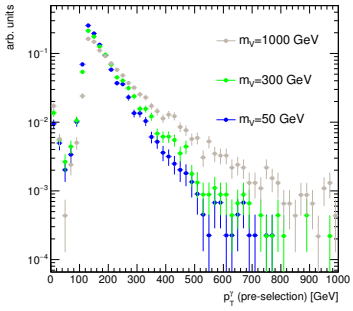


(a) Missing transverse momentum distribution for the photon+MET final state, for different mediator mass choices, for a DM mass of 10 GeV.

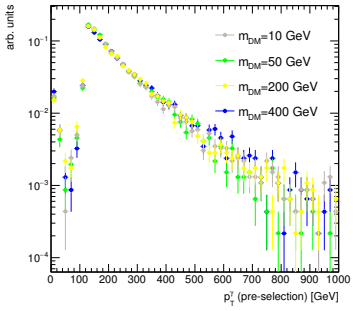


(b) Leading photon transverse momentum distribution for the photon+MET final state, for different DM mass choices, with a mediator mass of 1 TeV.

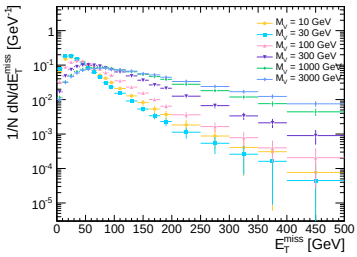


(c) Missing transverse momentum distribution for the leptonic Z+MET final state, for different mediator mass choices, for a DM mass of 15 GeV

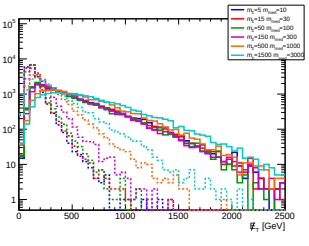

(d) Missing transverse momentum distribution for the hadronic W+MET final state.

Figure 5.3: Kinematic distributions relevant for searches with W, Z and photons in the final state, for the simplified model with a vector mediator exchanged in the $s-$channel.

Figure 5.4 shows the MET distribution for the hadronic Z+MET final state, with varying dark matter and mediator mass, before any selection. The acceptance for a series of simplified analysis cuts (MET>350 GeV, leading jet $p_T > 40$ GeV, minimum azimuthal angle between jet and MET > 0.4) applied at the generator level is shown in Figure 5.5. The parameter scan is still under discussion

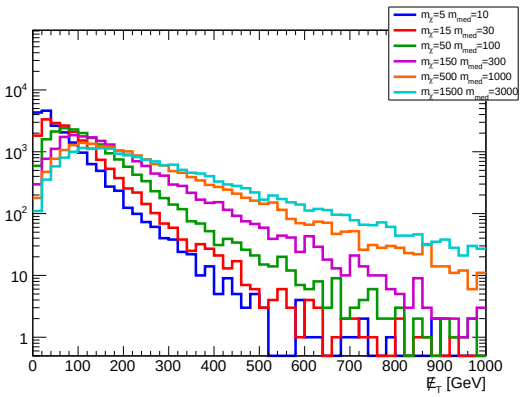


To do The parameter scan, and the conclusions that can be drawn from the plots below, need to be cross-checked with those in the monojet channel. (??)

Figure 5.4: Missing transverse momentum distribution for the hadronic Z+MET final state, for the simplified model with a colored scalar mediator exchanged in the $t-$channel.

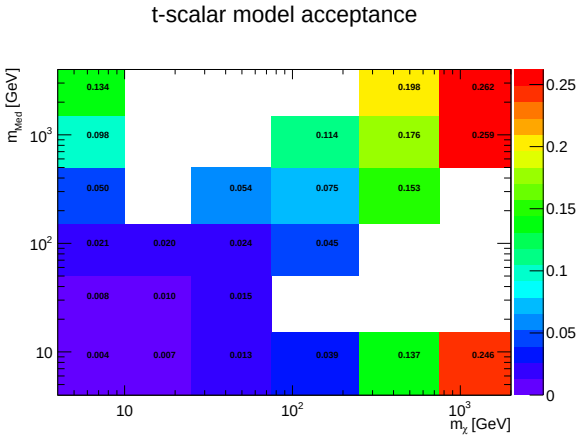


Figure 5.5: Acceptance table for the hadronic Z+MET final state, for the simplified model with a colored scalar mediator exchanged in the $t-$channel.

### 5.1.3 *Model implementation*

These models are generated at leading order with MadGraph 2.2.2, using Pythia8 for the parton shower. Parameter cards can be found on the Forum SVN repository [**?** ].

## 5.2 *EFT models with direct DM-boson couplings*

A complete list of effective operators with direct DM/boson couplings for Dirac DM, up to dimension 7, can be found in [CHLR13, CNS$^+$13, CHH15]. Higher dimensional operators, up to dimension 8, leading to Higgs+MET signatures, are mentioned in [CNS$^+$13, BLW14]. Despite the appearance of simplified models, we argue that the model independent approach of the EFTs is still relevant. Furthermore, not all EFT operators have a simplified model replacement.

### 5.2.1 *Dimension 5 operators*

The lowest dimension benchmark operators we may consider are effective dimension 5, such as the one depicted in Figure 5.6.

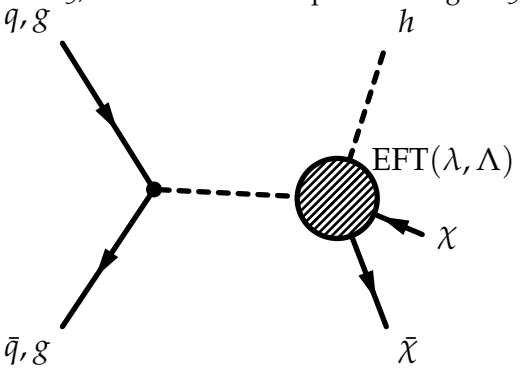


Figure 5.6: Diagram for EFT operators giving rise to a Higgs+MET signature.

Following the notation of [CNS$^+$13], models from this category have a Lagrangian that includes terms such as:

$$\frac{m_W^2}{\Lambda_5^3}\,\bar{\chi}\chi\,W^{+\mu}W_\mu^- + \frac{m_Z^2}{2\Lambda_5^3}\,\bar{\chi}\chi\,Z^\mu Z_\mu\,. \tag{5.1}$$

where $m_Z$ and $m_W$ are the masses of the $Z$ and $W$ boson, $W^\mu$ and $Z^\mu$ are the fields of the gauge bosons, $\chi$ denote the Dark Matter fields and $\Lambda_5$ is the effective field theory scale TodoNomenclature differs: $\Lambda_5$ vs $\lambda$. Note that these operators are of true dimension 7, but reduce to effective dimension 5 once Higgs vevs, contained in the W and Z mass terms, are inserted. As such, one expects these that operators would naturally arise in UV complete models where Dark Matter interacts via a Higgs portal where heavy mediators would couple to the Higgs or other fields in an extended Higgs sector. In such models the full theory may be expected to contain additional operators with Higgs-Dark Matter couplings.

Concentrating for the moment on mono-gauge boson signals, the above operator induces signatures with MET in conjunction with Z and W bosons at tree level, while at loop level it induces couplings to photon pairs and $Z\gamma$ through W loops. In these models, a clear relation exists between final states with photons, EW bosons and Higgs boson.

As shown in Fig. 5.7 kinematics of this model can be approximated by that of a simplified model including a high-mass scalar mediator exchanged in the s-channel. For this reason, the list of benchmark models with direct boson-DM couplings for photon, Z and W only includes dimension 7 operators: the scalar model with initial state radiation of an EW boson is already recommended and its results can be rescaled. The Higgs+MET analysis, however, will not consider the scalar simplified model as benchmark, due to the very low sensitivity in early LHC analyses, and will instead use this dimension 5 operator.

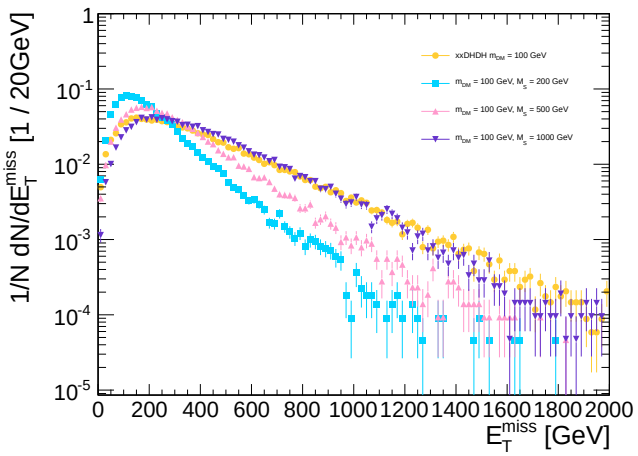


Figure 5.7: Comparison of the missing transverse momentum for the simplified model where a scalar mediator is exchanged in the s-channel and the model including a dimension-5 scalar contact operator, in the leptonic Z+MET final state

#### 5.2.1.1 *Parameter scan*

The two parameters of this model are the scale of new physics $\lambda$ and the DM particle mass. SM-DM coupling and new physics scale are related by $g_{\mathrm{DM}} = \frac{(246GeV)}{\lambda}$.

The initial value of the new physics scale $\lambda$ chosen for the sample generation is 3 TeV; this does not affect the signal kinematics,

To do Clarify the reason why this happens in Madgraph through explicit Lagrangian terms? (**??**)

and the cross-section of the samples can be rescaled according to the $\lambda^3$ dependence when deriving the constraints on this scale.

The DM mass values for the benchmark points to be simulated are chosen to span a sufficient Dark Matter range leading to different kinematics, that is within the LHC sensitivity for early searches and that is consistent across the various signatures and EFT operators. We therefore start the mass scan at $m_{\mathrm{DM}}$ =1 GeV, where collider experiments are complementary to direct and indirect detection and choose the last point corresponding to a DM mass of 1 TeV. We recommend a scan in seven mass points, namely:

$$m_{\mathrm{DM}} = 1, 10, 50, 100, 200, 400, 800, 1300 GeV.$$

A set of kinematic distributions from the Higgs+MET signature where the Higgs decays into two $b-$quarks is shown in Fig. 5.2, for points similar to those of the grid scan proposed.

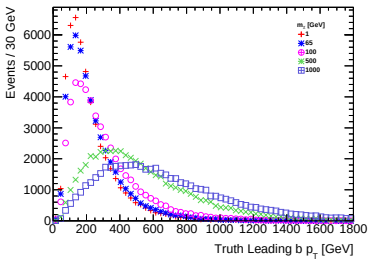


(a) Leading $b-$jet transverse momentum

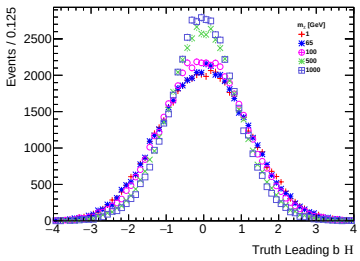


(b) Leading $b-$jet pseudorapidity

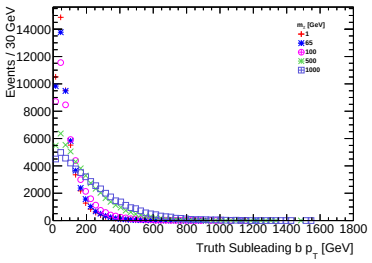


(c) Leading $b-$jet transverse momentum

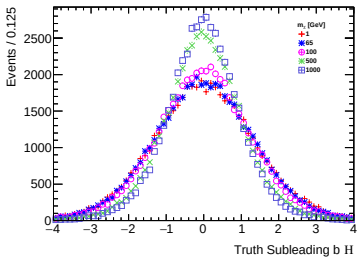


(d) Leading $b-$jet pseudorapidity

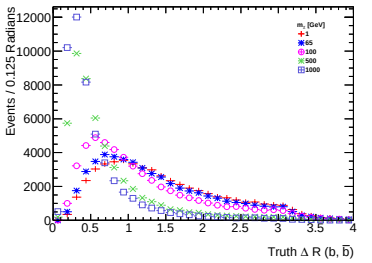


(e) Angular distance between the two leading $b-$jets

Figure 5.8: Comparison of the kinematic distributions for the two leading $b-$ jets (from the Higgs decay) in the model with direct interactions between the Higgs boson and the DM particle, when varying the DM mass.

### 5.2.2 *Dimension 7 operators*

The dimension-7 benchmark models contain the $SU(2)_L \times U(1)_Y$ gauge-invariant couplings between DM fields and the kinetic terms

of the EW bosons. The CP-conserving scalar couplings of this type can be written as

$$\frac{c_1}{\Lambda_S^3}\,\bar{\chi}\chi\,B_{\mu\nu}B^{\mu\nu} + \frac{c_2}{\Lambda_S^3}\,\bar{\chi}\chi\,W^i_{\mu\nu}W^{i,\mu\nu}\,. \tag{5.2}$$

Here $B_{\mu\nu} = \partial_\mu B_\nu - \partial_\nu B_\mu$ and $W^i_{\mu\nu} = \partial_\mu W^i_\nu - \partial_\nu W^i_\mu + g_2\epsilon^{ijk}W^j_\mu W^k_\mu$ are the $U(1)_Y$ and $SU(2)_L$ field strength tensor, respectively, and $g_2$ denotes the weak coupling constant. In the case of the pseudoscalar couplings, one has instead

$$\frac{c_1}{\Lambda_P^3}\,\bar{\chi}\gamma_5\chi\,B_{\mu\nu}\tilde{B}^{\mu\nu} + \frac{c_2}{\Lambda_P^3}\,\bar{\chi}\gamma_5\chi\,W^i_{\mu\nu}\tilde{W}^{i,\mu\nu}\,, \tag{5.3}$$

where $\tilde{B}_{\mu\nu} = 1/2\,\epsilon_{\mu\nu\lambda\rho}B^{\lambda\rho}$ and $\tilde{W}^i_{\mu\nu} = 1/2\,\epsilon_{\mu\nu\lambda\rho}W^{i,\lambda\rho}$ are the dual field strength tensors. In addition to the CP-conserving interactions (5.2) and (5.3), there are also four CP-violating couplings that are obtained from the above operators by the replacement $\bar{\chi}\chi \leftrightarrow \bar{\chi}\gamma_5\chi$.

The effective interactions introduced in (5.2) and (5.3) appear in models of Rayleigh DM [**?** ]. Ultraviolet completions where the operators are generated through loops of states charged under $U(1)_Y$ and/or $SU(2)_L$ have been proposed in [**?** ] and their LHC signatures have been studied in [**?** ]. If these new charged particles are light, the high-$p_T$ gauge bosons that participate in the MET processes considered here are able to resolve the substructure of the loops. This generically suppresses the cross sections compared to the EFT predictions [HKU13], and thus will weaken the bounds on the interaction strengths of DM and the EW gauge bosons to some extent. Furthermore, the light charged mediators may be produced on-shell in $pp$ collisions, rendering direct LHC searches potentially more restrictive than MET searches. Making the above statements precise would require further studies beyond the timescale of this forum.

Since for $\Lambda_S = \Lambda_P$ the effective interactions (5.2) and (5.3) predict essentially the same value of the mono-photon, mono-$Z$ and mono-$W$ cross section [CNS$^+$13, CHH15], we consider below only the former couplings. We emphasise however that measurements of the jet-jet azimuthal angle difference in MET+$2j$ events may be used to disentangle whether DM couples more strongly to the combination $B_{\mu\nu}B^{\mu\nu}$ ($W^i_{\mu\nu}W^{i,\mu\nu}$) or the product $B_{\mu\nu}\tilde{B}^{\mu\nu}$ ($W^i_{\mu\nu}\tilde{W}^{i,\mu\nu}$) of field strength tensors [CHLR13, CHH15].

After EW symmetry breaking the interactions (5.2) induce direct couplings between pairs of DM particles and gauge bosons. The corresponding Feynman rule reads

$$\frac{4i}{\Lambda_S^3}\,g_{V_1V_2}\left(p_1^{\mu_2}p_2^{\mu_1} - g^{\mu_1\mu_2}\,p_1\cdot p_2\right), \tag{5.4}$$

where $p_i$ ($\mu_i$) denotes the momentum (Lorentz index) of the vector field $V_i$ and for simplicity the spinors associated with the DM fields

have been dropped. The couplings $g_{V_iV_j}$ take the form

$$\begin{aligned} g_{\gamma\gamma} &= c_w^2 c_1 + s_w^2 c_2 \,, \\ g_{\gamma Z} &= -s_w c_w \left(c_1 - c_2\right) \,, \\ g_{ZZ} &= s_w^2 c_1 + c_w^2 c_2 \,, \\ g_{WW} &= c_2 \,, \end{aligned} \tag{5.5}$$

with $s_w$ ($c_w$) the sine (cosine) of the weak mixing angle. Note that our coefficients $c_1$ and $c_2$ are identical to the coefficients $C_B$ and $C_W$ used in [CHH15], while they are related via $k_1 = \frac{1}{{c_w}^2} c_1$ and $k_2 = \frac{1}{{s_w}^2} c_2$ to the coefficients $k_1$ and $k_2$ introduced in [CNS+13].

The coefficients $c_1$ and $c_2$ appearing in (5.5) determine the relative importance of each of the MET channels and their correlations. For example, one observes that:

- Only $c_2$ enters the coupling between DM and $W$ bosons, meaning that only models with $c_2 \neq 0$ predict a mono-$W$ signal;
- If $c_1 = c_2$ the mono-photon (mono-$Z$) signal does not receive contributions from diagrams involving $Z$ (photon) exchange;
- Since numerically $c_w^2/s_w^2 \simeq 3.3$ the mono-photon channel is particularly sensitive to $c_1$.

#### 5.2.2.1 *Parameter scan*

As stated above and shown in Ref. [NCC+14], the kinematic distributions for dimension-7 scalar and pseudoscalar operators only shows small differences. This has been verified from a generator-level study: the signal acceptance after a simplified analysis selection (MET>350 GeV, leading jet $p_T > 40$ GeV, minimum azimuthal difference between either of the two jets and the MET direction $>$ 0.4) is roughly 70% for both. We therefore only suggest to generate one of the two models. TodoWhen we have the cross-sections for both, we can recommend the one with the highest cross-section.

The differences in kinematics for the various signatures are negligible when changing the coefficients $k_1$ and $k_2$, as shown in Figure **??**. Only the case $k_1 = k_2 = 1$ is generated as benchmark; other cases are left for reinterpretation as they will only need a rescaling of the cross-sections shown in Appendix B for the various DM mass points considered.

### 5.2.3 *Higher dimensional operators*

Many higher dimensional operators can induce signals of photons or $W/Z/H$ bosons in the final state. A complete list can be found in Refs. **??** and references therein.

Although with lower priority with respect to the operators above, a representative dimension-8 operators can be chosen as benchmark, with the form:

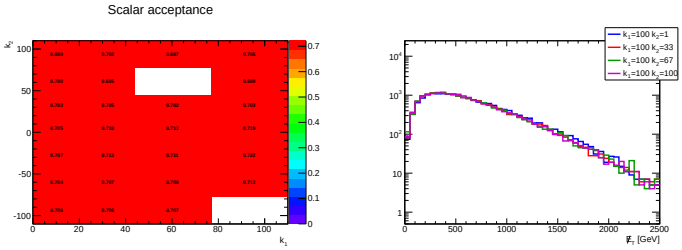


(a) Missing transverse momentum distribution.

(b) Acceptance.

Figure 5.9: MET distribution and acceptance for the dimension-7 model with a hadronically decaying Z in the final state, for the scalar and pseudoscalar operators representing direct interactions between DM and bosons.

$$\frac{1}{\Lambda^4}\bar{\chi}\gamma^\mu\chi B_{\mu\nu}H^\dagger D^\nu H$$

In this case, the new physics scale is $\Lambda$ is connected with the coupling of the DM as $y_\chi = \frac{1}{\Lambda^4}$.TodoIs more detail needed here? An advantage of this operator is that it includes all signatures with EW bosons, allowing to assess the relative sensitivity of the various channels with the same model. The kinematics for this operator is different with respect to other operators, leading to a harder MET spectrum, as illustrated by comparing the leading $b-$jet distribution for the dimension 5 operator to the dimension 8 operator.

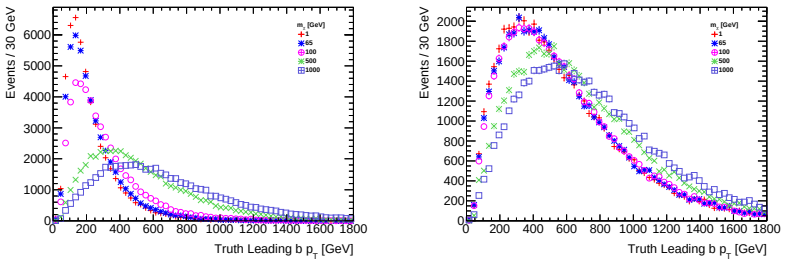


(a) Leading $b-$jet transverse momentum

(b) Leading $b-$jet transverse momentum

Figure 5.10: Comparison of the transverse momentum for the leading $b-$ jet from the Higgs decay for a dimension 5 and dimension 7 operator with direct boson-DM couplings.

### 5.2.4 *Validity of EW contact operators and possible completions*

It is important to remember that the operators described in this section may present problems in terms of the validity of the contact interaction approach for the energy scales reached at the LHC.

As outlined in [BLW14], designing very high MET search signal regions that are exclusively motivated by the hard MET spectra of the dimension 7 and 8 operators will mean that the momentum transfer in the selected events is larger. This in turn means that processes at that energy scale (mediators, particles exchanged in loops) are accessible, and a simple contact interaction will not be able to correctly describe the kinematics of these signals.

Contact interaction operators like the ones in this section remain useful tools for comparison of the sensitivity of different search channels, and for reinterpretation of other models under the correct assumptions. To date, there are no UV-complete models available for most of those operators: the dimension-7 operators are particularly challenging since their completion involves loops. However,

this may be the focus of future theoretical exploration: an example of a complete model for scalar DM corresponding to the dimension-5 operator is provided in the Appendix B. Providing results for the pure EFT limit of these models will prove useful to cross-check the implementation of future.

Given these considerations, the recommendations on the presentation of the results for these models are:

- Assess the percentage of events that pass the EFT validity condition, and present results using a truncation of the invalid events using the procedure in Section 6 alongside pure EFT results;
- Deliver fiducial limits on the cross section of any new physics events, without any model assumption, according to the guidelines in Appendix **??**.

### 5.2.5 *Model implementation*

These models are generated at leading order with MadGraph 2.2.2, using Pythia8 for the parton shower. Parameter cards can be found on the Forum SVN repository: [For15b] for dimension 5 operators and [For15b] for dimension 7.

## 5.3 *Specific simplified models including EW bosons, tailored to Higgs+MET searches*

Three benchmark simplified models [CDM+14, BLW14] are recommended for Higgs+MET searches:

- A model where a leptophobic vector mediator ($Z'_B$) is exchanged in the $s-$channel, radiates a Higgs boson and decays into two DM particles (Fig. 5.11 (a));
- A model where a scalar mediator $S$ couples to the SM only through the SM Higgs and decays to two DM particles (Fig. 5.12);
- A model where a vector $Z'$ is produced resonantly and decays into a Higgs boson plus an intermediate heavy pseudoscalar particle $A^0$, in turn decaying into two DM particles (Fig. 5.11 (b)).

To do AB: remove the extra Z in the diagram for the Mono-HZprimeqq (??)

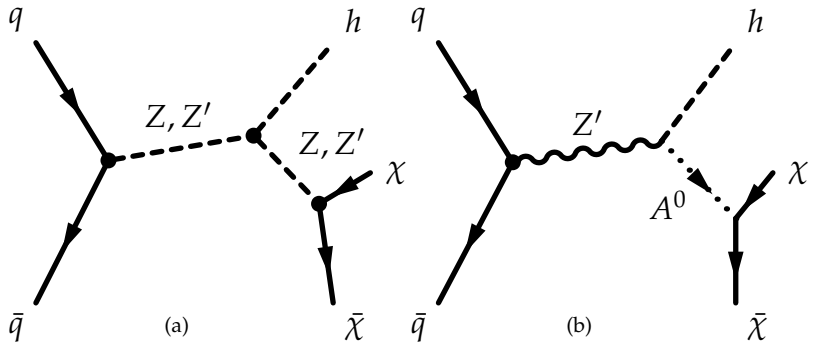


Figure 5.11: Feynman diagrams of leading order processes leading to Higgs+MET events: a model with a vector mediator ($Z'$) coupling with DM and with the Higgs boson $h$ **??**, and a 2HDM model with a new invisibly decaying pseudoscalar $A^0$ from the decay of an on-shell resonance $Z'$ giving rise to a Higgs+MET signature **??**.

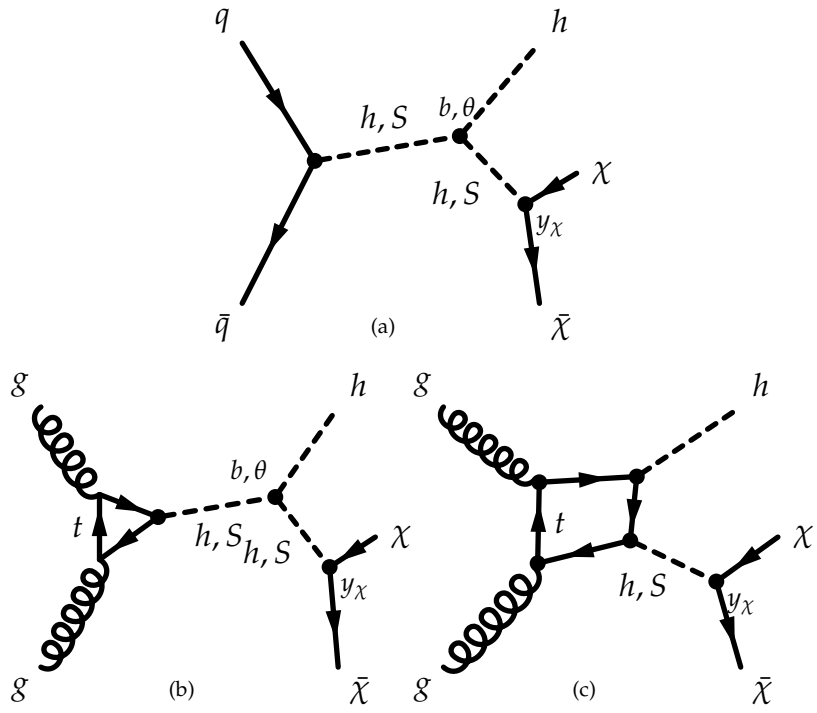


Figure 5.12: Feynman diagrams of leading order processes leading to Higgs+MET events for a model with a scalar mediator ($S$) coupling with DM and with the Higgs boson $h$.

These models are kinematically distinct from one another, as shown in the comparison of the MET spectra in Fig. 5.13 for high and low mediator masses. Figure 5.13 (a) shows the MET distribution for models with high mediator masses ($m_S = 1$ TeV, $m_{Z'} = 1$ TeV, $m_{A^0} = 1$ TeV) and DM mass of either 50 ($Z'_B$ and $A^0$ models) or 65 GeV (scalar mediator model). Figure 5.13 (b) shows the MET distribution for models with low mediator masses ($m_{Z'_B} = 100$ GeV, $m_{Z'} = 1$ TeV, $m_{A^0} = 100$ GeV) and DM mass of 1 TeV for all models.

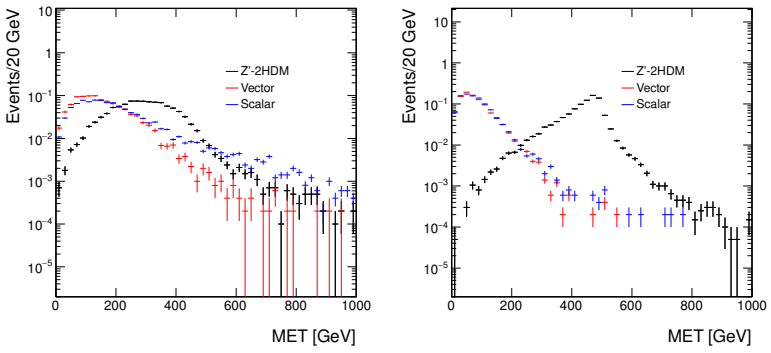


(a) High mediator mass

(b) Low mediator mass

Figure 5.13: Comparison of the missing transverse momentum distributions at generator level in different simplified models leading to a Higgs+MET signature. The model parameter settings are detailed in the text.

### 5.3.1 *MET+Higgs from a baryonic $Z'$*

The model shown in Fig. 5.11 (a) postulates a new gauge boson $Z'$ corresponding to a new $U(1)_B$ baryon number symmetry. The stable baryonic states included in this model are the DM candidate particles. The mass of the $Z'$ boson is acquired through a baryonic Higgs $h_B$, which mixes with the SM Higgs boson. The interactions between the $Z'$, the quarks and the DM are described by the follow-

ing Lagrangian:

$$L = g_q \bar{q} \gamma^\mu q Z'_\mu + g_\chi \bar{\chi} \gamma^\mu \chi Z'_\mu. \tag{5.6}$$

The quark couplings $g_q$ are fixed to be equal to one third of the gauge coupling $g_B$, while the DM coupling to the $Z'$ are proportional to the baryon number and to the gauge coupling ($g_\chi = B g_B$). No leptonic couplings of the $Z'$ are allowed, thus evading dilepton constraints. After incorporating the mixing of the baryonic and SM Higgs bosons, this model is is described by the following Lagrangian term at energies below $m_{Z'}$:

$$L_{\text{eff}} = -\frac{g_q g_\chi}{m^2_{Z'}} \bar{q} \gamma^\mu q \bar{\chi} \gamma_\mu \chi \left(1 + \frac{g_{hZ'Z'}}{m^2_{Z'}} h\right), \tag{5.7}$$

The first term of this equation gives rise to a term that is equivalent to the radiation of a jet (or another EW gauge boson) in the initial state. The second term describes the interaction between the $Z'$ and the SM Higgs boson, via the coupling $g_{hZ'Z'} = \frac{m_{Z'} 2 sin\theta}{v_B}$, where $sin\theta$ is the mixing angle between the SM Higgs and the baryonic Higgs $h_B$, and $v_B$ is the Baryonic Higgs vev.

#### 5.3.1.1 *Parameter scan*

The model is described by six parameters:

1. the mediator mass $m_{\text{med}}$, (also referred to as $m_{Z'}$)
2. mass of dark matter, $m_{DM}$
3. coupling of $Z'$ mediator to dark matter, $g_{\text{DM}}$
4. coupling of the mediator to quarks, $g_q$
5. mixing angle between baryonic Higgs $h_B$ and the SM-like Higgs boson, $\sin\theta$
6. coupling of the mediator to SM-like Higgs boson, $g_{hZ'Z'}$

The width of the $Z'$ mediator is calculated using all possible decays to SM particles (quarks) and to pairs of DM particles if kinematically allowed.

The dependence of the missing transverse momentum (MET) on the model parameters is studied by varying the parameters one at a time. The variation of parameters other than $m_{med}$ and $m_{DM}$ does not result in significant variations of the MET spectrum, as shown in Figures 5.14. Figure 5.15 shows that for an on-shell mediator, varying $m_{DM}$ with the other parameters fixed does not affect the MET distribution, while the distribution broadens significantly in the case of an off-shell mediator. For this reason, the same grid in $m_{\text{med}}$, $m_{\text{DM}}$ as for the vector mediator of the jet+MET search (Table **??**) is chosen as a starting point. The coupling $g_{hZ'Z'}$, along with $g_q$ and $g_{DM}$, are subject to perturbativity bounds:

$$g_q, g_\chi < 4\pi$$

and

$$g_{hZ'Z'} < \sqrt{4\pi} m_{Z'} \sin\theta$$

The value $g_{hZ'Z'}/m_{Z'} = 1.0$ is chosen as a benchmark value for the generation of Monte Carlo samples since it maximizes the cross section (as shown in the following paragraph) without violating the bounds. The mediator-DM coupling $g_{\mathrm{DM}}$ is fixed to 1, and the mediator-quark $g_q$ coupling is fixed to $1/3$. The kinematic distributions do not change as a function of these parameters, so results for other values of $g_{hZ'Z'}/m_{Z'}$, $g_{\mathrm{DM}}$ and $g_q$ can be obtained through rescaling by the appropriate cross sections.

Figs 5.16 and 5.17 show the kinematic distributions for the two leading jets in the $H \to \bar{b}b$ decay channel, for two values of the mediator mass and varying the DM mass.

Analyses should perform further studies, beyond those studies performed for the forum, to estimate the reach of the analysis with respect to all points in the grid and therefore decide on a smaller set of grid points to be generated.

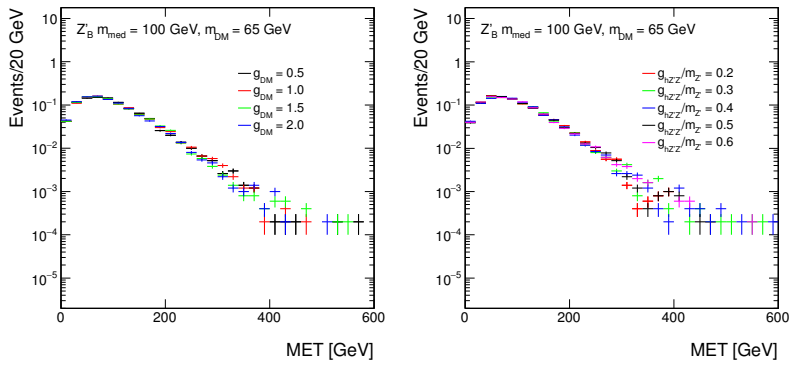


Figure 5.14: Missing transverse momentum distributions at generator level in the vector mediator scenario for different values of: the mediator-dark matter coupling $g_{\mathrm{DM}}$ (left), and the coupling between the mediator and the SM-like Higgs boson, scaled by the mediator mass, $g_{hZ'Z'}/m_{Z'}$ (right).

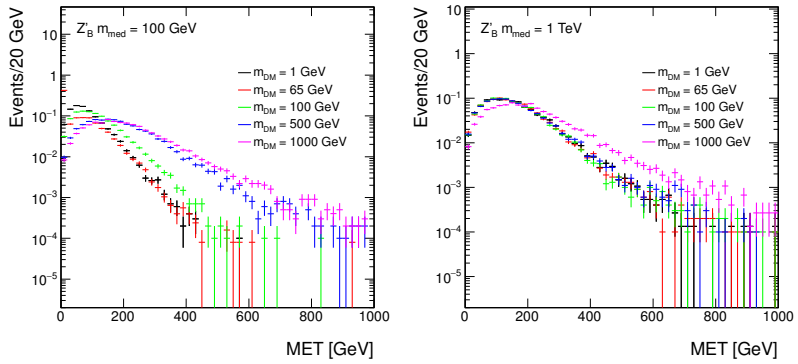


Figure 5.15: Missing transverse momentum distributions at generator level in the vector mediator scenario: for different values of the dark matter mass $m_{DM}$ and a mediator mass of $m_{\mathrm{med}}$ = 100 GeV (left) and $m_{\mathrm{med}}$ = 1 TeV (right).

### 5.3.1.2 *Cross-section scaling*

The dependence of the cross section of the $pp \to H\chi\bar{\chi} + X$ process on $g_{hZ'Z'}$ is shown in Figure 5.18. The curves have been fit to second-order polynomials. For $m_{med} = 100$ GeV, the fit function is

$$y = -0.12 - 3.4 \times 10^{-3} x + 2.7 \times 10^{-4} x^2$$

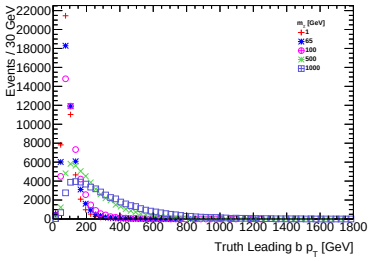


(a) Leading $b-$jet transverse momentum

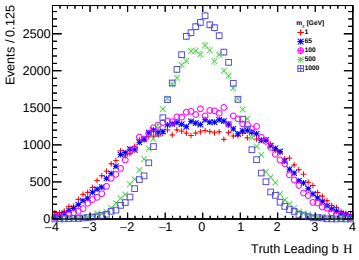


(b) Leading $b-$jet pseudorapidity

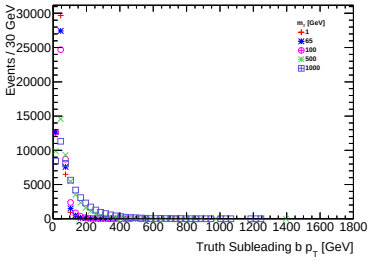


(c) Leading $b-$jet transverse momentum

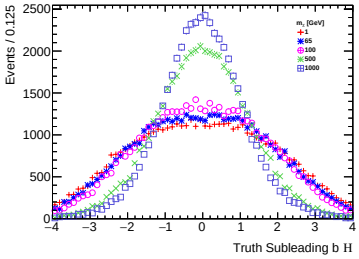


(d) Leading $b-$jet pseudorapidity

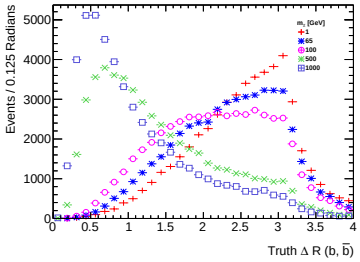


(e) Angular distance between the two leading $b-$jets

Figure 5.16: Comparison of the kinematic distributions for the two leading $b-$ jets ()from the Higgs decay) in the vector $Z'$ simplified model, when fixing the $Z'$ mass to 100 GeV and varying the DM mass.

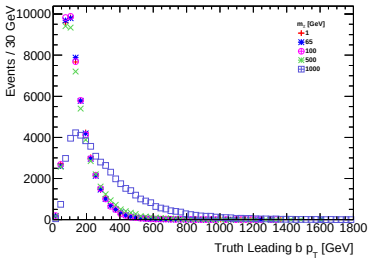


(a) Leading $b-$jet transverse momentum

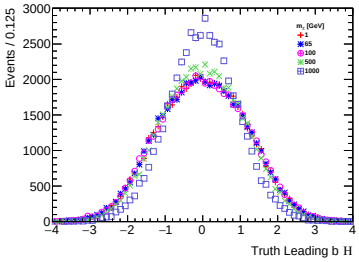


(b) Leading $b-$jet pseudorapidity

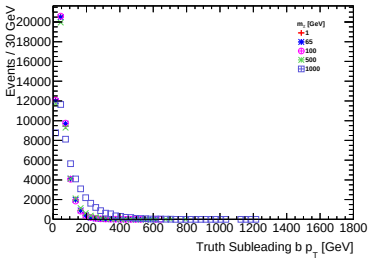


(c) Leading $b-$jet transverse momentum

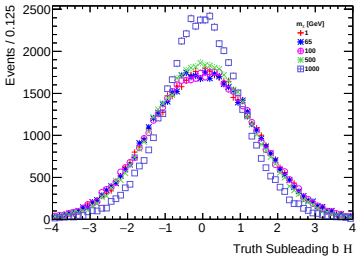


(d) Leading $b-$jet pseudorapidity

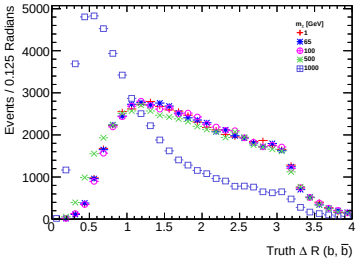


(e) Angular separation of the two leading $b$-jets

Figure 5.17: Comparison of the kinematic distributions for the two leading jets from the Higgs decay in the vector $Z'$ simplified model, when fixing the $Z'$ mass to 1000 GeV and varying the DM mass.

. For $m_{med} = 1$ TeV, the fit function is is

$$y = 0.0012 - 2.4 \times 10^{-7} x + 1.5 \times 10^{-7} x^2$$

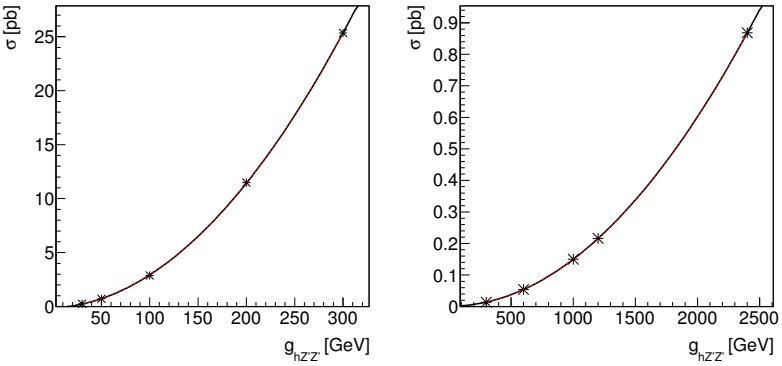


Figure 5.18: Cross section of the $pp \to H\chi\bar{\chi}$ process as a function of $g_{hZ'Z'}$ for $m_{Z'} = 100$ GeV (left) and $m_{Z'} = 1$ TeV (right). The fit functions are shown in the text.

### 5.3.2 *MET+Higgs from a scalar mediator*

A real scalar singlet $S$ coupling to DM can be introduced as a portal between SM and the dark sector through the Higgs field. The new scalar mixes with the SM Higgs boson, and couples to DM through a Yukawa term $y_\chi$. The relevant terms in the scalar potential are

$$\begin{aligned} V &\supset a|H|^2 S + b|H|^2 S^2 + \lambda_h |H|^4 \\ &\longrightarrow \tfrac{1}{2} a(h+v)^2 S + \tfrac{1}{2} b(h+v)^2 S^2 + \frac{\lambda_h}{4}(h+v)^4, \end{aligned} \tag{5.8}$$

where $a, b$ are new physics couplings and $\lambda_h$ is the Higgs quartic.

The additional Lagrangian terms for this model are:

$$L \supset -y_\chi \bar{\chi}\chi(cos\theta\, S - sin\theta\, h) - \frac{m_q}{v}\bar{q}q(cos\theta\, h + sin\theta\, S) \tag{5.9}$$

where $\theta$ is the mixing angle between the Higgs boson and the new scalar.

Mono-Higgs signals in this second model arise through processes shown in Fig. 5.12 (a,b), or through the radiation of a Higgs boson from the $t$ quark in the production loop, in Fig. 5.12 (c). The first two processes depend on the $h^2 S$ and $h S^2$ cubic terms in Eq. (5.8). At leading order in $\sin\theta$, these terms are

$$V_{\text{cubic}} \approx \frac{\sin\theta}{v}(2m_h^2 + m_S^2) h^2 S + b\, v\, h\, S^2 + ... \tag{5.10}$$

with $a$ and $\lambda_h$ expressed in terms of $\sin\theta$ and $m_h^2$, respectively. At leading order of $\sin\theta$, the $h^2 S$ term is fixed once the mass eigenvalues $m_h, m_S$ and mixing angle are specified. The $h\, S^2$ term is not fixed and remains a free parameter of the model, depending on the new physics coupling $b$.

#### 5.3.2.1 *Parameter scan*

The model is described by five parameters:

1. the Yukawa coupling of heavy scalar to dark matter, $g_{DM}$ (also referred to as $y_\chi$)
2. the mixing angle between heavy scalar and SM-like Higgs boson, $\sin\theta$;
3. the new physics coupling, $b$;
4. mass of heavy scalar, $m_S$, also termed $m_{\text{med}}$;
5. mass of dark matter, $m_{DM}$;

The mixing angle is constrained from current Higgs data to satisfy $\cos\theta = 1$ within 10% and therefore $\sin\theta \lesssim 0.4$. This provides a starting point for the parameter scan in this model: we recommend to set $\sin\theta = 0.3$. Figure 5.20 shows that there is no dependence of the kinematics from the value of this angle, and different values

can be obtained via rescaling the results for this mixing angle according to the relevant cross-section. It can also be observed from Figures 5.21 and 5.19 that the kinematics of this model follows that of the equivalent jet+MET model: only small changes are observed in the on-shell region, while the relevant distributions diverge when the mediator is off-shell. For this reason, the same grid in $m_{\text{med}}$, $m_{\text{DM}}$ as for the scalar mediator of the jet+MET search (Table **??**) is chosen as a starting point. The Yukawa coupling to DM $y_{DM}$ is set to 1, the new physics coupling between scalar and SM Higgs $b$ = 3. Results for other values can be obtained via a rescaling of the results for these parameters. More detailed studies are required to estimate the reach of the analysis with respect to all points in the grid and therefore decide on a smaller set of grid points to be generated; those are left to the individual analyses. **[TODO: can we get sensitivity to all the points for all signatures?]**

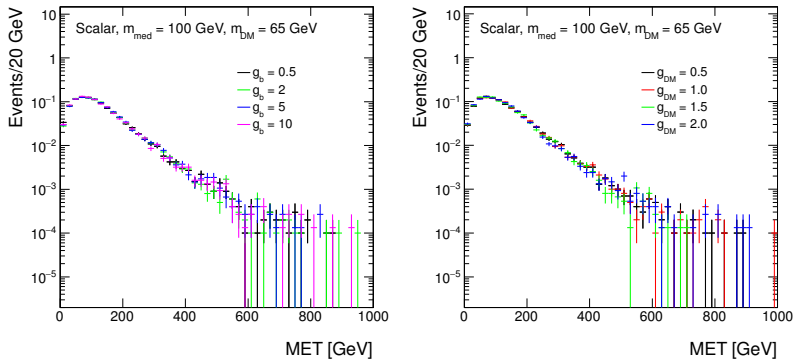


Figure 5.19: Missing transverse momentum distributions at generator level in the scalar mediator scenario, for different values of: the new physics coupling $g_b$ (left), and the mediator-dark matter coupling $g_{DM}$ (right).

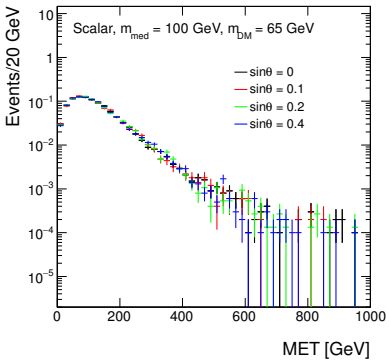


Figure 5.20: Missing transverse momentum distributions at generator level in the scalar mediator scenario: for different values of the mixing angle $\sin\theta$.

Figs. 5.22 and 5.23 show the kinematic distributions for the two leading jets in the $H \to \bar{b}b$ decay channel, for two values of the mediator mass and varying the DM mass.

### 5.3.3 *Higgs+MET signal from 2HDM model with a $Z'$ and a new pseudoscalar*

In this simplified model [BLW14], a new $Z'$ resonance decays to a Higgs boson $h$ plus a heavy pseudoscalar state $A^0$ in the 2HDM

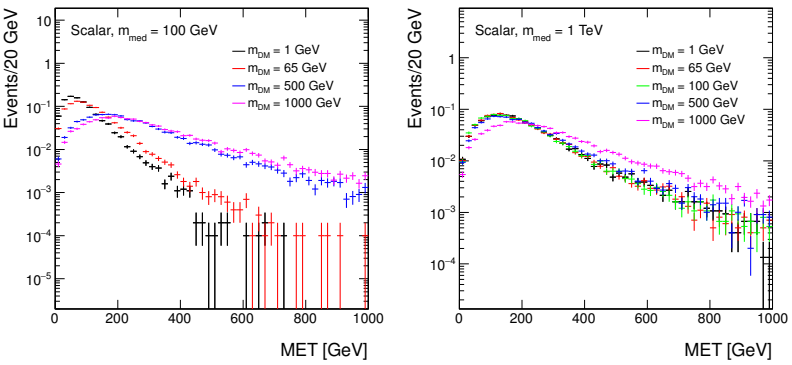


Figure 5.21: Missing transverse momentum distributions at generator level in the scalar mediator scenario: for different values of the dark matter mass $m_{DM}$ and a mediator mass of $m_{med}$ = 100 GeV (left) and $m_{med}$ = 1 TeV (right).

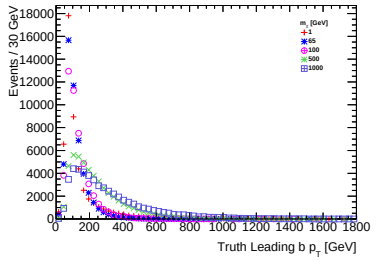


(a) Leading $b-$jet transverse momentum

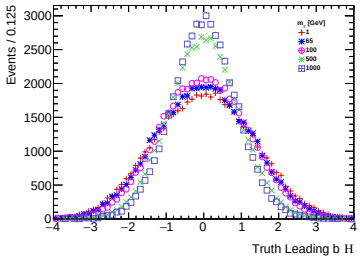


(b) Leading $b-$jet pseudorapidity

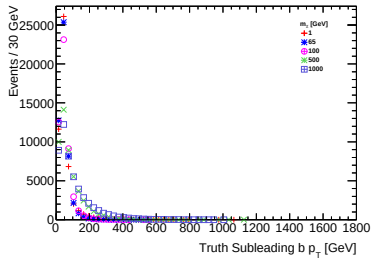


(c) Leading $b-$jet transverse momentum

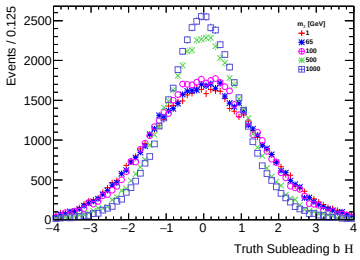


(d) Leading $b-$jet pseudorapidity

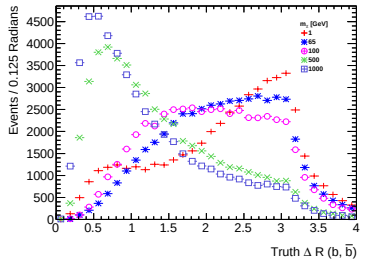


(e) Angular distance between the two leading $b-$jets

Figure 5.22: Comparison of the kinematic distributions for the two leading jets from the Higgs decay in the scalar simplified model, when fixing the new scalar mass to 100 GeV and varying the DM mass.

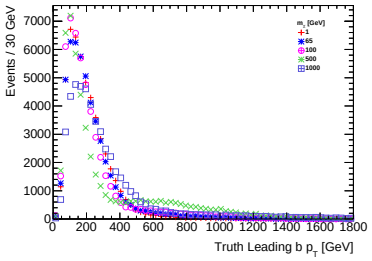


(a) Leading $b-$jet transverse momentum

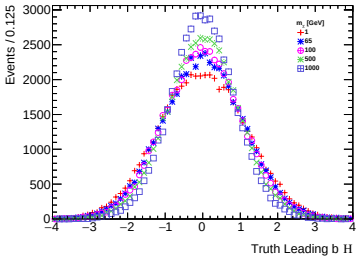


(b) Leading $b-$jet pseudorapidity

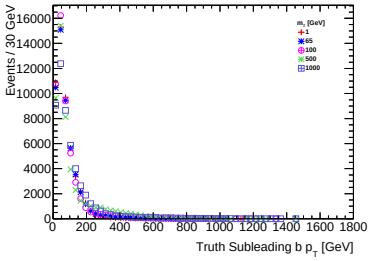


(c) Leading $b-$jet transverse momentum

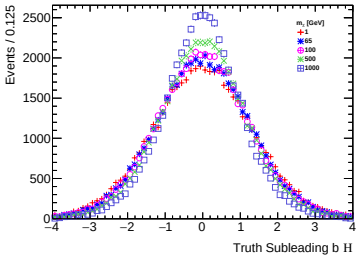


(d) Leading $b-$jet pseudorapidity

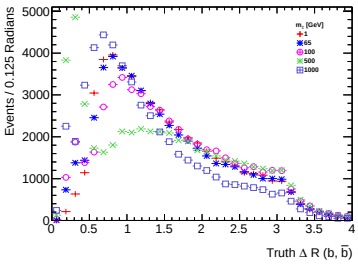


(e) Angular distance between the two leading $b-$jets

Figure 5.23: Comparison of the kinematic distributions for the two leading jets from the Higgs decay in the scalar simplified model, when fixing the new scalar mass to 1000 GeV and varying the DM mass.

framework, which in turn decays to a DM pair. This model is represented in the diagram in Fig. 5.11 (b).

The motivation for coupling the dark matter to the pseudoscalar is that dark matter coupling to a Higgs or $Z'$ boson is generically constrained by other signal channels and direct detection. An advantage of including this model is that it has different kinematics due to the on-shell $Z'$ production, where for heavy $Z'$ masses the MET and pT spectra are much harder. This model can satisfy electroweak precision tests and constraints from dijet resonance searches, and still give a potentially observable Higgs+MET signal.

This model comprises two doublets, where $\Phi_u$ couples to up-type quarks and $\Phi_d$ couples to down-type quarks and leptons:

$$-\mathcal{L} \supset y_u Q \tilde{\Phi}_u \bar{u} + y_d Q \Phi_d \bar{d} + y_e L \Phi_d \bar{e} + \text{h.c.} \tag{5.11}$$

After electroweak symmetry breaking, the Higgs doublets attain vevs $v_u$ and $v_d$, and in unitary gauge the doublets are parametrized as

$$\Phi_d = \frac{1}{\sqrt{2}} \begin{pmatrix} -\sin\beta\ H^+ \\ v_d - \sin\alpha\ h + \cos\alpha\ H - i\sin\beta\ A^0 \end{pmatrix} \quad ,$$
$$\Phi_u = \frac{1}{\sqrt{2}} \begin{pmatrix} \cos\beta\ H^+ \\ v_u + \cos\alpha\ h + \sin\alpha\ H + i\cos\beta\ A^0 \end{pmatrix} \tag{5.12}$$

where $h, H$ are neutral CP-even scalars and $A^0$ is a neutral CP-odd scalar. In this framework, $\tan\beta \equiv v_u/v_d$, and $\alpha$ is the mixing angle that diagonalizes the $h - H$ mass squared matrix. We take $\alpha = \beta - \pi/2$, in the limit where $h$ has SM-like couplings to fermions and gauge bosons as per Ref. [**?** ], and $\tan\beta \geq 0.3$ as implied from the perturbativity of the top Yukawa coupling. The Higgs vevs lead to $Z - Z'$ mass mixing, with a mixing parameter given by

$$\begin{aligned} \epsilon &\equiv \frac{1}{M_{Z'}^2 - M_Z^2} \frac{g g_z}{2\cos\theta_w} (z_d v_d^2 + z_u v_u^2) \\ &= \frac{(M_Z^0)^2}{M_{Z'}^2 - M_Z^2} \frac{2 g_z \cos\theta_w}{g} z_u \sin^2\beta. \end{aligned} \tag{5.13}$$

The production cross section for this model scales as $(g_z)^2$, as the decay width for this process to leading order in $\epsilon$ (Eq. 5.13) is

$$\Gamma_{Z' \to h A^0} = (g_z \cos\alpha \cos\beta)^2 \frac{|p|}{24\pi} \frac{|p|^2}{M_{Z'}^2}. \tag{5.14}$$

where the center of mass momentum for the decay products $|p| = \frac{1}{2M_{Z'}} \lambda^{1/2}(M_{Z'}^2, m_h^2, m_{A^0}^2)$, and $\lambda$ is the Källen triangle function.[1]

[1] $\lambda(c_1, c_2, c_3) \equiv c_1^2 + c_2^2 + c_3^2 - 2(c_1c_2 + c_2c_3 + c_3c_1)$

#### 5.3.3.1 *Parameter scan*

The model is described by five parameters:

- the pseudoscalar mass $M_{A^0}$,
- the DM mass $m_{\text{DM}}$,

- the $Z'$ mass, $M_{Z'}$,
- $\tan\beta(\equiv v_u/v_d)$,
- the $Z'$ coupling strength $g_z$.

To study the signal production and kinematic dependencies on these parameters, we produced signal samples varying each of the five parameters through MadGraph for the matrix element, PYTHIA for the parton shower, and DELPHES[dF+14] for a parameterized detector-level simulation.

As seen in Fig. 5.24, variations of $\tan\beta$ does not lead to any kinematic difference and the production cross section simply scales as a function of $\tan\beta$. Hence we recommend to fix $\tan\beta$ to unity in the signal generation.

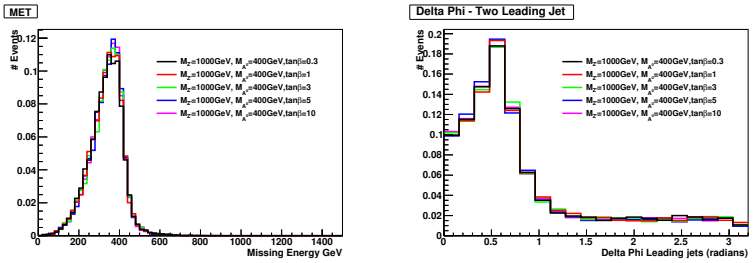


(a) MET distribution (b) $\Delta\phi$ distance between the two $b-$ jets

Figure 5.24: Kinematic distributions of the signal process varying $\tan\beta$, in the case of a Higgs boson decaying into two $b$ quarks, after parameterized detector simulation: no kinematic dependency is observed

Similarly, variations of $g_z$ do not lead to any kinematic changes. The value of $g_z$ for a given $M_{Z'}$ and $\tan\beta$ can be set according to the maximum value allowed by electroweak global fits and dijet constraints, as described in [BLW14]. Since this parameter does not influence the kinematics, we leave it up to individual analyses on whether they generate benchmark points only according to these external constraints **[TODO: add link to section as in summary. This is the same sentence we will put in for the mono-b model]**.

Since the DM pair are produced as a result of the decay of $A^0$, there are minimal kinematic changes when varying $M_{DM}$ as long as $M_{DM} < M_{A^0}/2$ so that $A^0$ production is on-shell, as shown in Fig. 5.25 and 5.26 (before detector simulation).

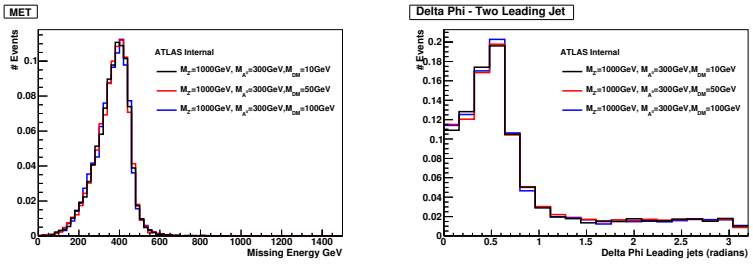


(a) MET distribution (b) $\Delta\phi$ distance between the two $b-$ jets

Figure 5.25: Kinematic distributions of the signal process varying $M_{DM}$: minimal kinematic dependency on $M_{DM}$ as expected when $A^0$ is produced on-shell. Plots shown for $M_{Z'} = 1000$ GeV, $M_{A^0} = 300$ GeV.

We recommend to produce signal events for a fixed $g_z = 0.8$, $\tan\beta = 1$ and $M_{DM} = 100$ GeV. For these values, we scan the 2-D parameter space of $M_{Z'}, M_{A^0}$ with $M_{Z'} = 600, 800, 1000, 1200, 1400$ GeV, and $M_{A^0} = 300, 400, 500, 600, 700, 800$ GeV with $M_{A^0} < M_{Z'} - m_h$,

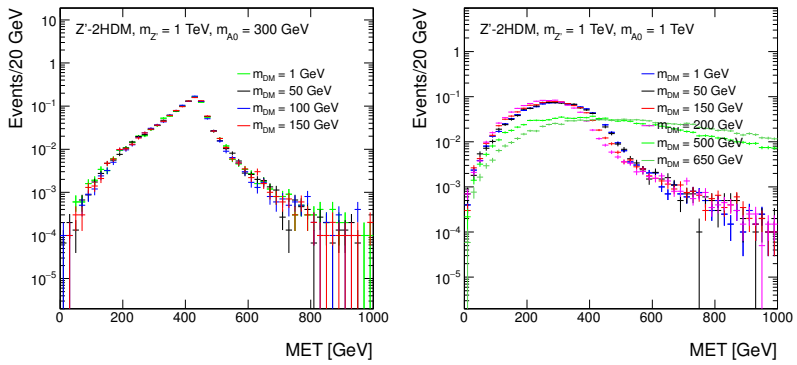


Figure 5.26: Missing transverse momentum distributions at generator level in the $Z'$+2HDM scenario for different values of the dark matter mass $m_{DM}$, with $m_{Z'}$ = 1 TeV and $m_{A^0}$ = 300 GeV (left) and $m_{A^0}$ = 1 TeV (right).

for a total of 24 points. The choice of scan is justified by the sensitivity study in **??**: the expected LHC sensitivity for Run-2 is up to $M_{Z'} \sim 1.5$ TeV. For the parameter scan, the DM mass is fixed to 100 GeV. For two $M_{Z'}$, $M_{A^0}$ value sets, we vary the DM mass to obtain sample cross section for rescaling results. All LO cross sections for the various parameter scan points are reported in Appendix B. The parameter scan excludes the off-shell region, as the cross-sections are suppressed and the LHC would not have any sensitivity to these benchmark points in early data.

The kinematic distributions with varying $M_{Z'}$ for fixed $M_{A^0}$ are shown in Fig. 5.27, while the dependency on $M_{A^0}$ is shown in Fig. 5.28.

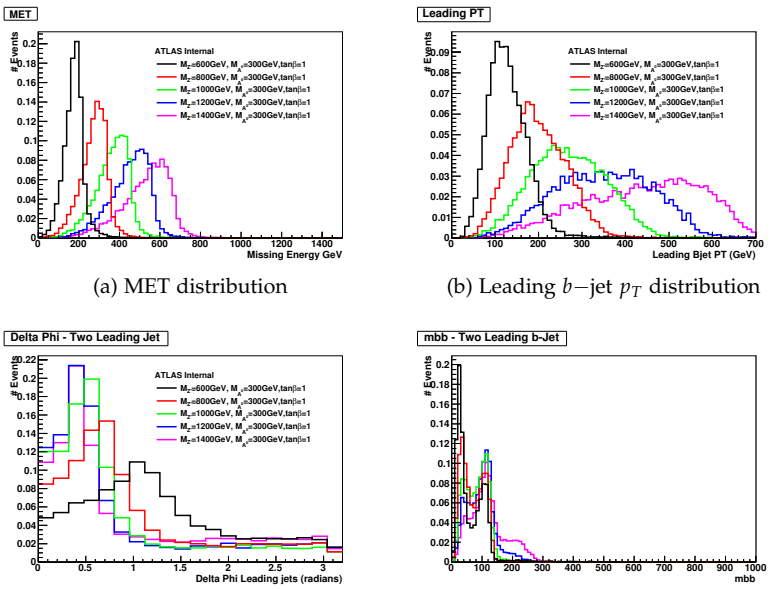


(a) MET distribution

(b) Leading $b-$jet $p_T$ distribution

(c) $\Delta\phi$ distance between the two $b-$ jets

(d) Dijet invariant mass

Figure 5.27: Kinematic distributions of the signal process varying $M_{Z'}$, for $M_{DM} = 100$ GeV, $M_{A^0} = 300$ GeV.

This model also allows for an additional source of Higgs plus MET signal with a similar kinematics (Fig. 5.29, shown with detector simulation samples) to the signal process from the decay of $Z' \to hZ$, where the $Z$ decays invisibly. The partial decay width for

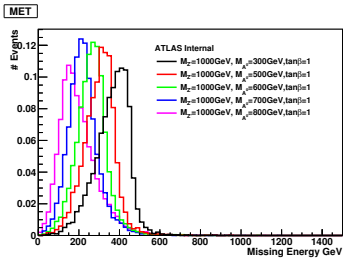


(a) MET distribution

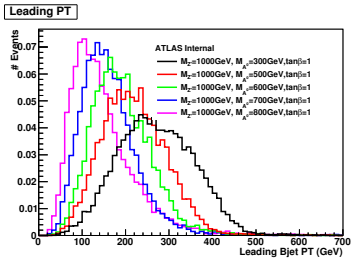


(b) Leading $b-$jet $p_T$ distribution

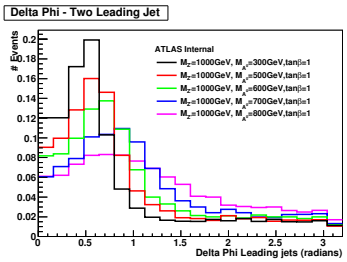


(c) $\Delta\phi$ distance between the two $b-$ jets

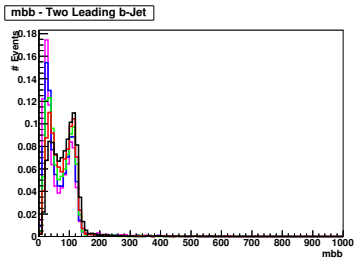


(d) Dijet invariant mass

Figure 5.28: Kinematic distributions of the signal process varying $M_{A^0}$, for $M_{DM} = 100$ GeV, $M_{Z'} = 1000$ GeV.

the $Z'$ is:

$$\Gamma_{Z' \to hZ} = (g_z \cos\alpha \sin\beta)^2 \frac{|p|}{24\pi} \left( \frac{|p|^2}{M_{Z'}^2} + 3\frac{M_Z^2}{M_{Z'}^2} \right), \qquad (5.15)$$

The values for the $Z'$ masses scanned for those samples should follow those of the previous samples, namely values of $M_{Z'} = 600, 800, 1000, 1200, 1400$ GeV. This signal process has no $M_A$ dependence.

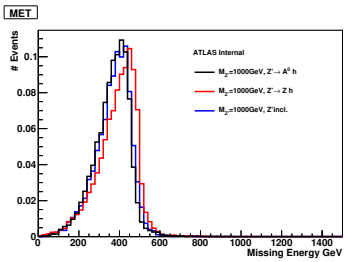


(a) MET distribution

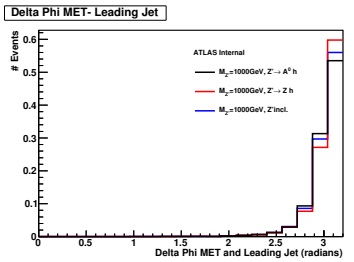


(b) Leading $b-$jet $p_T$ distribution

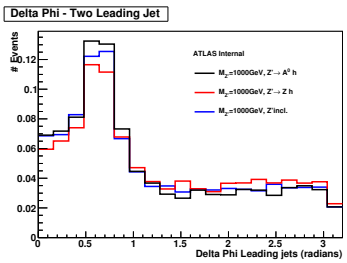


(c) $\Delta\phi$ distance between the two $b-$ jets

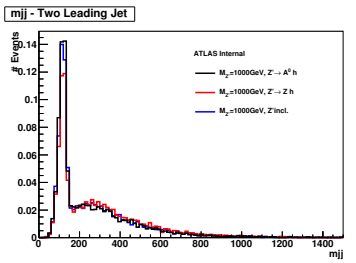


(d) Dijet invariant mass

Figure 5.29: Kinematic distributions of $Z' \to A^0 h$ exclusive production, $Z' \to Zh$ exclusive production and $Z'$ inclusive production for $M_{Z'} = 1000$ GeV and $M_{A^0} = 300$ GeV

# 6

# Validity of EFT approach

Effective Field Theories (EFTs) are an extremely useful tool for DM searches at the LHC. Given the current lack of indications about the nature of the DM particle and its interactions, a model independent interpretation of the collider bounds appears mandatory, especially in complementarity with the reinterpretation of the exclusion limits within a choice of simplified models, which cannot exhaust the set of possible completions of an effective Lagrangian. However EFTs must be used with caution at LHC energies, where the energy scale of the interaction is at a scale where the EFT approximation can no longer be assumed to be valid. To illustrate the problem, consider an effective interaction

$$(\bar{\psi}_{SM}\psi_{SM})(\bar{\psi}_{DM}\psi_{DM})\frac{g}{\Lambda^2}$$

that couples SM and DM fields. The strength of this interaction can be parametrized by $f = \frac{g}{\Lambda^2}$. A monojet signature can be generated by appling perturbation theory in the QCD coupling. The resulting Feynman diagram will contain a quark propagator with virtuality $\sqrt{-q^2}$. For a fixed $f$, a small value of $g$ will require a small value of $\Lambda$. The EFT approximation breaks down if $\sqrt{-q^2} > \Lambda$. On the other hand, large $\Lambda$ implies large $g$, raising the question if perturbation theory is even applicable.

Here we summarise some methods that can be used to ensure the validity of the EFT approximation. These methods are described in detail in Refs. [BDSMR14**?** , BDSJ$^+$14, A$^+$15, RWZ15].

## 6.1 Outline of the procedure described in Refs. [**?** A$^+$15]

For a tree-level interaction between DM and the Standard Model (SM) via some mediator with mass $M$, the EFT approximation corresponds to expanding the propagator in powers of $Q_{\rm tr}^2/M^2$, truncating at lowest order, and combining the remaining parameters into a single parameter $M_*$ (also called $\Lambda$). For an example scenario with a $Z'$-type mediator (leading to some combination of operators D5 to D8 in the EFT limit) this corresponds to setting

$$\frac{g_{\rm DM}g_q}{Q_{\rm tr}^2 - M^2} = -\frac{g_{\rm DM}g_q}{M^2}\left(1 + \frac{Q_{\rm tr}^2}{M^2} + \mathcal{O}\left(\frac{Q_{\rm tr}^4}{M^4}\right)\right) \simeq -\frac{1}{{M_*}^2}, \qquad (6.1)$$

where $Q_{\rm tr}$ is the momentum carried by the mediator, and $g_{\rm DM}$, $g_q$ are the DM-mediator and quark-mediator couplings respectively. Similar expressions exist for other operators. Clearly the condition that must be satisfied for this approximation to be valid is that $Q_{\rm tr}^2 < M^2 = g_{\rm DM} g_q {M_*}^2$.

We can use this condition to enforce the validity of the EFT approximation by restricting the signal (after the imposition of the event selection of the analysis) to events for which $Q_{\rm tr}^2 < M^2$. This truncated signal can then be used to derive the new, truncated limit on $M_*$ as a function of $(m_{\rm DM}, g_{\rm DM} g_q)$.

For the example D5-like operator, $\sigma \propto {M_*}^{-4}$, and so there is a simple rule for converting a rescaled cross section into a rescaled constraint on $M_*$ if the original limit is based on a simple cut-and-count procedure. Defining $\sigma_{\rm EFT}^{\rm cut}$ as the cross section truncated such that all events pass the condition $\sqrt{g_{\rm DM} g_q} M_*^{\rm rescaled} > Q_{\rm tr}$, we have

$$M_*^{\rm rescaled} = \left( \frac{\sigma_{\rm EFT}}{\sigma_{\rm EFT}^{\rm cut}} \right)^{1/4} M_*^{\rm original}, \tag{6.2}$$

which can be solved for $M_*^{\rm rescaled}$ via either iteration or a scan (note that $M_*^{\rm rescaled}$ appears on both the LHS and RHS of the equation). Similar relations exist for a given UV completion of each operator. The details and application of this procedure to ATLAS results can be found in Ref. [A$^+$15] for a range of operators. Since this method uses the physical couplings and energy scale $Q_{\rm tr}$, it gives the strongest possible constraints in the EFT limit while remaining robust by ensuring the validity of the EFT approximation.

## 6.2 *Outline of the procedure described in Ref. [RWZ15]*

In [RWZ15] a procedure to extract model independent and consistent bounds within the EFT is described. This procedure can be applied to any effective Lagrangian describing the interactions between the DM and the SM, and provides limits that can be directly reinterpreted in any completion of the EFT.

The range of applicability of the EFT is defined by a mass scale $M_{\text{cut}}$, a parameter which marks the upper limit of the range of energy scales at which the EFT can be used reliably, independently of the particular completion of the model. Regardless of the details of the full theory, the energy scale probing the validity of the EFT is less than or equal to the centre-of-mass energy $E_{\text{cm}}$, the total invariant mass of the hard final states of the reaction. Therefore, the condition ensuring the validity of the EFT is, by definition of $M_{\text{cut}}$,

$$E_{\text{cm}} < M_{\text{cut}} \,. \tag{6.3}$$

For example, in the specific case of a tree level mediation with a single mediator, $M_{\text{cut}}$ can be interpreted as the mass of that mediator.

There are then at least three free parameters describing an EFT: the DM mass $m_{\text{DM}}$, the scale $M_*$ of the interaction, and the cutoff scale $M_{\text{cut}}$.

We can use the same technique as above to restrict the signal to the events for which $E_{\text{cm}} < M_{\text{cut}}$, using only these events to derive the exclusion limits on $M_*$ as a function of $(m_{\text{DM}}, M_{\text{cut}})$. We can also define an *effective coupling strength* $M_{\text{cut}} = g_* M_*$, where $g_*$ is a free parameter that substitutes the parameter $M_{\text{cut}}$, and therefore derive exclusions on $M_*$ as a function of $(m_{\text{DM}}, g_*)$. This allows us to see how much of the theoretically allowed parameter space has been actually tested and how much is still unexplored; For example, in the $Z'$-type model considered above, $g_*$ is equal to $\sqrt{g_{\text{DM}} g_q}$. The resulting plots are shown in [RWZ15] for a particular effective operator.

The advantage of this procedure is that the obtained bounds can be directly and easily recast in any completion of the EFT, by computing the parameters $M_*$, $M_{\text{cut}}$ in the full model as functions of the parameters of the complete theory. On the other hand, the resulting limits will be weaker than those obtained using $Q_{\text{tr}}$ and a specific UV completion.

## 6.3 *EFT validity recommendations*

## 6.4 *Recommendation for contact interaction theories with simplified models available*

...to be written...

## 6.5 *Recommendation for truncation of theories with no simplified models available*

$M_{\text{cut}}$ is related to physical couplings and masses only in a UV complete theory, and so is effectively a free parameter. It makes sense to choose $M_{\text{cut}}$ such that we identify the transition region where the EFT stops being a good description of UV complete theories. This can be done using R, which is defined as the fraction of events for which $\hat{s} > M_{\text{cut}}^2$.

For large values of $M_{\text{cut}}$, no events are thrown away in the truncation procedure, and R=1. As $M_{\text{cut}}$ becomes smaller, eventually all events are thrown away in the truncation procedure, i.e. R=0, and the EFT gives no exclusion limits for the chosen acceptance.

We propose a rough scan over $M_{\text{cut}}$, such that we find the values of $M_{\text{cut}}$ for which R ranges from, say, 0.1 to 1. We can then perform a scan over (several, your choice) values of $M_{\text{cut}}$, showing the truncated limit for each one.

When R=0, there is no limit. When R reaches 1, the truncated limit is identical to the original limit.

# A
# Appendix: Implementation of Models

## A.1 Implementation of s-channel models

There are several matrix element implementations of the DM production through spin-0 and spin-1 mediators.

For a spin-1 mediator, the implementation in POWHEG generates DM pair production with 1 parton at next-to-leading order (NLO), whilst MADGRAPH and MCFM are at leading order (LO). As shown in POWHEG Ref. [HKR13], including NLO corrections result in an enhancement in the cross section as compared to LO and though this is not significant, it does lead to a substantial reduction in the dependence on the choice of the renormalization and factorization scale and hence the theoretical uncertainty on the signal prediction. Since NLO calculations are available for the process in POWHEG, we recommend to proceed with POWHEG as the generator of choice.

For a spin-0 mediator, the top-quark loop is the most important consideration. The matrix element implementation of the s-channel spin-0 mediated DM production is available in POWHEG with the full top-loop calculation at LO [HR15]. The POWHEG implementation includes the finite top quark mass dependence for DM pair production with 1 parton at LO. For consistency with the spin-1 generation, we recommend using POWHEG for this case as well.

Here, we document some specific settings for the Dark Matter models needed to run the POWHEG generation:

- The POWHEG implementation allows to generate a single sample that provides sufficient statistics in all signal regions. POWHEG generates weighted events and the `bornsuppfact` parameter is used to set the event suppression factor according to

$$F(k_{\mathrm{T}}) = \frac{k_{\mathrm{T}}^2}{k_{\mathrm{T}}^2 + \texttt{bornsuppfact}^2} \,. \tag{A.1}$$

  In this way, the events at, for instance low $\not{E}_T$, are suppressed and receive higher event weights which ensures higher statistics at high $\not{E}_T$. We recommend to set `bornsuppfact` to 1000.

- The `bornktmin` parameter allows to suppress the low $\not{E}_T$ region even further by starting the generation at a certain value of $k_{\mathrm{T}}$. It

is recommended to set this parameter to half the lower analysis $\not{E}_T$ cut, for the event selection used in the CMS/ATLAS monojet analyses for instance the proposed value for `bornktmin` is 150. However, this parameter should be set keeping in mind the event selection of all the analyses that will use these signal samples and hence a threshold lower than 150 may be required.

- Set `runningwidth` to 0.
- Set `mass_low` and `mass_high` to -1.
- The minimal values for `ncall1`, `itmx1`, `ncall2`, `itmx2` are 250000, 5, 1000000, 5 for the DMV model, respectively. In order to increase speed, set `foldsci` and `foldy` to 2 and keep `foldphi` at 1.
- The minimal values for `ncall1`, `itmx1`, `ncall2`, `itmx2` are 100000, 5, 100000, 5 for the DMS_tloop model, respectively.
- Allow negative weights for the DMV model by setting `withnegweights` to 1.
- Since the DMS_tloop model is a leading order process, set `LOevents` and `bornonly` are set to 1 internally.
- Automatic calculation of systematic uncertainties associated with the choice of hard scale and PDFs.

**[Comment on proper PDF sets to use, concerns about sea quark PDF in b-initiated diagrams (perhaps the latter belongs in the b-flavored DM section]**

## *A.2 CKKW parton matching implementation*

The parton matching techniques are implemented in the mono-jet like MC generation in order to avoid double counting the partons from matrix elements and parton showering. The CKKW matching is better developed and preferred [A$^+$14c] [A$^+$08]. As the illustration sample, the EFT D5 samples are generated with `MadGraph5_aMC@NLO` version 2.2.2. The technical implementations are shown as below.

On the generator side, i.e., `MadGraph5_aMC@NLO`:

- `ickkw = 0`
- `ktdurham =` matching scale
- `dparameter = 0.4`
- `dokt = T`
- `ptj=20`
- `drjj=0`
- `mmjj=0`

- `ptj1min=0`

On the parton showering side, i.e., `Pythia 8`:

- `Merging:ktType = 1`
- `Merging:TMS =` matching scale
- `1000022:all = chi chi  2 0 0 30.0 0.0 0.0 0.0 0.0`
- `1000022:isVisible = false`
- `Merging:doKTMerging = on`
- `Merging:Process = pp>chi,1000022chi ,-1000022`
- `Merging:nJetMax = 2`

The matching scales should be the same for the generation and parton showering. In `MadGraph5_aMC@NLO`, the particle data group ID `1000022` is used for weakly interacting dark matter candidates, which should be informed to `Pythia 8`.

In this test we are generating the process with up to two parton emissions, so the command `Merging:nJetMax = 2` is applied to `Pythia 8`. The different parton emission cases are generated separately:

- `p p > chi chi`
- `p p > chi chi  j`
- `p p > chi chi  j j`

Two matching scales are tested at 30 and 80 GeV. The differential jet rates are shown in Fig. A.1 for matching scale 30 GeV and Fig. A.2 for 80 GeV. The 80 GeV matching scale gives smoother distribution, which is desired to avoid artifical effect due to parton matching. There will be a small tink around the matching scale for both cases.

To compare the effect in a finer step, the matching scales at 30, 50, 70, 80 and 90 GeV are plotted in FigA.3. Globally good agreement is seen among different matching scales, with some difference observed around the matching scale. A closer look in this range shows that the 80 and 90 GeV matching scales produce very close distributions, so it is safe to use 80 GeV as the baseline matching scale.

The MC distributions for the missing transverse energy and transverse momenta for the leading and subleading jets are plotted in Fig.. For the mono-jet analysis, usually a missing transverse energy cut larger than 300 GeV is applied for offline selection, which makes the contribution of the 0-parton emission case negligible in the mono-jet analysis.

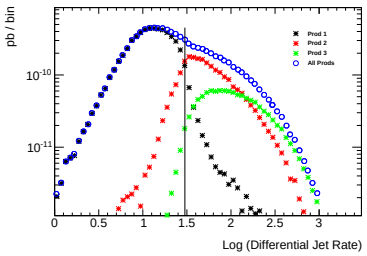


(a) $1 \to 2$ parton process

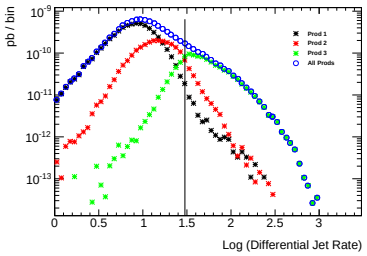


(b) $2 \to 3$ parton process

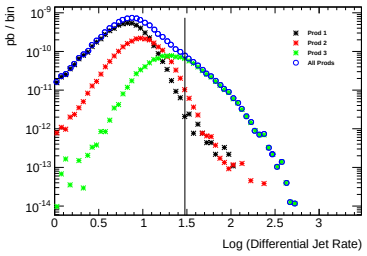


(c) $3 \to 4$ parton process

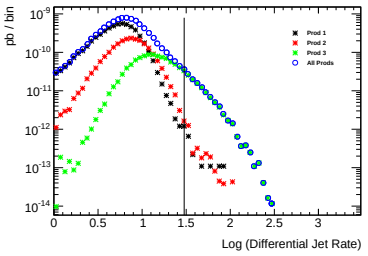


(d) $4 \to 5$ parton process

Figure A.1: Jet differential rates distributions for EFT D5 sample with CKKW matching scale at 30 GeV. 0-, 1- and 2-parton emission cases are generated separatedly. A vertical line is drawn at the matching scale.

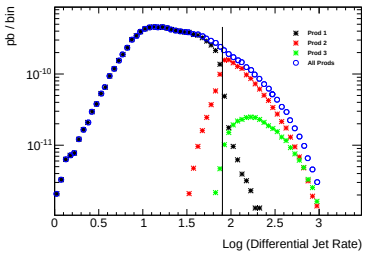


(a) $1 \to 2$ parton process

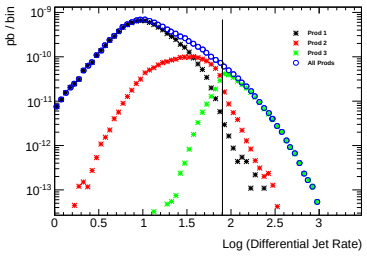


(b) $2 \to 3$ parton process

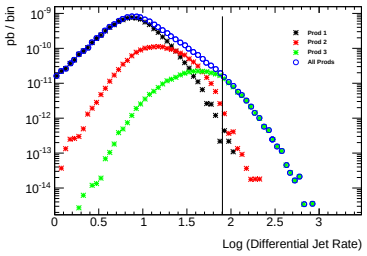


(c) $3 \to 4$ parton process

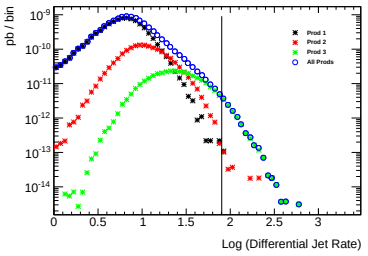


(d) $4 \to 5$ parton process

Figure A.2: Jet differential rates distributions for EFT D5 sample with CKKW matching scale at 80 GeV. 0-, 1- and 2-parton emission cases are generated separatedly. A vertical line is drawn at the matching scale.

## *A.3 Parton emission generation*

In order to describe the signal kinematics correctly and save time in MC generation, the parton emissions will only be generated up to a certain numbers of parton and ignore the cases with more partons. The later ones usually have cross sections small enough and limited contribution in the interested kinematic regions.

It is found that the 3- or more-parton emission cases are negligible in our intersted regions, but the 2-parton emission case has significant contributions. The 0- and 1-parton emissions are out of discussion since they give the baseline signature in this analysis. The impacts of 2- and 3-parton emissions are quantified in this section.

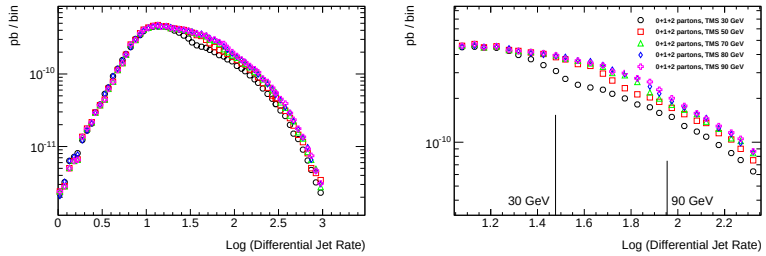


(a) $1 \to 2$ parton process

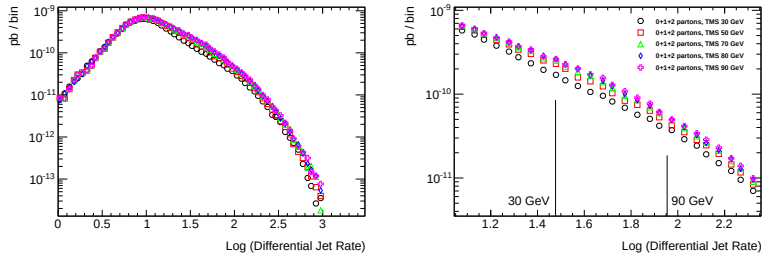


(b) $2 \to 3$ parton process

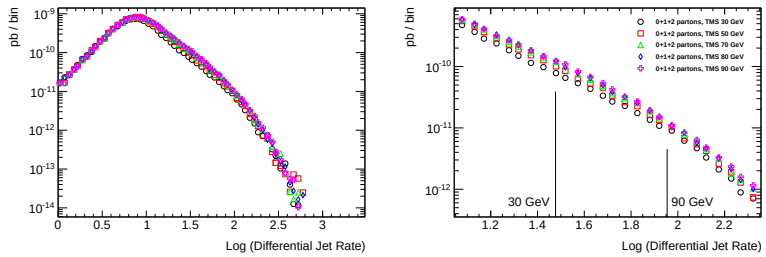


(c) $3 \to 4$ parton process

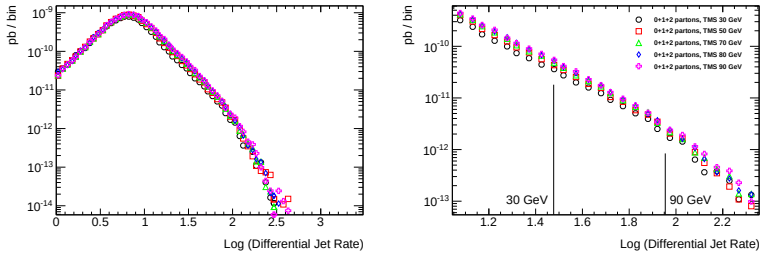


(d) $4 \to 5$ parton process

Figure A.3: Jet differential rates distributions for EFT D5 sample with CKKW matching scale at 30, 50, 70, 80 and 90 GeV. 0-, 1- and 2-parton emission cases are generated separatedly and the total merged contribution is shown. A closer look is shown around the matching scale.

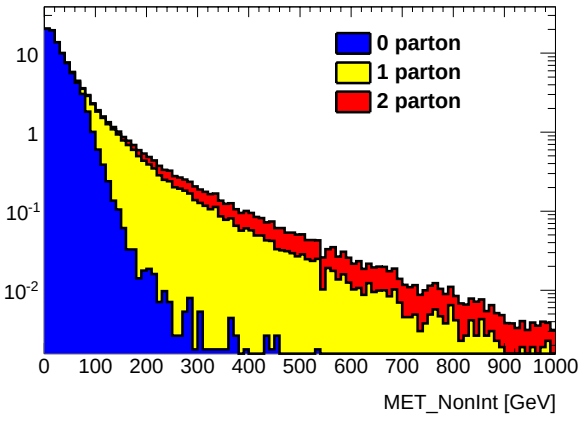


Figure A.4: Missing transverse momentum distributions for EFT D5 sample with CKKW matching scale at 80 GeV. 0-, 1- and 2-parton emission cases are generated separatedly and added together by cross sections. The 0-parton emission case has very limited contribution for missing transverse energy larger than 300 GeV region.

Here the 0-, 1-, 2- and 3-parton emissions are generated separately and requested in matching step with `Merging:nJetMax=3` and scale at 80 GeV in Pythia8for 0+1+2+3 parton emission case, while `Merging:nJetMax=2` requested for 0+1+2 case and `Merging:nJetMax=1` requested for 0+1 case. The MET distribution is plotted in Fig.A.5, while the jet multiplicity is shown in Fig.A.6.

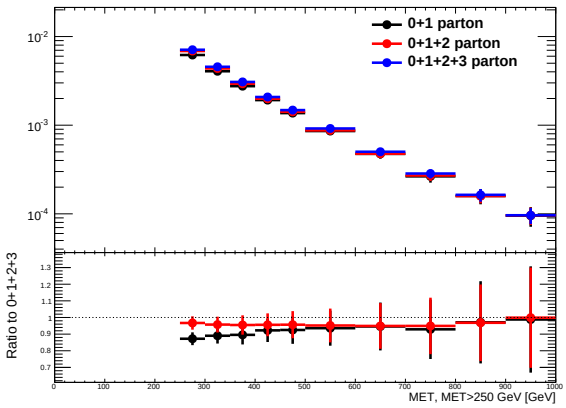


Figure A.5: Missing transverse momentum distributions for EFT D5 sample with CKKW matching scale at 80 GeV. 0-, 1-, 2- and 3-parton emission cases are generated separatedly and added together by cross sections.

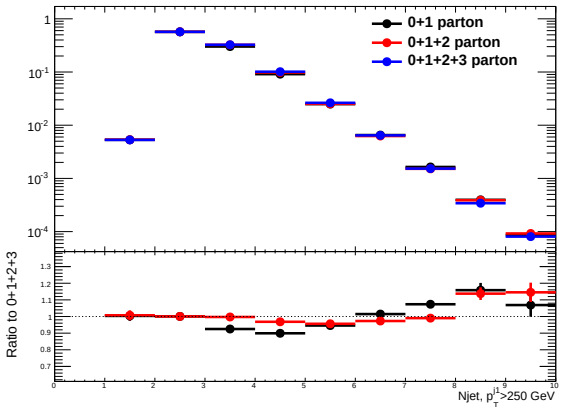


Figure A.6: Jet multiplicity distribution for EFT D5 sample with CKKW matching scale at 80 GeV. 0-, 1-, 2- and 3-parton emission cases are generated separatedly and added together by cross sections.

With the ATLAS run-I baseline cut (MET and leading jet $p_T$ larger than 250 GeV, less than 4 jets), the 0+1 parton emission has 17.4% yield less compared to 0+1+2+3 parton emission, while the 0+1+2 has 2.2% less. With MET>400 GeV, 0+1 parton emission has 16.8% yield less and 0+1+2 parton emission has 2.4% less compared to 0+1+2+3 parton emission. With MET>600 GeV, 0+1 parton emission has 16.5% yield less and 0+1+2 parton emission has 2.9% less compared to 0+1+2+3 parton emission. The same numbers hold if a sysmetric cut is added on leading jet transverse momentum.

## *A.4 Model implementation for mono-Higgs models*

All three Higgs+MET models are generated at leading order with MadGraph 2.2.2, using Pythia8 for the parton shower. The MadGraph implementations of the scalar and vector models can be

found on the Forum SVN repository [For15c], while the 2HDM model can be found at this link [For15a].

In all cases, it is recommended not to handle the $h$ decay through MadGraph as it does not include the proper $h$ branching ratios, or, if using MadGraph, then the resulting cross section should be rescaled to match onto the correct branching ratio.

### Madgraph details for scalar mediator Higgs+MET model

In this model, the contribution from the $ggh$S box is included through an effective Lagrangian evaluated in the large $m_t$ limit. This may overestimate the rates of the $h + \not{E}_T$ signal [HKU13], but a full evaluation is left to future studies.

### Madgraph details for 2HDM Higgs+MET model

The two couplings that can be changed in the Madgraph model follow the nomenclature below:

- `Tb` - $\tan\beta$
- `gz` - $g_z$, gauge coupling of $Z'$ to quarks

The other couplings are not changed, including `gx` (the $A\bar{\chi}\chi$ coupling) which has little impact on the signal. $\sin\alpha$ is fixed internally such that $\cos(\beta - \alpha) = 0$. The width of the $Z'$ and $A$ can be computed automatically within Madgraph. The couplings here don't affect the signal kinematics, so they can be fixed to default values and then the signal rates can be scaled appropriately.

The nomenclature for the masses in the Madgraph model is:

- `MZp` - PDG ID 32 - $Z'$
- `MA0` - PDG ID 28 - $A$
- `MX` - PDG ID 1000022 - dark matter particle

The other masses are unchanged and do not affect the result. Both $Z' \to hZ(\bar{\nu}\nu)$ and $Z' \to hA(\bar{\chi}\chi)$ contribute to the final state, scaling different with model parameters. We recommend to generate them separately, and then add the two signal processes together weighted by cross sections.

# B

# Appendix: Detailed studies for EW models

## B.1 Further W+MET models with possible cross-section enhancements

As pointed out in Ref. [BCD+15], the mono-$W$ signature can probe the iso-spin violating interactions of dark matter with quarks. The relevant operators after the electroweak symmetry breaking is

$$\frac{1}{\Lambda^2}\overline{\chi}\gamma_\mu\chi\left(\overline{u}_L\gamma^\mu u_L + \xi\bar{d}_L\gamma^\mu d_L\right) . \tag{B.1}$$

Here, we only keep the left-handed quarks because the right-handed quarks do not radiate a $W$-gauge boson from the weak interaction. As the LHC constraints the cutoff to higher values, it is also important to know the corresponding operators before the electroweak symmetry. At the dimension-six level, the following operator

$$\frac{c_6}{\Lambda^2}\overline{\chi}\gamma_\mu\chi\,\overline{Q}_L\gamma^\mu Q_L \tag{B.2}$$

conserves iso-spin and provides us $\xi = 1$ [**?** ]. At the dimension-eight level, new operators appear to induce iso-spin violation and can be

$$\frac{c_8^d}{\Lambda^4}\overline{\chi}\gamma_\mu\chi\,(H\overline{Q}_L)\gamma^\mu(Q_L H^\dagger) + \frac{c_8^u}{\Lambda^4}\overline{\chi}\gamma_\mu\chi\,(\tilde{H}\overline{Q}_L)\gamma^\mu(Q_L\tilde{H}^\dagger) . \tag{B.3}$$

After inputting the vacuum expectation value of the Higgs field, we have

$$\xi = \frac{c_6 + c_8^d\, v_{\rm EW}^2/2\Lambda^2}{c_6 + c_8^u\, v_{\rm EW}^2/2\Lambda^2} . \tag{B.4}$$

For a nonzero $c_6$ and $v_{\rm EW} \ll \Lambda$, the iso-spin violation effects are suppressed. On the other hand, the values of $c_6$, $c_8^d$ and $c_8^u$ depend on the UV-models.

There is one possible UV-model to obtain a zero value for $c_6$ and non-zero values for $c_8^d$ and $c_8^u$. One can have the dark matter and the SM Higgs field charged under a new $U(1)'$. There is a small mass mixing between SM $Z$-boson and the new $Z'$ with a mixing angle of $\mathcal{O}(v_{\rm EW}^2/M_{Z'}^2)$. After integrating out $Z'$, one has different effective dark matter couplings to $u_L$ and $d_L$ fields, which are proportional to their couplings to the $Z$ boson. For this model, we have $c_6 = 0$ and

$$\xi = \frac{-\frac{1}{2} + \frac{1}{3}\sin^2\theta_W}{\frac{1}{2} - \frac{2}{3}\sin^2\theta_W} \approx -2.7 \tag{B.5}$$

and order of unity.

## B.2 Simplified model corresponding to dimension-5 EFT operator

As an example of a simplified model corresponding to the dimension-5 EFT operator described in Section 5.2, we consider a Higgs portal with a scalar mediator. Models of this kind are among the most concise versions of simplified models that produce couplings of Dark Matter to pairs of gauge-bosons. Scalar fields may couple directly to pairs of electroweak gauge bosons, but must carry part of the electroweak vev. One may thus consider a simple model where Dark Matter couples to a a scalar singlet mediator, which mixes with the fields in the Higgs sector.

$$L \subset m_s S^2 + \lambda S^2 H^2 + \lambda^{'} S H^2 + y S \chi \overline{\chi} \tag{B.6}$$

Where H is a field in the Higgs sector that contains part of the electroweak vev, S is a heavy scalar singlet and $\chi$ is a Dark Matter field. There is then an S channel diagram where DM pairs couple to the singlet field S, which then mixes with a Higgs-sector field, and couples to W and Z bosons. This diagram contains 2 insertions of EW symmetry breaking fields, corresponding in form to the effective dimension-5 operator in the previous section.

## B.3 Tabulated cross-sections

### B.3.1 photon+MET signal, s-channel vector mediator model

### B.3.2 Higgs+MET signal, vector mediator model

Figure B.1 shows the cross sections in this vector mediator model in the $m_{med}$ vs $m_{DM}$ plane. The tabulated values can be found in Table B.1

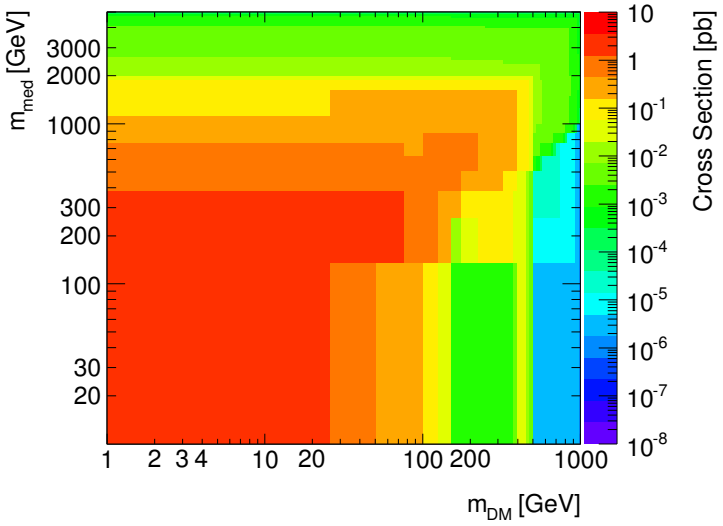


Figure B.1: Cross section of the $pp \rightarrow H\chi\bar{\chi}$ process in units of pico-barn for the vector mediator model.

| $m_{DM}$ [GeV] | $m_{med}$ [GeV] | $\sigma_{pp\to h\chi\bar{\chi}}$ [pb] |
|---|---|---|
| 1 | 10 | 0.0003835 |
| 1 | 20 | 0.0003177 |
| 1 | 50 | 0.0001467 |
| 1 | 100 | 0.0001065 |
| 1 | 200 | 6.867e-05 |
| 1 | 300 | 7.388e-05 |
| 1 | 500 | 7.858e-05 |
| 1 | 1000 | 4.327e-05 |
| 1 | 2000 | 4.018e-05 |
| 1 | 5000 | 3.336e-05 |
| 10 | 10 | 3.603e-06 |
| 10 | 15 | 1.477e-05 |
| 10 | 50 | 0.0001547 |
| 10 | 100 | 0.0001104 |
| 10 | 5000 | 4.5e-05 |
| 50 | 10 | 1.401e-07 |
| 50 | 50 | 2.099e-07 |
| 50 | 95 | 2.813e-05 |
| 50 | 200 | 4.82e-05 |
| 50 | 300 | 7.485e-05 |
| 50 | 5000 | 3.384e-05 |
| 150 | 10 | 4.833e-09 |
| 150 | 295 | 3.65e-08 |
| 150 | 500 | 6.463e-07 |
| 150 | 5000 | 2.407e-08 |
| 500 | 10 | 8.672e-12 |
| 500 | 500 | 1.157e-11 |
| 500 | 995 | 5.254e-10 |
| 500 | 2000 | 7.138e-10 |
| 500 | 5000 | 5.87e-10 |
| 1000 | 10 | 5.946e-14 |
| 1000 | 1000 | 1.546e-13 |
| 1000 | 1995 | 8.316e-12 |
| 1000 | 5000 | 2.112e-11 |

Table B.1: Cross section of the $pp \to h\chi\bar{\chi}$ process in units of pico-barn for the vector mediator model.

### B.3.3 *Higgs+MET signal, scalar mediator model*

Figure B.2 shows the cross sections of the $pp \to H\chi\bar{\chi}$ process in this vector mediator model in the $m_{med}$ vs $m_{DM}$ plane. The tabulated values can be found in Table B.2

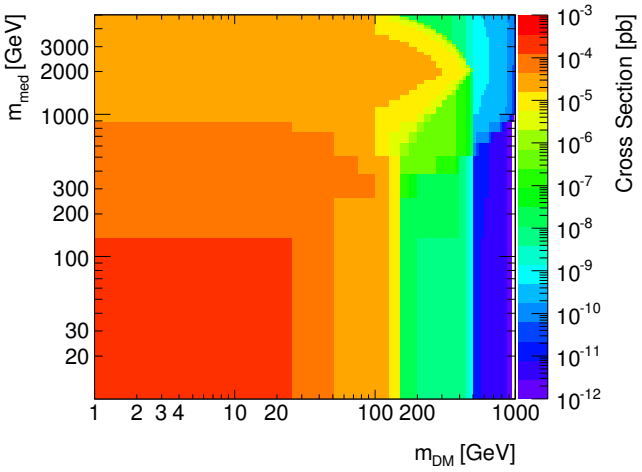


Figure B.2: Cross section of the $pp \to H\chi\bar{\chi}$ process in units of picobarn for the scalar mediator model.

### B.3.4 *Higgs+MET signal from 2HDM model with a $Z'$ and a new pseudoscalar*

The leading order cross-sections from the Madgraph generator for the signal samples are listed in Tables B.3, B.4, B.5, for the various scan points recommended.

| $m_{DM}$ [GeV] | $m_{med}$ [GeV] | $\sigma_{pp\to h\chi\bar{\chi}}$ [pb] |
|---|---|---|
| 1 | 10 | 2.389 |
| 1 | 20 | 2.483 |
| 1 | 50 | 2.98 |
| 1 | 100 | 2.881 |
| 1 | 200 | 2.344 |
| 1 | 300 | 2.041 |
| 1 | 500 | 0.9328 |
| 1 | 1000 | 0.1524 |
| 1 | 2000 | 0.008919 |
| 1 | 5000 | 1.39e-05 |
| 10 | 10 | 0.01895 |
| 10 | 15 | 0.7378 |
| 10 | 50 | 2.929 |
| 10 | 100 | 2.875 |
| 10 | 5000 | 1.387e-05 |
| 50 | 10 | 0.0003215 |
| 50 | 50 | 0.01127 |
| 50 | 95 | 0.2784 |
| 50 | 200 | 1.868 |
| 50 | 300 | 1.759 |
| 50 | 5000 | 1.391e-05 |
| 150 | 10 | 4.786e-06 |
| 150 | 200 | 0.004841 |
| 150 | 295 | 0.156 |
| 150 | 500 | 0.575 |
| 150 | 5000 | 1.391e-05 |
| 500 | 10 | 6.296e-09 |
| 500 | 500 | 2.855e-05 |
| 500 | 995 | 0.008244 |
| 500 | 2000 | 0.007899 |
| 500 | 5000 | 1.355e-05 |
| 1000 | 10 | 3.78e-11 |
| 1000 | 1000 | 7.372e-07 |
| 1000 | 1995 | 0.0004346 |
| 1000 | 5000 | 1.245e-05 |

Table B.2: Cross section of the $pp \to h\chi\bar{\chi}$ process in units of pico-barn for the scalar mediator.

| $M_{Z'}$ (GeV) | $M_{A^0}(GeV)$ | $\sigma$ [pb] |
|---|---|---|
| 600 | 300 | 1.55E-01 |
| 600 | 400 | 2.18E-02 |
| 800 | 300 | 8.30E-02 |
| 800 | 400 | 2.72E-02 |
| 800 | 500 | 1.09E-02 |
| 800 | 600 | 2.98E-03 |
| 1000 | 300 | 3.74E-02 |
| 1000 | 400 | 1.53E-02 |
| 1000 | 500 | 8.91E-03 |
| 1000 | 600 | 4.89E-03 |
| 1000 | 700 | 2.21E-03 |
| 1000 | 800 | 7.05E-04 |
| 1200 | 300 | 1.70E-02 |
| 1200 | 400 | 7.65E-03 |
| 1200 | 500 | 5.14E-03 |
| 1200 | 600 | 3.52E-03 |
| 1200 | 700 | 2.25E-03 |
| 1200 | 800 | 1.27E-03 |
| 1400 | 300 | 8.00E-03 |
| 1400 | 400 | 3.79E-03 |
| 1400 | 500 | 2.75E-03 |
| 1400 | 600 | 2.09E-03 |
| 1400 | 700 | 1.58E-03 |
| 1400 | 800 | 1.06E-03 |

Table B.3: LO cross-sections for $Z' \rightarrow A^0h$ samples, varying $M_{Z'}$ and $M_{A^0}$, keeping the DM mass fixed to 100 GeV. The columns from left to right describe $M_{Z'}$, $M_{A^0}$ and the sample cross section in pb.

| $M_{Z'}$ (GeV) | $M_{A^0}(GeV)$ | $M_{DM}(GeV)$ | $\sigma$ [pb] |
|---|---|---|---|
| 1000 | 300 | 10 | 3.76E-02 |
| 1000 | 300 | 50 | 3.75E-02 |
| 1200 | 600 | 10 | 3.64E-03 |
| 1200 | 600 | 20 | 3.07E-03 |

Table B.4: LO cross-sections for $Z' \rightarrow A^0h$ samples, when varying $M_{DM}$. The columns from left to right describe $M_{Z'}$, $M_{A^0}$, $M_{DM}$, and the sample cross section in pb.

| $M_{Z'}$ (GeV) | $\sigma$ [pb] |
|---|---|
| 600 | 1.15E-01 |
| 800 | 3.21E-02 |
| 1000 | 1.13E-02 |
| 1200 | 4.54E-03 |
| 1400 | 2.00E-03 |

Table B.5: LO cross-sections for $Z' \rightarrow Zh$ exclusive samples, varying $M_{Z'}$. The columns from left to right describe $M_{Z'}$ and the sample cross section in pb.

# C

# Appendix: Table of cross sections for $t\bar{t}$+MET searches

## C.1 Relic density constraints for b−flavored Dark Matter

For Dirac fermion DM the relic density is governed primarily by the $s$-wave annihilation cross section, which is given approximately given by:

$$\langle \sigma v \rangle = \frac{3g^4}{32\pi} \frac{m_\chi^2 \sqrt{1-(m_b/m_\chi)^2}}{\left(m_\Phi^2 + m_\chi^2 - m_b^2\right)} \approx \frac{3g^4 m_\chi^2}{32\pi(m_\Phi^2 + m_\chi^2)} \qquad \text{(C.1)}$$

We assume $\langle \sigma v \rangle = 1.5$ pb.

Figure C.1 shows the weights obtained for various dark matter and mediator massed required to obtain the correct relic density observed in the early universe.

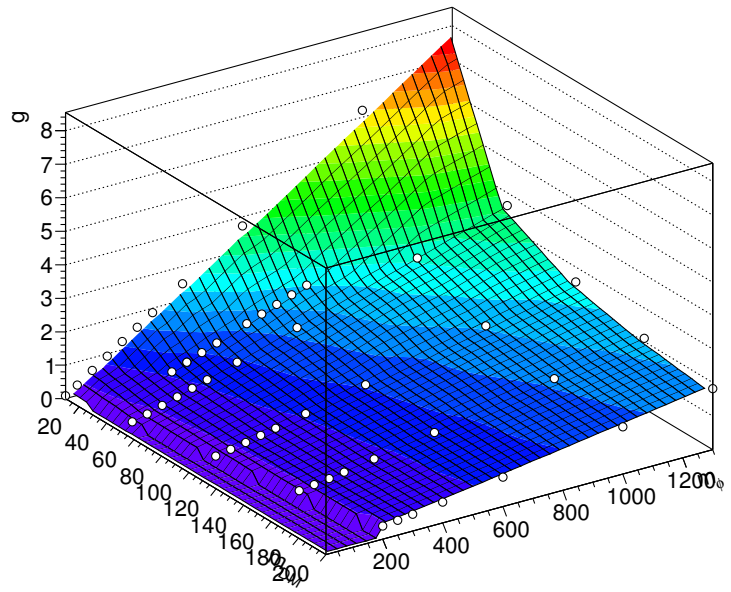


Figure C.1: Coupling constants required to obtain correct relic density in the early universe .

| $m_\chi$ | $m_\Phi$ | $\sigma$ [pb] | $m_\chi$ | $m_\Phi$ | $\sigma$ [pb] |
|---|---|---|---|---|---|
| 100 | 1000 | 5.48E-03 | 150 | 600 | 1.23E-01 |
| 100 | 100 | 1.91E-02 | 200 | 1000 | 4.94E-03 |
| 100 | 1300 | 8.90E-04 | 200 | 1300 | 7.82E-04 |
| 100 | 150 | 6.66E+00 | 200 | 200 | 2.66E-03 |
| 100 | 200 | 9.86E+00 | 200 | 250 | 6.48E-01 |
| 100 | 250 | 7.67E+00 | 200 | 300 | 1.69E+00 |
| 100 | 300 | 4.12E+00 | 200 | 400 | 9.41E-01 |
| 100 | 400 | 1.11E+00 | 200 | 600 | 1.16E-01 |
| 100 | 600 | 1.30E-01 | 35 | 250 | 9.75E+00 |
| 10 | 1000 | 5.80E-03 | 35 | 300 | 4.56E+00 |
| 10 | 100 | 7.84E+01 | 35 | 350 | 2.22E+00 |
| 10 | 10 | 4.09E-01 | 35 | 400 | 1.19E+00 |
| 10 | 1300 | 9.53E-04 | 35 | 500 | 3.76E-01 |
| 10 | 150 | 3.95E+01 | 35 | 550 | 2.24E-01 |
| 10 | 200 | 2.12E+01 | 35 | 600 | 1.37E-01 |
| 10 | 250 | 9.92E+00 | 35 | 650 | 8.62E-02 |
| 10 | 300 | 4.57E+00 | 35 | 700 | 5.54E-02 |
| 10 | 400 | 1.20E+00 | 50 | 1000 | 5.72E-03 |
| 10 | 50 | 1.59E+02 | 50 | 100 | 3.25E+01 |
| 10 | 600 | 1.38E-01 | 50 | 1300 | 9.34E-04 |
| 150 | 1000 | 5.22E-03 | 50 | 150 | 2.84E+01 |
| 150 | 1300 | 8.37E-04 | 50 | 200 | 1.84E+01 |
| 150 | 150 | 6.64E-03 | 50 | 250 | 9.52E+00 |
| 150 | 200 | 1.87E+00 | 50 | 300 | 4.49E+00 |
| 150 | 250 | 3.86E+00 | 50 | 400 | 1.17E+00 |
| 150 | 300 | 3.35E+00 | 50 | 50 | 7.06E-02 |
| 150 | 400 | 1.03E+00 | 50 | 600 | 1.36E-01 |

Table C.1: Dark matter masses $m_\chi$ and mediator masses $m_\Phi$ generated for $g = 1$ for 13 TeV. The resulting production cross sections are given in pb.

## C.2 Cross sections for b−flavored Dark Matter

## C.3 Cross sections for the $t\bar{t}$+DM scalar simplified model

Table C.5: Cross section calculation for each coupling choice and minimal width assumption for the $t\bar{t}$+DM scalar simplified model grid

| Coupling (g) | $m_{Phi}$ [GeV] | $m_\chi$ [GeV] | $\Gamma_{min}$ [GeV] | $\sigma$ [pb] |
|---|---|---|---|---|
| 0.1 | 10 | 1 | 0.00374 | 0.1955 ± 0.00066 |
| 0.1 | 20 | 1 | 0.00785 | 0.1054 ± 0.00031 |
| 0.1 | 50 | 1 | 0.0199 | 0.03011 ± 9.1e-05 |
| 0.1 | 100 | 1 | 0.0398 | 0.006867 ± 2.5e-05 |
| 0.1 | 200 | 1 | 0.0797 | 0.0009397 ± 2.6e-06 |
| 0.1 | 300 | 1 | 0.120 | 0.0002942 ± 1e-06 |
| 0.1 | 500 | 1 | 0.311 | 5.289e-05 ± 1.9e-07 |
| 0.1 | 1000 | 1 | 0.881 | 3.717e-06 ± 1.5e-08 |

Continued on next page

Table C.5 – continued from previous page

| Coupling (g) | $m_{Phi}$ [GeV] | $m_{\chi}$ [GeV] | $\Gamma_{min}$ [GeV] | $\sigma$ [pb] |
|---|---|---|---|---|
| 0.1 | 2000 | 1 | 1.91 | 7.81e-08 ± 3.2e-10 |
| 0.1 | 5000 | 1 | 4.89 | 1.111e-11 ± 5.5e-14 |
| 0.1 | 10 | 10 | 6.33 | 9.418e-06 ± 3.6e-08 |
| 0.1 | 50 | 10 | 0.0153 | 0.03016 ± 8.1e-05 |
| 0.1 | 100 | 10 | 0.0375 | 0.00686 ± 2.2e-05 |
| 0.1 | 5000 | 10 | 4.89 | 1.095e-11 ± 5.8e-14 |
| 0.1 | 15 | 10 | 3.84 | 1.2e-05 ± 4.8e-08 |
| 0.1 | 10 | 50 | 6.33 | 1.914e-07 ± 7.2e-10 |
| 0.1 | 50 | 50 | 2.34e-05 | 2.323e-07 ± 8.8e-10 |
| 0.1 | 200 | 50 | 0.0518 | 0.0009421 ± 2.8e-06 |
| 0.1 | 300 | 50 | 0.100 | 0.0002954 ± 9.8e-07 |
| 0.1 | 5000 | 50 | 4.88 | 1.059e-11 ± 5.3e-14 |
| 0.1 | 95 | 50 | 4.66e-05 | 6.548e-07 ± 2.3e-09 |
| 0.1 | 10 | 150 | 6.33 | 8.684e-09 ± 4.1e-11 |
| 0.1 | 200 | 150 | 0.000107 | 1.296e-08 ± 5.3e-11 |
| 0.1 | 500 | 150 | 0.214 | 3.92e-05 ± 1.6e-07 |
| 0.1 | 5000 | 150 | 4.87 | 9.079e-12 ± 5.9e-14 |
| 0.1 | 295 | 150 | 0.000185 | 3.969e-08 ± 2e-10 |
| 0.1 | 10 | 500 | 6.33 | 7.367e-11 ± 3.2e-13 |
| 0.1 | 500 | 500 | 0.112 | 9.86e-11 ± 3.9e-13 |
| 0.1 | 2000 | 500 | 1.63 | 5.953e-08 ± 2.3e-10 |
| 0.1 | 5000 | 500 | 4.77 | 5.768e-12 ± 2.6e-14 |
| 0.1 | 995 | 500 | 0.480 | 8.67e-10 ± 3.6e-12 |
| 0.1 | 10 | 1000 | 6.33 | 6.576e-13 ± 2.8e-15 |
| 0.1 | 1000 | 1000 | 0.483 | 9.426e-13 ± 4.2e-15 |
| 0.1 | 5000 | 1000 | 4.43 | 4.314e-12 ± 2e-14 |
| 0.1 | 1995 | 1000 | 1.11 | 1.589e-11 ± 9.2e-14 |
| 0.3 | 10 | 1 | 0.0337 | 1.766 ± 0.006 |
| 0.3 | 20 | 1 | 0.0706 | 0.9493 ± 0.0029 |
| 0.3 | 50 | 1 | 0.179 | 0.2695 ± 0.00082 |
| 0.3 | 100 | 1 | 0.358 | 0.06159 ± 0.00021 |
| 0.3 | 200 | 1 | 0.717 | 0.008466 ± 2.4e-05 |
| 0.3 | 300 | 1 | 1.08 | 0.002649 ± 8.5e-06 |
| 0.3 | 500 | 1 | 2.80 | 0.0004741 ± 1.6e-06 |
| 0.3 | 1000 | 1 | 7.93 | 3.349e-05 ± 1.3e-07 |
| 0.3 | 2000 | 1 | 17.2 | 7.227e-07 ± 3.2e-09 |
| 0.3 | 5000 | 1 | 44.0 | 5.42e-10 ± 3.5e-12 |
| 0.3 | 10 | 10 | 5.70 | 0.0007633 ± 2.5e-06 |
| 0.3 | 50 | 10 | 0.138 | 0.2706 ± 0.00082 |
| 0.3 | 100 | 10 | 0.337 | 0.06182 ± 0.00022 |
| 0.3 | 5000 | 10 | 44.0 | 5.386e-10 ± 2.7e-12 |
| 0.3 | 15 | 10 | 3.45e-05 | 0.0009761 ± 3.6e-06 |
| 0.3 | 10 | 50 | 5.70 | 1.561e-05 ± 6.1e-08 |
| 0.3 | 50 | 50 | 0.000210 | 1.892e-05 ± 7.3e-08 |
| 0.3 | 200 | 50 | 0.466 | 0.008444 ± 2.2e-05 |

Continued on next page

Table C.5 – continued from previous page

| Coupling (g) | $m_{Phi}$ [GeV] | $m_{\chi}$ [GeV] | $\Gamma_{min}$ [GeV] | $\sigma$ [pb] |
|---|---|---|---|---|
| 0.3 | 300 | 50 | 0.902 | 0.002677 ± 7.7e-06 |
| 0.3 | 5000 | 50 | 44.0 | 5.012e-10 ± 3.1e-12 |
| 0.3 | 95 | 50 | 0.000420 | 5.306e-05 ± 2.3e-07 |
| 0.3 | 10 | 150 | 5.70 | 7.02e-07 ± 3.3e-09 |
| 0.3 | 200 | 150 | 0.000962 | 1.051e-06 ± 4.1e-09 |
| 0.3 | 500 | 150 | 1.92 | 0.000351 ± 1.3e-06 |
| 0.3 | 5000 | 150 | 43.9 | 3.805e-10 ± 2.4e-12 |
| 0.3 | 295 | 150 | 0.00166 | 3.211e-06 ± 1.5e-08 |
| 0.3 | 10 | 500 | 5.70 | 5.945e-09 ± 2.7e-11 |
| 0.3 | 500 | 500 | 1.01 | 7.991e-09 ± 4.9e-11 |
| 0.3 | 2000 | 500 | 14.7 | 5.347e-07 ± 2.3e-09 |
| 0.3 | 5000 | 500 | 42.9 | 1.264e-10 ± 6.9e-13 |
| 0.3 | 995 | 500 | 4.32 | 7.039e-08 ± 3e-10 |
| 0.3 | 10 | 1000 | 5.70 | 5.302e-11 ± 2.4e-13 |
| 0.3 | 1000 | 1000 | 4.35 | 7.606e-11 ± 3.4e-13 |
| 0.3 | 5000 | 1000 | 39.8 | 4.887e-11 ± 2.1e-13 |
| 0.3 | 1995 | 1000 | 10.0 | 1.279e-09 ± 6.4e-12 |
| 0.7 | 10 | 1 | 0.183 | 9.624 ± 0.034 |
| 0.7 | 20 | 1 | 0.384 | 5.129 ± 0.015 |
| 0.7 | 50 | 1 | 0.974 | 1.461 ± 0.0048 |
| 0.7 | 100 | 1 | 1.95 | 0.3324 ± 0.0014 |
| 0.7 | 200 | 1 | 3.90 | 0.04588 ± 0.00013 |
| 0.7 | 300 | 1 | 5.86 | 0.01442 ± 5e-05 |
| 0.7 | 500 | 1 | 15.2 | 0.002548 ± 9.6e-06 |
| 0.7 | 1000 | 1 | 43.2 | 0.0001813 ± 8.9e-07 |
| 0.7 | 2000 | 1 | 93.7 | 4.478e-06 ± 1.9e-08 |
| 0.7 | 5000 | 1 | 239 | 1.504e-08 ± 6.7e-11 |
| 0.7 | 10 | 10 | 3.10e-05 | 0.02264 ± 8.3e-05 |
| 0.7 | 50 | 10 | 0.752 | 1.462 ± 0.0041 |
| 0.7 | 100 | 10 | 1.84 | 0.3347 ± 0.0011 |
| 0.7 | 5000 | 10 | 239 | 1.494e-08 ± 6.7e-11 |
| 0.7 | 15 | 10 | 0.000188 | 0.02881 ± 0.00011 |
| 0.7 | 10 | 50 | 3.10e-05 | 0.0004597 ± 1.8e-06 |
| 0.7 | 50 | 50 | 0.00114 | 0.0005588 ± 2.3e-06 |
| 0.7 | 200 | 50 | 2.54 | 0.0458 ± 0.00013 |
| 0.7 | 300 | 50 | 4.91 | 0.01433 ± 4.9e-05 |
| 0.7 | 5000 | 50 | 239 | 1.363e-08 ± 6.9e-11 |
| 0.7 | 95 | 50 | 0.00228 | 0.00157 ± 7.3e-06 |
| 0.7 | 10 | 150 | 3.10e-05 | 2.097e-05 ± 8.5e-08 |
| 0.7 | 200 | 150 | 0.00524 | 3.123e-05 ± 1.6e-07 |
| 0.7 | 500 | 150 | 10.5 | 0.001889 ± 6.8e-06 |
| 0.7 | 5000 | 150 | 239 | 1.018e-08 ± 5.2e-11 |
| 0.7 | 295 | 150 | 0.00906 | 9.511e-05 ± 4e-07 |
| 0.7 | 10 | 500 | 3.10e-05 | 1.78e-07 ± 6.8e-10 |
| 0.7 | 500 | 500 | 5.48 | 2.373e-07 ± 9.8e-10 |

Continued on next page

Table C.5 – continued from previous page

| Coupling (g) | $m_{Phi}$ [GeV] | $m_{\chi}$ [GeV] | $\Gamma_{min}$ [GeV] | $\sigma$ [pb] |
|---|---|---|---|---|
| 0.7 | 2000 | 500 | 80.0 | 2.877e-06 ± 1.2e-08 |
| 0.7 | 5000 | 500 | 234 | 2.682e-09 ± 1.7e-11 |
| 0.7 | 995 | 500 | 23.5 | 1.939e-06 ± 7.3e-09 |
| 0.7 | 10 | 1000 | 3.10e-05 | 1.584e-09 ± 7.6e-12 |
| 0.7 | 1000 | 1000 | 23.7 | 2.26e-09 ± 1.1e-11 |
| 0.7 | 5000 | 1000 | 217 | 5.244e-10 ± 2.4e-12 |
| 0.7 | 1995 | 1000 | 54.52 | 3.227e-08 ± 1.4e-10 |
| 1. | 10 | 1 | 0.374 | 19.59 ± 0.062 |
| 1. | 20 | 1 | 0.785 | 10.48 ± 0.03 |
| 1. | 50 | 1 | 1.99 | 2.941 ± 0.0091 |
| 1. | 100 | 1 | 3.98 | 0.6723 ± 0.0024 |
| 1. | 200 | 1 | 7.97 | 0.09327 ± 0.00029 |
| 1. | 300 | 1 | 12.0 | 0.0295 ± 0.00011 |
| 1. | 500 | 1 | 31.1 | 0.00518 ± 2.2e-05 |
| 1. | 1000 | 1 | 88.1 | 0.0003687 ± 1.7e-06 |
| 1. | 2000 | 1 | 191 | 1.034e-05 ± 4.6e-08 |
| 1. | 5000 | 1 | 489 | 6.17e-08 ± 2.4e-10 |
| 1. | 10 | 10 | 6.33e-05 | 0.09487 ± 0.00036 |
| 1. | 50 | 10 | 1.53 | 2.942 ± 0.0083 |
| 1. | 100 | 10 | 3.75 | 0.6732 ± 0.0023 |
| 1. | 5000 | 10 | 489 | 6.138e-08 ± 2.3e-10 |
| 1. | 15 | 10 | 0.000384 | 0.1202 ± 0.0005 |
| 1. | 10 | 50 | 6.33e-05 | 0.001906 ± 8.4e-06 |
| 1. | 50 | 50 | 0.00234 | 0.002329 ± 1e-05 |
| 1. | 200 | 50 | 5.18 | 0.09224 ± 0.00025 |
| 1. | 300 | 50 | 10.0 | 0.02901 ± 0.0001 |
| 1. | 5000 | 50 | 488 | 5.616e-08 ± 2.2e-10 |
| 1. | 95 | 50 | 0.00466 | 0.006558 ± 2.7e-05 |
| 1. | 10 | 150 | 6.33e-05 | 8.634e-05 ± 4e-07 |
| 1. | 200 | 150 | 0.0107 | 0.00013 ± 5.7e-07 |
| 1. | 500 | 150 | 21.4 | 0.003754 ± 1.9e-05 |
| 1. | 5000 | 150 | 487 | 4.162e-08 ± 1.8e-10 |
| 1. | 295 | 150 | 0.0185 | 0.000394 ± 1.6e-06 |
| 1. | 10 | 500 | 6.33e-05 | 7.356e-07 ± 3.3e-09 |
| 1. | 500 | 500 | 11.2 | 9.894e-07 ± 5e-09 |
| 1. | 2000 | 500 | 163 | 5.808e-06 ± 2.4e-08 |
| 1. | 5000 | 500 | 477 | 1.048e-08 ± 5.7e-11 |
| 1. | 995 | 500 | 48.0 | 7.3e-06 ± 3.2e-08 |
| 1. | 10 | 1000 | 6.33e-05 | 6.607e-09 ± 2.7e-11 |
| 1. | 1000 | 1000 | 48.3 | 9.433e-09 ± 4e-11 |
| 1. | 5000 | 1000 | 443 | 1.7e-09 ± 1e-11 |
| 1. | 1995 | 1000 | 111 | 1.108e-07 ± 5.7e-10 |
| 1.5 | 10 | 1 | 0.842 | 44.1 ± 0.16 |
| 1.5 | 20 | 1 | 1.77 | 23.19 ± 0.078 |
| 1.5 | 50 | 1 | 4.47 | 6.471 ± 0.02 |

Continued on next page

Table C.5 – continued from previous page

| Coupling (g) | $m_{Phi}$ [GeV] | $m_{\chi}$ [GeV] | $\Gamma_{min}$ [GeV] | $\sigma$ [pb] |
|---|---|---|---|---|
| 1.5 | 100 | 1 | 8.96 | 1.478 ± 0.0061 |
| 1.5 | 200 | 1 | 17.9 | 0.2074 ± 0.00068 |
| 1.5 | 300 | 1 | 26.9 | 0.0657 ± 0.00024 |
| 1.5 | 500 | 1 | 69.9 | 0.01123 ± 5.6e-05 |
| 1.5 | 1000 | 1 | 198 | 0.0008135 ± 3.5e-06 |
| 1.5 | 2000 | 1 | 430 | 2.873e-05 ± 1.2e-07 |
| 1.5 | 5000 | 1 | 1099 | 2.964e-07 ± 1.2e-09 |
| 1.5 | 10 | 10 | 0.000143 | 0.4772 ± 0.0019 |
| 1.5 | 50 | 10 | 3.45 | 6.499 ± 0.022 |
| 1.5 | 100 | 10 | 8.43 | 1.469 ± 0.0056 |
| 1.5 | 5000 | 10 | 1099 | 2.932e-07 ± 1.3e-09 |
| 1.5 | 15 | 10 | 0.000863 | 0.613 ± 0.0022 |
| 1.5 | 10 | 50 | 0.000143 | 0.009661 ± 3.4e-05 |
| 1.5 | 50 | 50 | 0.00526 | 0.0118 ± 4.2e-05 |
| 1.5 | 200 | 50 | 11.7 | 0.2032 ± 0.00064 |
| 1.5 | 300 | 50 | 22.6 | 0.06446 ± 0.00024 |
| 1.5 | 5000 | 50 | 1099 | 2.687e-07 ± 1.2e-09 |
| 1.5 | 95 | 50 | 0.0105 | 0.03298 ± 0.00013 |
| 1.5 | 10 | 150 | 0.000143 | 0.0004384 ± 1.8e-06 |
| 1.5 | 200 | 150 | 0.0241 | 0.0006557 ± 2.7e-06 |
| 1.5 | 500 | 150 | 48.1 | 0.008036 ± 3.9e-05 |
| 1.5 | 5000 | 150 | 1097 | 2.008e-07 ± 1.4e-09 |
| 1.5 | 295 | 150 | 0.0416 | 0.002022 ± 8.3e-06 |
| 1.5 | 10 | 500 | 0.000143 | 3.712e-06 ± 1.5e-08 |
| 1.5 | 500 | 500 | 25.2 | 5.001e-06 ± 1.9e-08 |
| 1.5 | 2000 | 500 | 367 | 1.223e-05 ± 6e-08 |
| 1.5 | 5000 | 500 | 1072 | 4.885e-08 ± 2.7e-10 |
| 1.5 | 995 | 500 | 108 | 2.975e-05 ± 1.5e-07 |
| 1.5 | 10 | 1000 | 0.000143 | 3.342e-08 ± 1.5e-10 |
| 1.5 | 1000 | 1000 | 109 | 4.786e-08 ± 2.1e-10 |
| 1.5 | 5000 | 1000 | 996 | 6.688e-09 ± 3.1e-11 |
| 1.5 | 1995 | 1000 | 250 | 3.982e-07 ± 2.2e-09 |
| 2. | 10 | 1 | 1.50 | 78.28 ± 0.3 |
| 2. | 20 | 1 | 3.14 | 40.52 ± 0.13 |
| 2. | 50 | 1 | 7.95 | 11.12 ± 0.038 |
| 2. | 100 | 1 | 15.9 | 2.531 ± 0.011 |
| 2. | 200 | 1 | 31.9 | 0.3644 ± 0.0012 |
| 2. | 300 | 1 | 47.8 | 0.1157 ± 0.00053 |
| 2. | 500 | 1 | 124 | 0.01917 ± 9e-05 |
| 2. | 1000 | 1 | 353 | 0.001382 ± 6.1e-06 |
| 2. | 2000 | 1 | 765 | 5.899e-05 ± 2.7e-07 |
| 2. | 5000 | 1 | 1954 | 8.392e-07 ± 3.4e-09 |
| 2. | 10 | 10 | 0.0002532 | 1.509 ± 0.0052 |
| 2. | 50 | 10 | 6.14 | 11.19 ± 0.037 |
| 2. | 100 | 10 | 15.0 | 2.513 ± 0.0091 |

Continued on next page

Table C.5 – continued from previous page

| Coupling (g) | $m_{Phi}$ [GeV] | $m_{\chi}$ [GeV] | $\Gamma_{min}$ [GeV] | $\sigma$ [pb] |
|---|---|---|---|---|
| 2. | 5000 | 10 | 1954 | 8.317e-07 ± 3.6e-09 |
| 2. | 15 | 10 | 0.00153 | 1.923 ± 0.0066 |
| 2. | 10 | 50 | 0.000253 | 0.03065 ± 0.00011 |
| 2. | 50 | 50 | 0.00934 | 0.03716 ± 0.00018 |
| 2. | 200 | 50 | 20.7 | 0.3487 ± 0.0011 |
| 2. | 300 | 50 | 40.1 | 0.1114 ± 0.00041 |
| 2. | 5000 | 50 | 1953 | 7.612e-07 ± 4e-09 |
| 2. | 95 | 50 | 0.0187 | 0.1045 ± 0.0005 |
| 2. | 10 | 150 | 0.000253 | 0.001376 ± 6.3e-06 |
| 2. | 200 | 150 | 0.0428 | 0.002081 ± 9.1e-06 |
| 2. | 500 | 150 | 85.5 | 0.01343 ± 5.5e-05 |
| 2. | 5000 | 150 | 1950 | 5.605e-07 ± 3e-09 |
| 2. | 295 | 150 | 0.0740 | 0.006316 ± 2.8e-05 |
| 2. | 10 | 500 | 0.000253 | 1.177e-05 ± 4.8e-08 |
| 2. | 500 | 500 | 44.8 | 1.586e-05 ± 8.6e-08 |
| 2. | 2000 | 500 | 653 | 1.953e-05 ± 9.5e-08 |
| 2. | 5000 | 500 | 1907 | 1.333e-07 ± 6.5e-10 |
| 2. | 995 | 500 | 192 | 7.427e-05 ± 3.9e-07 |
| 2. | 10 | 1000 | 0.000253 | 1.056e-07 ± 5e-10 |
| 2. | 1000 | 1000 | 193 | 1.507e-07 ± 6.7e-10 |
| 2. | 5000 | 1000 | 1771 | 1.624e-08 ± 6.7e-11 |
| 2. | 1995 | 1000 | 445 | 8.764e-07 ± 5.3e-09 |
| 2.5 | 10 | 1 | 2.34 | 122.2 ± 0.44 |
| 2.5 | 20 | 1 | 4.90 | 61.98 ± 0.21 |
| 2.5 | 50 | 1 | 12.4 | 16.62 ± 0.057 |
| 2.5 | 100 | 1 | 24.9 | 3.788 ± 0.016 |
| 2.5 | 200 | 1 | 49.8 | 0.551 ± 0.0021 |
| 2.5 | 300 | 1 | 74.7 | 0.1762 ± 0.00073 |
| 2.5 | 500 | 1 | 194 | 0.02816 ± 0.00014 |
| 2.5 | 1000 | 1 | 551 | 0.001971 ± 8.5e-06 |
| 2.5 | 2000 | 1 | 1195 | 9.628e-05 ± 4.1e-07 |
| 2.5 | 5000 | 1 | 3053 | 1.685e-06 ± 6.9e-09 |
| 2.5 | 10 | 10 | 0.000396 | 3.687 ± 0.016 |
| 2.5 | 50 | 10 | 9.59 | 16.9 ± 0.064 |
| 2.5 | 100 | 10 | 23.4 | 3.755 ± 0.014 |
| 2.5 | 5000 | 10 | 3053 | 1.68e-06 ± 6.7e-09 |
| 2.5 | 15 | 10 | 0.00240 | 4.719 ± 0.016 |
| 2.5 | 10 | 50 | 0.000396 | 0.07571 ± 0.00036 |
| 2.5 | 50 | 50 | 0.0146 | 0.09133 ± 0.00038 |
| 2.5 | 200 | 50 | 32.4 | 0.5224 ± 0.0016 |
| 2.5 | 300 | 50 | 62.6 | 0.1667 ± 0.00074 |
| 2.5 | 5000 | 50 | 3052 | 1.519e-06 ± 8e-09 |
| 2.5 | 95 | 50 | 0.0291 | 0.2547 ± 0.00089 |
| 2.5 | 10 | 150 | 0.000396 | 0.003396 ± 1.7e-05 |
| 2.5 | 200 | 150 | 0.0668 | 0.005081 ± 2.2e-05 |

Continued on next page

Table C.5 – continued from previous page

| Coupling (g) | $m_{Phi}$ [GeV] | $m_{\chi}$ [GeV] | $\Gamma_{min}$ [GeV] | $\sigma$ [pb] |
|---|---|---|---|---|
| 2.5 | 500 | 150 | 133 | 0.01954 ± 8.7e-05 |
| 2.5 | 5000 | 150 | 3046 | 1.123e-06 ± 6.5e-09 |
| 2.5 | 295 | 150 | 0.116 | 0.01551 ± 6.8e-05 |
| 2.5 | 10 | 500 | 0.000396 | 2.874e-05 ± 1.2e-07 |
| 2.5 | 500 | 500 | 69.95 | 3.883e-05 ± 1.9e-07 |
| 2.5 | 2000 | 500 | 1020 | 2.555e-05 ± 1.2e-07 |
| 2.5 | 5000 | 500 | 2979 | 2.592e-07 ± 1.3e-09 |
| 2.5 | 995 | 500 | 300 | 0.0001417 ± 8e-07 |
| 2.5 | 10 | 1000 | 0.0003957 | 2.584e-07 ± 1.2e-09 |
| 2.5 | 1000 | 1000 | 302.2 | 3.668e-07 ± 1.5e-09 |
| 2.5 | 5000 | 1000 | 2767 | 2.841e-08 ± 1.3e-10 |
| 2.5 | 1995 | 1000 | 695.4 | 1.487e-06 ± 7.2e-09 |
| 3. | 10 | 1 | 3.369 | 176.2 ± 0.67 |
| 3. | 20 | 1 | 7.061 | 87.59 ± 0.35 |
| 3. | 50 | 1 | 17.88 | 22.91 ± 0.078 |
| 3. | 100 | 1 | 35.83 | 5.118 ± 0.024 |
| 3. | 200 | 1 | 71.71 | 0.7647 ± 0.0027 |
| 3. | 300 | 1 | 107.6 | 0.2474 ± 0.001 |
| 3. | 500 | 1 | 279.8 | 0.0379 ± 0.00019 |
| 3. | 1000 | 1 | 793.2 | 0.002521 ± 1.4e-05 |
| 3. | 2000 | 1 | 1720 | 0.0001342 ± 4.9e-07 |
| 3. | 5000 | 1 | 4396 | 2.668e-06 ± 1e-08 |
| 3. | 10 | 10 | 0.0005698 | 7.631 ± 0.029 |
| 3. | 50 | 10 | 13.81 | 23.27 ± 0.083 |
| 3. | 100 | 10 | 33.73 | 5.138 ± 0.019 |
| 3. | 5000 | 10 | 4396 | 2.62e-06 ± 1e-08 |
| 3. | 15 | 10 | 0.003453 | 9.7 ± 0.044 |
| 3. | 10 | 50 | 0.0005698 | 0.1553 ± 0.00062 |
| 3. | 50 | 50 | 0.02102 | 0.1886 ± 0.0008 |
| 3. | 200 | 50 | 46.61 | 0.7242 ± 0.0023 |
| 3. | 300 | 50 | 90.2 | 0.2308 ± 0.0012 |
| 3. | 5000 | 50 | 4395 | 2.394e-06 ± 1.4e-08 |
| 3. | 95 | 50 | 0.04196 | 0.5301 ± 0.0019 |
| 3. | 10 | 150 | 0.0005698 | 0.007036 ± 3.3e-05 |
| 3. | 200 | 150 | 0.09621 | 0.01053 ± 4.4e-05 |
| 3. | 500 | 150 | 192.4 | 0.02598 ± 0.00012 |
| 3. | 5000 | 150 | 4387 | 1.767e-06 ± 1.2e-08 |
| 3. | 295 | 150 | 0.1664 | 0.03185 ± 0.00013 |
| 3. | 10 | 500 | 0.0005698 | 5.989e-05 ± 2.7e-07 |
| 3. | 500 | 500 | 100.7 | 7.985e-05 ± 3.1e-07 |
| 3. | 2000 | 500 | 1469 | 3.073e-05 ± 1.6e-07 |
| 3. | 5000 | 500 | 4290 | 3.921e-07 ± 1.8e-09 |
| 3. | 995 | 500 | 432.1 | 0.0002263 ± 9.7e-07 |
| 3. | 10 | 1000 | 0.0005698 | 5.337e-07 ± 2.3e-09 |
| 3. | 1000 | 1000 | 435.1 | 7.512e-07 ± 4.1e-09 |

Continued on next page

Table C.5 – continued from previous page

| Coupling (g) | $m_{Phi}$ [GeV] | $m_{\chi}$ [GeV] | $\Gamma_{min}$ [GeV] | $\sigma$ [pb] |
|---|---|---|---|---|
| 3. | 5000 | 1000 | 3984 | 4.011e-08 ± 1.7e-10 |
| 3. | 1995 | 1000 | 1001 | 2.15e-06 ± 1e-08 |
| 3.5 | 10 | 1 | 4.585 | 242 ± 0.94 |
| 3.5 | 20 | 1 | 9.611 | 116.6 ± 0.36 |
| 3.5 | 50 | 1 | 24.34 | 29.39 ± 0.093 |
| 3.5 | 100 | 1 | 48.77 | 6.585 ± 0.027 |
| 3.5 | 200 | 1 | 97.6 | 0.993 ± 0.0042 |
| 3.5 | 300 | 1 | 146.4 | 0.3235 ± 0.0019 |
| 3.5 | 500 | 1 | 380.8 | 0.04713 ± 0.00021 |
| 3.5 | 1000 | 1 | 1080 | 0.00299 ± 1.5e-05 |
| 3.5 | 2000 | 1 | 2341 | 0.0001649 ± 6.2e-07 |
| 3.5 | 5000 | 1 | 5984 | 3.53e-06 ± 1.8e-08 |
| 3.5 | 10 | 10 | 0.0007756 | 14.23 ± 0.052 |
| 3.5 | 50 | 10 | 18.79 | 30.44 ± 0.11 |
| 3.5 | 100 | 10 | 45.91 | 6.51 ± 0.024 |
| 3.5 | 5000 | 10 | 5984 | 3.514e-06 ± 1.3e-08 |
| 3.5 | 15 | 10 | 0.004699 | 18.1 ± 0.067 |
| 3.5 | 10 | 50 | 0.0007756 | 0.2893 ± 0.0011 |
| 3.5 | 50 | 50 | 0.02861 | 0.3505 ± 0.0017 |
| 3.5 | 200 | 50 | 63.45 | 0.9325 ± 0.0035 |
| 3.5 | 300 | 50 | 122.8 | 0.2972 ± 0.0014 |
| 3.5 | 5000 | 50 | 5982 | 3.185e-06 ± 1.7e-08 |
| 3.5 | 95 | 50 | 0.05711 | 0.981 ± 0.0043 |
| 3.5 | 10 | 150 | 0.0007756 | 0.01295 ± 6.7e-05 |
| 3.5 | 200 | 150 | 0.131 | 0.01947 ± 8.7e-05 |
| 3.5 | 500 | 150 | 261.9 | 0.03264 ± 0.00016 |
| 3.5 | 5000 | 150 | 5971 | 2.316e-06 ± 1.3e-08 |
| 3.5 | 295 | 150 | 0.2265 | 0.05947 ± 0.00026 |
| 3.5 | 10 | 500 | 0.0007756 | 0.0001104 ± 4.8e-07 |
| 3.5 | 500 | 500 | 137.1 | 0.0001486 ± 7.1e-07 |
| 3.5 | 2000 | 500 | 2000 | 3.401e-05 ± 1.5e-07 |
| 3.5 | 5000 | 500 | 5839 | 5.061e-07 ± 2.6e-09 |
| 3.5 | 995 | 500 | 588.1 | 0.0003275 ± 1.4e-06 |
| 3.5 | 10 | 1000 | 0.0007756 | 9.835e-07 ± 4.7e-09 |
| 3.5 | 1000 | 1000 | 592.2 | 1.401e-06 ± 7.5e-09 |
| 3.5 | 5000 | 1000 | 5423 | 4.878e-08 ± 2.5e-10 |
| 3.5 | 1995 | 1000 | 1363 | 2.809e-06 ± 1.2e-08 |

Table C.6: Cross section calculation for each coupling choice and minimal width assumption for the $t\bar{t}$+DM pseudoscalar simplified model grid

| Coupling (g) | $m_{Phi}$ [GeV] | $m_{\chi}$ [GeV] | $\Gamma_{min}$ [GeV] | $\sigma$ [pb] |
|---|---|---|---|---|
| 0.1 | 10 | 1 | 0.004 | 0.004237 ± 1.8e-05 |

Continued on next page

Table C.6 – continued from previous page

| Coupling (g) | $m_{Phi}$ [GeV] | $m_{\chi}$ [GeV] | $\Gamma_{min}$ [GeV] | $\sigma$ [pb] |
|---|---|---|---|---|
| 0.1 | 20 | 1 | 0.008 | 0.003931 ± 1.5e-05 |
| 0.1 | 50 | 1 | 0.02 | 0.003005 ± 1.4e-05 |
| 0.1 | 100 | 1 | 0.04 | 0.001905 ± 8.1e-06 |
| 0.1 | 200 | 1 | 0.08 | 0.0008608 ± 3.3e-06 |
| 0.1 | 300 | 1 | 0.12 | 0.0004105 ± 1.6e-06 |
| 0.1 | 500 | 1 | 0.413 | 5.591e-05 ± 2.2e-07 |
| 0.1 | 1000 | 1 | 0.949 | 3.961e-06 ± 1.7e-08 |
| 0.1 | 2000 | 1 | 1.95 | 7.961e-08 ± 3.2e-10 |
| 0.1 | 5000 | 1 | 4.9 | 1.19e-11 ± 7.1e-14 |
| 0.1 | 10 | 10 | 2.0 | 1.489e-06 ± 9.6e-09 |
| 0.1 | 50 | 10 | 0.018 | 0.003 ± 1.5e-05 |
| 0.1 | 100 | 10 | 0.04 | 0.001926 ± 1e-05 |
| 0.1 | 5000 | 10 | 4.9 | 1.179e-11 ± 6.2e-14 |
| 0.1 | 15 | 10 | 5.9 | 1.798e-06 ± 1e-08 |
| 0.1 | 10 | 50 | 2.0 | 2.42e-07 ± 1.1e-09 |
| 0.1 | 50 | 50 | 2.5e-05 | 2.97e-07 ± 1.2e-09 |
| 0.1 | 200 | 50 | 0.069 | 0.0008585 ± 4.7e-06 |
| 0.1 | 300 | 50 | 0.11 | 0.0004108 ± 1.7e-06 |
| 0.1 | 5000 | 50 | 4.9 | 1.166e-11 ± 6.5e-14 |
| 0.1 | 95 | 50 | 5.4e-05 | 1.065e-06 ± 5.7e-09 |
| 0.1 | 10 | 150 | 2.0 | 2.359e-08 ± 1.2e-10 |
| 0.1 | 200 | 150 | 0.00019 | 4.119e-08 ± 2e-10 |
| 0.1 | 500 | 150 | 0.37 | 4.953e-05 ± 1.9e-07 |
| 0.1 | 5000 | 150 | 4.9 | 1.066e-11 ± 7.3e-14 |
| 0.1 | 295 | 150 | 0.00063 | 3.366e-07 ± 1.8e-09 |
| 0.1 | 10 | 500 | 2.0 | 2.276e-10 ± 9.7e-13 |
| 0.1 | 500 | 500 | 0.21 | 3.261e-10 ± 1.4e-12 |
| 0.1 | 2000 | 500 | 1.84 | 7.296e-08 ± 2.9e-10 |
| 0.1 | 5000 | 500 | 4.86 | 6.723e-12 ± 3.1e-14 |
| 0.1 | 995 | 500 | 0.55 | 1.418e-08 ± 9.2e-11 |
| 0.1 | 10 | 1000 | 2.0 | 2.593e-12 ± 1.2e-14 |
| 0.1 | 1000 | 1000 | 0.55 | 3.939e-12 ± 1.5e-14 |
| 0.1 | 5000 | 1000 | 4.74 | 4.964e-12 ± 2.1e-14 |
| 0.1 | 1995 | 1000 | 1.15 | 4.176e-10 ± 2.2e-12 |
| 0.3 | 10 | 1 | 0.035 | 0.03821 ± 0.0002 |
| 0.3 | 20 | 1 | 0.071 | 0.03519 ± 0.00017 |
| 0.3 | 50 | 1 | 0.179 | 0.02707 ± 0.00012 |
| 0.3 | 100 | 1 | 0.359 | 0.01728 ± 7e-05 |
| 0.3 | 200 | 1 | 0.718 | 0.007718 ± 3e-05 |
| 0.3 | 300 | 1 | 1.08 | 0.003678 ± 1.5e-05 |
| 0.3 | 500 | 1 | 3.72 | 0.0004992 ± 1.9e-06 |
| 0.3 | 1000 | 1 | 8.54 | 3.541e-05 ± 1.5e-07 |
| 0.3 | 2000 | 1 | 17.5 | 7.434e-07 ± 2.9e-09 |
| 0.3 | 5000 | 1 | 44.1 | 6.065e-10 ± 3.3e-12 |
| 0.3 | 10 | 10 | 1.8e-05 | 0.0001216 ± 7.6e-07 |

Continued on next page

Table C.6 – continued from previous page

| Coupling (g) | $m_{Phi}$ [GeV] | $m_{\chi}$ [GeV] | $\Gamma_{min}$ [GeV] | $\sigma$ [pb] |
|---|---|---|---|---|
| 0.3 | 50 | 10 | 0.164 | 0.0273 ± 0.00013 |
| 0.3 | 100 | 10 | 0.351 | 0.01718 ± 6.8e-05 |
| 0.3 | 5000 | 10 | 44.1 | 6.164e-10 ± 4.3e-12 |
| 0.3 | 15 | 10 | 5.3e-05 | 0.0001503 ± 8.7e-07 |
| 0.3 | 10 | 50 | 1.8e-05 | 1.985e-05 ± 1e-07 |
| 0.3 | 50 | 50 | 0.000226 | 2.405e-05 ± 1.1e-07 |
| 0.3 | 200 | 50 | 0.622 | 0.007692 ± 2.8e-05 |
| 0.3 | 300 | 50 | 1.02 | 0.003682 ± 1.5e-05 |
| 0.3 | 5000 | 50 | 44.1 | 6.003e-10 ± 3.4e-12 |
| 0.3 | 95 | 50 | 0.00049 | 8.676e-05 ± 5.3e-07 |
| 0.3 | 10 | 150 | 1.8e-05 | 1.91e-06 ± 8.5e-09 |
| 0.3 | 200 | 150 | 0.00173 | 3.362e-06 ± 1.4e-08 |
| 0.3 | 500 | 150 | 3.36 | 0.0004437 ± 1.9e-06 |
| 0.3 | 5000 | 150 | 44.1 | 5.071e-10 ± 2.9e-12 |
| 0.3 | 295 | 150 | 0.00568 | 2.746e-05 ± 1.9e-07 |
| 0.3 | 10 | 500 | 1.8e-05 | 1.837e-08 ± 8.7e-11 |
| 0.3 | 500 | 500 | 1.93 | 2.647e-08 ± 1.1e-10 |
| 0.3 | 2000 | 500 | 16.6 | 6.605e-07 ± 2.6e-09 |
| 0.3 | 5000 | 500 | 43.8 | 1.956e-10 ± 1e-12 |
| 0.3 | 995 | 500 | 4.93 | 1.111e-06 ± 5.3e-09 |
| 0.3 | 10 | 1000 | 1.8e-05 | 2.107e-10 ± 8.3e-13 |
| 0.3 | 1000 | 1000 | 4.96 | 3.169e-10 ± 1.3e-12 |
| 0.3 | 5000 | 1000 | 42.6 | 6.77e-11 ± 3.4e-13 |
| 0.3 | 1995 | 1000 | 10.4 | 3.021e-08 ± 1.4e-10 |
| 0.7 | 10 | 1 | 0.191 | 0.213 ± 0.0011 |
| 0.7 | 20 | 1 | 0.389 | 0.1942 ± 0.00094 |
| 0.7 | 50 | 1 | 0.975 | 0.1483 ± 0.00074 |
| 0.7 | 100 | 1 | 1.95 | 0.09367 ± 0.00043 |
| 0.7 | 200 | 1 | 3.91 | 0.04172 ± 0.00017 |
| 0.7 | 300 | 1 | 5.89 | 0.01991 ± 7.9e-05 |
| 0.7 | 500 | 1 | 20.3 | 0.002681 ± 1.3e-05 |
| 0.7 | 1000 | 1 | 46.5 | 0.0001949 ± 8.2e-07 |
| 0.7 | 2000 | 1 | 95.5 | 4.648e-06 ± 2.2e-08 |
| 0.7 | 5000 | 1 | 240 | 1.714e-08 ± 7.6e-11 |
| 0.7 | 10 | 10 | 9.78e-05 | 0.00357 ± 1.7e-05 |
| 0.7 | 50 | 10 | 0.895 | 0.1482 ± 0.0007 |
| 0.7 | 100 | 10 | 1.91 | 0.09343 ± 0.00038 |
| 0.7 | 5000 | 10 | 240 | 1.71e-08 ± 8e-11 |
| 0.7 | 15 | 10 | 0.000289 | 0.004422 ± 2.6e-05 |
| 0.7 | 10 | 50 | 9.78e-05 | 0.0005819 ± 2.5e-06 |
| 0.7 | 50 | 50 | 0.00123 | 0.0007124 ± 3.3e-06 |
| 0.7 | 200 | 50 | 3.39 | 0.04143 ± 0.00018 |
| 0.7 | 300 | 50 | 5.55 | 0.01998 ± 9.3e-05 |
| 0.7 | 5000 | 50 | 240 | 1.661e-08 ± 1e-10 |
| 0.7 | 95 | 50 | 0.00266 | 0.002575 ± 1.7e-05 |

Continued on next page

Table C.6 – continued from previous page

| Coupling (g) | $m_{Phi}$ [GeV] | $m_{\chi}$ [GeV] | $\Gamma_{min}$ [GeV] | $\sigma$ [pb] |
|---|---|---|---|---|
| 0.7 | 10 | 150 | 9.78e-05 | 5.65e-05 ± 2.9e-07 |
| 0.7 | 200 | 150 | 0.0094 | 9.979e-05 ± 4.8e-07 |
| 0.7 | 500 | 150 | 18.3 | 0.002329 ± 1.3e-05 |
| 0.7 | 5000 | 150 | 240 | 1.393e-08 ± 6.7e-11 |
| 0.7 | 295 | 150 | 0.0309 | 0.0008152 ± 4e-06 |
| 0.7 | 10 | 500 | 9.78e-05 | 5.458e-07 ± 2.2e-09 |
| 0.7 | 500 | 500 | 10.5 | 7.888e-07 ± 3.2e-09 |
| 0.7 | 2000 | 500 | 90.3 | 3.71e-06 ± 1.6e-08 |
| 0.7 | 5000 | 500 | 238 | 4.666e-09 ± 3e-11 |
| 0.7 | 995 | 500 | 26.9 | 2.182e-05 ± 9.7e-08 |
| 0.7 | 10 | 1000 | 9.78e-05 | 6.257e-09 ± 2.7e-11 |
| 0.7 | 1000 | 1000 | 27 | 9.46e-09 ± 3.7e-11 |
| 0.7 | 5000 | 1000 | 232 | 9.897e-10 ± 5.3e-12 |
| 0.7 | 1995 | 1000 | 56.4 | 4.386e-07 ± 2.2e-09 |
| 1. | 10 | 1 | 0.39 | 0.4409 ± 0.0014 |
| 1. | 20 | 1 | 0.793 | 0.3992 ± 0.0016 |
| 1. | 50 | 1 | 1.99 | 0.3032 ± 0.0015 |
| 1. | 100 | 1 | 3.98 | 0.1909 ± 0.001 |
| 1. | 200 | 1 | 7.98 | 0.0836 ± 0.00035 |
| 1. | 300 | 1 | 12 | 0.03999 ± 0.00016 |
| 1. | 500 | 1 | 41.3 | 0.005408 ± 2.2e-05 |
| 1. | 1000 | 1 | 94.9 | 0.0003973 ± 1.7e-06 |
| 1. | 2000 | 1 | 195 | 1.087e-05 ± 5.2e-08 |
| 1. | 5000 | 1 | 490 | 7.022e-08 ± 2.8e-10 |
| 1. | 10 | 10 | 0.0002 | 0.01499 ± 8.4e-05 |
| 1. | 50 | 10 | 1.83 | 0.3034 ± 0.0016 |
| 1. | 100 | 10 | 3.9 | 0.1901 ± 0.00085 |
| 1. | 5000 | 10 | 490 | 7.023e-08 ± 3e-10 |
| 1. | 15 | 10 | 0.000589 | 0.01863 ± 9.3e-05 |
| 1. | 10 | 50 | 0.0002 | 0.002444 ± 1.2e-05 |
| 1. | 50 | 50 | 0.00251 | 0.002979 ± 1.5e-05 |
| 1. | 200 | 50 | 6.91 | 0.08382 ± 0.00036 |
| 1. | 300 | 50 | 11.3 | 0.03989 ± 0.00015 |
| 1. | 5000 | 50 | 490 | 6.831e-08 ± 4.1e-10 |
| 1. | 95 | 50 | 0.00544 | 0.01067 ± 5.7e-05 |
| 1. | 10 | 150 | 0.0002 | 0.0002364 ± 1.1e-06 |
| 1. | 200 | 150 | 0.0192 | 0.0004124 ± 1.8e-06 |
| 1. | 500 | 150 | 37.4 | 0.004611 ± 1.9e-05 |
| 1. | 5000 | 150 | 489 | 5.698e-08 ± 2.5e-10 |
| 1. | 295 | 150 | 0.0631 | 0.003365 ± 1.7e-05 |
| 1. | 10 | 500 | 0.0002 | 2.279e-06 ± 8.7e-09 |
| 1. | 500 | 500 | 21.4 | 3.275e-06 ± 1.4e-08 |
| 1. | 2000 | 500 | 184 | 7.611e-06 ± 3.7e-08 |
| 1. | 5000 | 500 | 486 | 1.867e-08 ± 1.2e-10 |
| 1. | 995 | 500 | 54.8 | 6.171e-05 ± 2.5e-07 |

Continued on next page

Table C.6 – continued from previous page

| Coupling (g) | $m_{Phi}$ [GeV] | $m_{\chi}$ [GeV] | $\Gamma_{min}$ [GeV] | $\sigma$ [pb] |
|---|---|---|---|---|
| 1. | 10 | 1000 | 0.0002 | 2.595e-08 ± 1e-10 |
| 1. | 1000 | 1000 | 55.1 | 3.933e-08 ± 1.5e-10 |
| 1. | 5000 | 1000 | 474 | 3.536e-09 ± 1.8e-11 |
| 1. | 1995 | 1000 | 115 | 1.103e-06 ± 5e-09 |
| 1.5 | 10 | 1 | 0.878 | 1.041 ± 0.004 |
| 1.5 | 20 | 1 | 1.78 | 0.9304 ± 0.0037 |
| 1.5 | 50 | 1 | 4.48 | 0.6793 ± 0.003 |
| 1.5 | 100 | 1 | 8.96 | 0.4189 ± 0.002 |
| 1.5 | 200 | 1 | 17.9 | 0.1836 ± 0.00074 |
| 1.5 | 300 | 1 | 27 | 0.08863 ± 0.00038 |
| 1.5 | 500 | 1 | 93 | 0.01129 ± 5.5e-05 |
| 1.5 | 1000 | 1 | 214 | 0.000878 ± 4.1e-06 |
| 1.5 | 2000 | 1 | 439 | 3.1e-05 ± 1.2e-07 |
| 1.5 | 5000 | 1 | 1103 | 3.408e-07 ± 1.6e-09 |
| 1.5 | 10 | 10 | 0.000449 | 0.0747 ± 0.00036 |
| 1.5 | 50 | 10 | 4.11 | 0.6777 ± 0.0032 |
| 1.5 | 100 | 10 | 8.78 | 0.424 ± 0.002 |
| 1.5 | 5000 | 10 | 1103 | 3.418e-07 ± 1.3e-09 |
| 1.5 | 15 | 10 | 0.00133 | 0.09382 ± 0.00049 |
| 1.5 | 10 | 50 | 0.000449 | 0.01227 ± 6.9e-05 |
| 1.5 | 50 | 50 | 0.00566 | 0.01488 ± 7.4e-05 |
| 1.5 | 200 | 50 | 15.5 | 0.1861 ± 0.00087 |
| 1.5 | 300 | 50 | 25.5 | 0.08815 ± 0.00041 |
| 1.5 | 5000 | 50 | 1103 | 3.334e-07 ± 2e-09 |
| 1.5 | 95 | 50 | 0.0122 | 0.05397 ± 0.00029 |
| 1.5 | 10 | 150 | 0.000449 | 0.0012 ± 6.1e-06 |
| 1.5 | 200 | 150 | 0.0432 | 0.002092 ± 9.1e-06 |
| 1.5 | 500 | 150 | 84.1 | 0.009493 ± 4.2e-05 |
| 1.5 | 5000 | 150 | 1102 | 2.739e-07 ± 1.5e-09 |
| 1.5 | 295 | 150 | 0.142 | 0.01722 ± 0.00011 |
| 1.5 | 10 | 500 | 0.000449 | 1.147e-05 ± 4.7e-08 |
| 1.5 | 500 | 500 | 48.2 | 1.659e-05 ± 6.5e-08 |
| 1.5 | 2000 | 500 | 415 | 1.716e-05 ± 9e-08 |
| 1.5 | 5000 | 500 | 1094 | 8.722e-08 ± 3.9e-10 |
| 1.5 | 995 | 500 | 123 | 0.0001753 ± 6.8e-07 |
| 1.5 | 10 | 1000 | 0.000449 | 1.32e-07 ± 5.2e-10 |
| 1.5 | 1000 | 1000 | 124 | 1.975e-07 ± 7.7e-10 |
| 1.5 | 5000 | 1000 | 1065 | 1.508e-08 ± 6.2e-11 |
| 1.5 | 1995 | 1000 | 259 | 2.741e-06 ± 1.3e-08 |
| 2. | 10 | 1 | 1.56 | 1.962 ± 0.0076 |
| 2. | 20 | 1 | 3.17 | 1.718 ± 0.0064 |
| 2. | 50 | 1 | 7.96 | 1.217 ± 0.0061 |
| 2. | 100 | 1 | 15.9 | 0.7382 ± 0.0029 |
| 2. | 200 | 1 | 31.9 | 0.3179 ± 0.0015 |
| 2. | 300 | 1 | 48 | 0.1503 ± 0.00067 |

Continued on next page

Table C.6 – continued from previous page

| Coupling (g) | $m_{Phi}$ [GeV] | $m_{\chi}$ [GeV] | $\Gamma_{min}$ [GeV] | $\sigma$ [pb] |
|---|---|---|---|---|
| 2. | 500 | 1 | 165 | 0.01871 ± 0.0001 |
| 2. | 1000 | 1 | 380 | 0.001487 ± 9.1e-06 |
| 2. | 2000 | 1 | 780 | 6.481e-05 ± 3e-07 |
| 2. | 5000 | 1 | 1961 | 9.619e-07 ± 3.9e-09 |
| 2. | 10 | 10 | 0.000799 | 0.2395 ± 0.0012 |
| 2. | 50 | 10 | 7.3 | 1.217 ± 0.0051 |
| 2. | 100 | 10 | 15.6 | 0.7347 ± 0.003 |
| 2. | 5000 | 10 | 1961 | 9.544e-07 ± 4.6e-09 |
| 2. | 15 | 10 | 0.00236 | 0.2973 ± 0.0015 |
| 2. | 10 | 50 | 0.000799 | 0.03855 ± 0.00018 |
| 2. | 50 | 50 | 0.0101 | 0.04728 ± 0.00022 |
| 2. | 200 | 50 | 27.6 | 0.3166 ± 0.0016 |
| 2. | 300 | 50 | 45.3 | 0.149 ± 0.00061 |
| 2. | 5000 | 50 | 1960 | 9.34e-07 ± 4.6e-09 |
| 2. | 95 | 50 | 0.0217 | 0.1717 ± 0.00096 |
| 2. | 10 | 150 | 0.000799 | 0.003778 ± 1.8e-05 |
| 2. | 200 | 150 | 0.0768 | 0.006619 ± 2.7e-05 |
| 2. | 500 | 150 | 149 | 0.01511 ± 8.1e-05 |
| 2. | 5000 | 150 | 1959 | 7.835e-07 ± 3.9e-09 |
| 2. | 295 | 150 | 0.253 | 0.05408 ± 0.00031 |
| 2. | 10 | 500 | 0.000799 | 3.638e-05 ± 1.5e-07 |
| 2. | 500 | 500 | 85.8 | 5.258e-05 ± 2.4e-07 |
| 2. | 2000 | 500 | 736.9 | 2.857e-05 ± 1.7e-07 |
| 2. | 5000 | 500 | 1945 | 2.44e-07 ± 1.1e-09 |
| 2. | 995 | 500 | 219.2 | 0.0003371 ± 1.4e-06 |
| 2. | 10 | 1000 | 0.0007987 | 4.139e-07 ± 1.7e-09 |
| 2. | 1000 | 1000 | 220.5 | 6.26e-07 ± 2.8e-09 |
| 2. | 5000 | 1000 | 1894 | 3.818e-08 ± 1.5e-10 |
| 2. | 1995 | 1000 | 460.1 | 4.794e-06 ± 2.4e-08 |
| 2.5 | 10 | 1 | 2.44 | 3.313 ± 0.016 |
| 2.5 | 20 | 1 | 4.95 | 2.805 ± 0.013 |
| 2.5 | 50 | 1 | 12.4 | 1.92 ± 0.01 |
| 2.5 | 100 | 1 | 24.9 | 1.131 ± 0.0054 |
| 2.5 | 200 | 1 | 49.9 | 0.4734 ± 0.0021 |
| 2.5 | 300 | 1 | 75.0 | 0.2216 ± 0.0012 |
| 2.5 | 500 | 1 | 258 | 0.02611 ± 0.00012 |
| 2.5 | 1000 | 1 | 593 | 0.002111 ± 1e-05 |
| 2.5 | 2000 | 1 | 1218 | 0.0001072 ± 4.2e-07 |
| 2.5 | 5000 | 1 | 3064 | 1.927e-06 ± 9.9e-09 |
| 2.5 | 10 | 10 | 0.00125 | 0.5815 ± 0.0026 |
| 2.5 | 50 | 10 | 11.4 | 1.928 ± 0.011 |
| 2.5 | 100 | 10 | 24.4 | 1.131 ± 0.006 |
| 2.5 | 5000 | 10 | 3064 | 1.937e-06 ± 9.9e-09 |
| 2.5 | 15 | 10 | 0.00368 | 0.7216 ± 0.0041 |
| 2.5 | 10 | 50 | 0.00125 | 0.09521 ± 0.00048 |

Continued on next page

Table C.6 – continued from previous page

| Coupling (g) | $m_{Phi}$ [GeV] | $m_{\chi}$ [GeV] | $\Gamma_{min}$ [GeV] | $\sigma$ [pb] |
|---|---|---|---|---|
| 2.5 | 50 | 50 | 0.0157 | 0.1158 ± 0.00055 |
| 2.5 | 200 | 50 | 43.2 | 0.475 ± 0.0018 |
| 2.5 | 300 | 50 | 70.8 | 0.2214 ± 0.0012 |
| 2.5 | 5000 | 50 | 3064 | 1.868e-06 ± 1e-08 |
| 2.5 | 95 | 50 | 0.034 | 0.421 ± 0.0022 |
| 2.5 | 10 | 150 | 0.00125 | 0.009221 ± 4.6e-05 |
| 2.5 | 200 | 150 | 0.12 | 0.01604 ± 6.7e-05 |
| 2.5 | 500 | 150 | 234 | 0.0206 ± 8.7e-05 |
| 2.5 | 5000 | 150 | 3062 | 1.55e-06 ± 7.6e-09 |
| 2.5 | 295 | 150 | 0.395 | 0.1314 ± 0.0007 |
| 2.5 | 10 | 500 | 0.00125 | 8.948e-05 ± 3.4e-07 |
| 2.5 | 500 | 500 | 134 | 0.0001273 ± 5e-07 |
| 2.5 | 2000 | 500 | 1151 | 3.922e-05 ± 1.8e-07 |
| 2.5 | 5000 | 500 | 3039 | 4.732e-07 ± 2e-09 |
| 2.5 | 995 | 500 | 343 | 0.0005315 ± 2.5e-06 |
| 2.5 | 10 | 1000 | 0.00125 | 1.014e-06 ± 4.2e-09 |
| 2.5 | 1000 | 1000 | 345 | 1.522e-06 ± 7e-09 |
| 2.5 | 5000 | 1000 | 2960 | 6.909e-08 ± 3.6e-10 |
| 2.5 | 1995 | 1000 | 719 | 6.791e-06 ± 3.3e-08 |
| 3. | 10 | 1 | 3.51 | 5.17 ± 0.021 |
| 3. | 20 | 1 | 7.13 | 4.262 ± 0.017 |
| 3. | 50 | 1 | 17.9 | 2.814 ± 0.014 |
| 3. | 100 | 1 | 35.9 | 1.595 ± 0.0073 |
| 3. | 200 | 1 | 71.8 | 0.651 ± 0.0028 |
| 3. | 300 | 1 | 108 | 0.3028 ± 0.0014 |
| 3. | 500 | 1 | 372 | 0.03314 ± 0.00019 |
| 3. | 1000 | 1 | 854 | 0.002641 ± 1.5e-05 |
| 3. | 2000 | 1 | 1754 | 0.0001496 ± 5.3e-07 |
| 3. | 5000 | 1 | 4412 | 3.035e-06 ± 1.4e-08 |
| 3. | 10 | 10 | 0.0018 | 1.214 ± 0.0059 |
| 3. | 50 | 10 | 16.4 | 2.849 ± 0.012 |
| 3. | 100 | 10 | 35.1 | 1.611 ± 0.0071 |
| 3. | 5000 | 10 | 4412 | 3.031e-06 ± 2.1e-08 |
| 3. | 15 | 10 | 0.00530 | 1.509 ± 0.0076 |
| 3. | 10 | 50 | 0.00178 | 0.1967 ± 0.00093 |
| 3. | 50 | 50 | 0.0226 | 0.242 ± 0.0012 |
| 3. | 200 | 50 | 62.2 | 0.6533 ± 0.0033 |
| 3. | 300 | 50 | 102 | 0.3011 ± 0.0013 |
| 3. | 5000 | 50 | 4412 | 2.974e-06 ± 1.6e-08 |
| 3. | 95 | 50 | 0.0489 | 0.8669 ± 0.0046 |
| 3. | 10 | 150 | 0.0018 | 0.01918 ± 8.3e-05 |
| 3. | 200 | 150 | 0.173 | 0.03357 ± 0.00015 |
| 3. | 500 | 150 | 336 | 0.02601 ± 0.00013 |
| 3. | 5000 | 150 | 4409 | 2.417e-06 ± 1.1e-08 |
| 3. | 295 | 150 | 0.568 | 0.2747 ± 0.0017 |

Continued on next page

Table C.6 – continued from previous page

| Coupling (g) | $m_{Phi}$ [GeV] | $m_{\chi}$ [GeV] | $\Gamma_{min}$ [GeV] | $\sigma$ [pb] |
|---|---|---|---|---|
| 3. | 10 | 500 | 0.0018 | 0.0001847 ± 7.2e-07 |
| 3. | 500 | 500 | 193 | 0.0002634 ± 1.2e-06 |
| 3. | 2000 | 500 | 1658 | 4.736e-05 ± 2.1e-07 |
| 3. | 5000 | 500 | 4376 | 7.254e-07 ± 3.1e-09 |
| 3. | 995 | 500 | 493 | 0.0007379 ± 3e-06 |
| 3. | 10 | 1000 | 0.0018 | 2.087e-06 ± 9.5e-09 |
| 3. | 1000 | 1000 | 496 | 3.142e-06 ± 1.3e-08 |
| 3. | 5000 | 1000 | 4263 | 9.753e-08 ± 4e-10 |
| 3. | 1995 | 1000 | 1035 | 8.775e-06 ± 3.8e-08 |
| 3.5 | 10 | 1 | 4.78 | 7.684 ± 0.025 |
| 3.5 | 20 | 1 | 9.71 | 6.209 ± 0.026 |
| 3.5 | 50 | 1 | 24.4 | 3.911 ± 0.024 |
| 3.5 | 100 | 1 | 48.8 | 2.138 ± 0.011 |
| 3.5 | 200 | 1 | 97.7 | 0.8426 ± 0.0034 |
| 3.5 | 300 | 1 | 147 | 0.3824 ± 0.0018 |
| 3.5 | 500 | 1 | 506 | 0.03921 ± 0.00026 |
| 3.5 | 1000 | 1 | 1163 | 0.003103 ± 1.6e-05 |
| 3.5 | 2000 | 1 | 2387 | 0.0001824 ± 8e-07 |
| 3.5 | 5000 | 1 | 6005 | 4.039e-06 ± 2.6e-08 |
| 3.5 | 10 | 10 | 0.00245 | 2.231 ± 0.011 |
| 3.5 | 50 | 10 | 22.4 | 3.911 ± 0.021 |
| 3.5 | 100 | 10 | 47.8 | 2.133 ± 0.0093 |
| 3.5 | 5000 | 10 | 6005 | 4.037e-06 ± 1.9e-08 |
| 3.5 | 15 | 10 | 0.00722 | 2.777 ± 0.013 |
| 3.5 | 10 | 50 | 0.00245 | 0.3644 ± 0.0016 |
| 3.5 | 50 | 50 | 0.0308 | 0.4471 ± 0.002 |
| 3.5 | 200 | 50 | 84.7 | 0.8484 ± 0.0041 |
| 3.5 | 300 | 50 | 139 | 0.3844 ± 0.002 |
| 3.5 | 5000 | 50 | 6005 | 3.938e-06 ± 2.2e-08 |
| 3.5 | 95 | 50 | 0.0666 | 1.603 ± 0.01 |
| 3.5 | 10 | 150 | 0.00245 | 0.03531 ± 0.00018 |
| 3.5 | 200 | 150 | 0.235 | 0.0618 ± 0.00027 |
| 3.5 | 500 | 150 | 458 | 0.03087 ± 0.00015 |
| 3.5 | 5000 | 150 | 6001 | 3.227e-06 ± 1.6e-08 |
| 3.5 | 295 | 150 | 0.773 | 0.5139 ± 0.0026 |
| 3.5 | 10 | 500 | 0.00245 | 0.0003434 ± 1.5e-06 |
| 3.5 | 500 | 500 | 263 | 0.0004874 ± 2e-06 |
| 3.5 | 2000 | 500 | 2257 | 5.311e-05 ± 2.5e-07 |
| 3.5 | 5000 | 500 | 5956 | 9.439e-07 ± 4.7e-09 |
| 3.5 | 995 | 500 | 672 | 0.0009553 ± 3.7e-06 |
| 3.5 | 10 | 1000 | 0.00245 | 3.857e-06 ± 1.9e-08 |
| 3.5 | 1000 | 1000 | 675 | 5.748e-06 ± 2.4e-08 |
| 3.5 | 5000 | 1000 | 5802 | 1.197e-07 ± 6.2e-10 |
| 3.5 | 1995 | 1000 | 1409 | 1.037e-05 ± 4.9e-08 |

| $m_\chi$ | $m_\Phi$ | $\sigma$ [pb] | $m_\chi$ | $m_\Phi$ | $\sigma$ [pb] |
|---|---|---|---|---|---|
| 100 | 1000 | 1.50E-02 | 150 | 600 | 1.22E-01 |
| 100 | 100 | 1.13E-04 | 200 | 1000 | 7.04E-03 |
| 100 | 1300 | 7.05E-03 | 200 | 1300 | 2.11E-03 |
| 100 | 150 | 6.12E+00 | 200 | 200 | 6.29E-05 |
| 100 | 200 | 9.60E+00 | 200 | 250 | 5.83E-01 |
| 100 | 250 | 7.57E+00 | 200 | 300 | 1.64E+00 |
| 100 | 300 | 4.01E+00 | 200 | 400 | 9.08E-01 |
| 100 | 400 | 1.06E+00 | 200 | 600 | 1.11E-01 |
| 100 | 600 | 1.45E-01 | 35 | 250 | 9.62E+00 |
| 10 | 1000 | 3.55E-01 | 35 | 300 | 4.56E+00 |
| 10 | 100 | 7.67E+01 | 35 | 350 | 2.35E+00 |
| 10 | 10 | 2.43E-05 | 35 | 400 | 1.33E+00 |
| 10 | 1300 | 2.35E-01 | 35 | 500 | 5.48E-01 |
| 10 | 150 | 3.92E+01 | 35 | 550 | 3.80E-01 |
| 10 | 200 | 2.13E+01 | 35 | 600 | 2.76E-01 |
| 10 | 250 | 1.05E+01 | 35 | 650 | 2.07E-01 |
| 10 | 300 | 5.57E+00 | 35 | 700 | 1.60E-01 |
| 10 | 400 | 2.35E+00 | 50 | 1000 | 3.69E-02 |
| 10 | 50 | 1.51E+02 | 50 | 100 | 3.07E+01 |
| 10 | 600 | 8.16E-01 | 50 | 1300 | 2.39E-02 |
| 150 | 1000 | 9.44E-03 | 50 | 150 | 2.76E+01 |
| 150 | 1300 | 3.44E-03 | 50 | 200 | 1.82E+01 |
| 150 | 150 | 8.84E-05 | 50 | 250 | 9.31E+00 |
| 150 | 200 | 1.69E+00 | 50 | 300 | 4.40E+00 |
| 150 | 250 | 3.76E+00 | 50 | 400 | 1.22E+00 |
| 150 | 300 | 3.29E+00 | 50 | 50 | 1.04E-04 |
| 150 | 400 | 9.83E-01 | 50 | 600 | 2.14E-01 |

Table C.2: Dark matter masses $m_\chi$ and mediator masses $m_\Phi$ generated such that relic density constraints are fullfilled for 13 TeV. The resulting production cross sections are given in pb.

## *C.4 Cross sections for the $b\bar{b}$+DM scalar simplified model*

**[TODO: add cross-sections, they will be available with plots]**

| $m_\chi$ | $m_\Phi$ | $\sigma$ [pb] | $m_\chi$ | $m_\Phi$ | $\sigma$ [pb] |
|---|---|---|---|---|---|
| 100 | 1000 | 1.50E-02 | 150 | 600 | 1.22E-01 |
| 100 | 100 | 1.13E-04 | 200 | 1000 | 7.04E-03 |
| 100 | 1300 | 7.05E-03 | 200 | 1300 | 2.11E-03 |
| 100 | 150 | 6.12E+00 | 200 | 200 | 6.29E-05 |
| 100 | 200 | 9.60E+00 | 200 | 250 | 5.83E-01 |
| 100 | 250 | 7.57E+00 | 200 | 300 | 1.64E+00 |
| 100 | 300 | 4.01E+00 | 200 | 400 | 9.08E-01 |
| 100 | 400 | 1.06E+00 | 200 | 600 | 1.11E-01 |
| 100 | 600 | 1.45E-01 | 35 | 250 | 9.62E+00 |
| 10 | 1000 | 3.55E-01 | 35 | 300 | 4.56E+00 |
| 10 | 100 | 7.67E+01 | 35 | 350 | 2.35E+00 |
| 10 | 10 | 2.43E-05 | 35 | 400 | 1.33E+00 |
| 10 | 1300 | 2.35E-01 | 35 | 500 | 5.48E-01 |
| 10 | 150 | 3.92E+01 | 35 | 550 | 3.80E-01 |
| 10 | 200 | 2.13E+01 | 35 | 600 | 2.76E-01 |
| 10 | 250 | 1.05E+01 | 35 | 650 | 2.07E-01 |
| 10 | 300 | 5.57E+00 | 35 | 700 | 1.60E-01 |
| 10 | 400 | 2.35E+00 | 50 | 1000 | 3.69E-02 |
| 10 | 50 | 1.51E+02 | 50 | 100 | 3.07E+01 |
| 10 | 600 | 8.16E-01 | 50 | 1300 | 2.39E-02 |
| 150 | 1000 | 9.44E-03 | 50 | 150 | 2.76E+01 |
| 150 | 1300 | 3.44E-03 | 50 | 200 | 1.82E+01 |
| 150 | 150 | 8.84E-05 | 50 | 250 | 9.31E+00 |
| 150 | 200 | 1.69E+00 | 50 | 300 | 4.40E+00 |
| 150 | 250 | 3.76E+00 | 50 | 400 | 1.22E+00 |
| 150 | 300 | 3.29E+00 | 50 | 50 | 1.04E-04 |
| 150 | 400 | 9.83E-01 | 50 | 600 | 2.14E-01 |

Table C.3: Dark matter masses $m_\chi$ and mediator masses $m_\Phi$ generated such that relic density constraints are fullfilled for 13 TeV. The resulting production cross sections are given in pb.

| $m_\chi$ | $m_\Phi$ | $\sigma$ [pb] | $m_\chi$ | $m_\Phi$ | $\sigma$ [pb] |
|---|---|---|---|---|---|
| 100 | 1000 | 1.53E-03 | 150 | 600 | 1.61E-02 |
| 100 | 100 | 2.21E-05 | 200 | 1000 | 5.46E-04 |
| 100 | 1300 | 7.91E-04 | 200 | 1300 | 1.54E-04 |
| 100 | 150 | 1.58E+00 | 200 | 200 | 9.52E-06 |
| 100 | 200 | 2.48E+00 | 200 | 250 | 1.22E-01 |
| 100 | 250 | 1.82E+00 | 200 | 300 | 3.53E-01 |
| 100 | 300 | 8.77E-01 | 200 | 400 | 1.65E-01 |
| 100 | 400 | 1.94E-01 | 200 | 600 | 1.43E-02 |
| 100 | 600 | 2.00E-02 | 35 | 250 | 2.32E+00 |
| 10 | 1000 | 5.61E-02 | 35 | 300 | 1.00E+00 |
| 10 | 100 | 2.36E+01 | 35 | 350 | 4.73E-01 |
| 10 | 10 | 6.53E-06 | 35 | 400 | 2.51E-01 |
| 10 | 1300 | 3.62E-02 | 35 | 500 | 9.23E-02 |
| 10 | 150 | 1.12E+01 | 35 | 550 | 6.07E-02 |
| 10 | 200 | 5.61E+00 | 35 | 600 | 4.20E-02 |
| 10 | 250 | 2.50E+00 | 35 | 650 | 3.02E-02 |
| 10 | 300 | 1.21E+00 | 35 | 700 | 2.25E-02 |
| 10 | 400 | 4.53E-01 | 50 | 1000 | 4.70E-03 |
| 10 | 50 | 4.83E+01 | 50 | 100 | 8.88E+00 |
| 10 | 600 | 1.34E-01 | 50 | 1300 | 3.34E-03 |
| 150 | 1000 | 8.21E-04 | 50 | 150 | 7.83E+00 |
| 150 | 1300 | 3.07E-04 | 50 | 200 | 4.80E+00 |
| 150 | 150 | 1.52E-05 | 50 | 250 | 2.25E+00 |
| 150 | 200 | 3.93E-01 | 50 | 300 | 9.67E-01 |
| 150 | 250 | 8.86E-01 | 50 | 400 | 2.28E-01 |
| 150 | 300 | 7.19E-01 | 50 | 50 | 2.37E-05 |
| 150 | 400 | 1.79E-01 | 50 | 600 | 3.15E-02 |

Table C.4: Dark matter masses $m_\chi$ and mediator masses $m_\Phi$ generated for such that relic density constraints are fullfilled for 8 TeV. The resulting production cross sections are given in pb.

# D
# Appendix: Presentation of experimental results for reinterpretation

To do Add a section on specific information that is necessary to have from experimentalists in DM searches (**??**)

Along with the design of new searches to hunt for new physics at the LHC, it is important to consider information needed in order to reinterpret the searches outside of the collaborations. The following is a non-exhaustive list of recommendations in order to make reinterpretation easier and faster. This appendix details considerations for reimplementation of the analysis as well as for using the simplified model results directly given by the collaborations.

One of the important developments in recent years is an active development of the analyses recasting codes [DFK+15, CDFW14, KSTR15]. The aim of these codes is to provide a public library of reimplemented and validated LHC analyses. Such libraries can then be used to analyse validity of a BSM scenario in a systematic and effective manner. The availability of public libraries further facilitates a unified framework and can lead to an organised and central structure to preserve LHC information in a long run.

In order to be able to develop such codes, it is important to get complete and systematic information from the collaborations.

- **Data digitisation**: Availability of digitised data is one of the primary requirement. All information given by collaborations in the form of plots should be made available in a digitised format. Platforms such as HepData can be used in oder to maintain a centralised manner. In case when HepData can not be used, digitised data can be provided via analyses twiki pages. This information primarily includes expected and observed exclusion lines along with their $\pm 1\sigma$ uncertainty, expected and observed upper limits in case of simplified models, efficiency maps and all kinematic distributions as reported in the analysis. Units should be clearly specified. If the digitised figures are made available as a C macro or a ROOT file, the names of the objects should be clearly identifiable e.g. expected upper limits of a particular topology/model given as a ROOT file can be labeled as `KEY: TH2D ExpectedUpperLimit;1`. Furthermore, these digitised files can potentially contain more information (larger axes ranges) than displayed on the plot. This will help facilitate understand what happens beyond the limits displayed in the plot, e.g. a dis-

tribution for number of jets can be artificially limited to a point in the plot (for the purpose of clarity of figure) , however, this artificial limit leads to a sharp cutoff in the plot. While validating the analysis it is often necessary to compare the distributions beyond such artificial limits, having this information digitised will be of a great help in such cases.

## *D.1 Reimplementing analyses*

This section lists information necessary in order to reimplement an analysis. Analysis reimplementation usually consists of several stages. Usually, one starts with reading the analysis note carefully, following which the preselection and event selection cuts are identified. These are then mimicked using a code typically written in C++. The detector simulation is carried out by using public detector simulation softwares e.g. Delphes [dF+14]. The resulting ROOT file is then analysed using the C++ code written in the previous step.

- **Analysis documentation**: The collaborations should provide a cutflow table with every analysis, such a cutflow table will naturally define the order of cuts implemented in an analysis. There are several preselection criteria which can not be easily simulated in phenomenology, e.g. MET cleaning. Numbers should be provided after such cuts so that theorists can rescale their number of events in order to account for such cuts. Efficiencies of several reconstructed objects are given as an input to detector simulation softwares like Delphes. It is thus very useful to get parametrised efficiencies for reconstructed objects (as a function of the rapidity $\eta$ and/or transverse momentum $p_T$), along with the working points at which they were evaluated (e.g. loose, tight selection). Object definitions should be clearly identifiable.

- **Validation**: Validation corresponds to re-deriving the results as given by collaborations in order to verify that the implementation of the analysis is correct. Usually most of the bug catching takes place in the phase of validation. The following items are necessary in order to recreate the results.

  - Monte Carlo generators: Monte Carlo generators along with the exact versions used to produce the event files should be listed.
  - Production cross sections: The order of production cross sections (e.g. LO,NLO,NLL) as well as the codes which were used to compute them should be provided. A table of reference cross sections for several values of particle masses such as ones provided by SUSY cross section working group will be highly appreciated.
  - Process Generation: Details of the generated process, detailing number of additional partons generated.

  - Availability of the LHE files: LHE files (detailing at least a few events if not the entire file) corresponding to the benchmarks listed in the analysis should be made available in order to cross check process generation. For models concerning SUSY, corresponding SLHA files of benchmark files should also be details. Special attention should be paid to list the parameters which change the production cross section or kinematics of the process e.g. mixing angles.
  - Process cards: Process cards includes PDF choices, details of matching algorithms and scales and details of process generation. If process cards are not available, above items should be clearly identified.
  - MadGraph model files: For models which are not already implemented in MadGraph, availability of the corresponding model files is highly desired. It details the exact notation used in the model and hence sets up a complete framework. In case MadGraph is not used, enough information should be provided in order to clearly identify the underlying model used for interpretations.

- **Limit setting**: Detailed description of the likelihood used in order to derive the limits should be given, this can contain statistical procedure within the analysis text itself, however direct availability of the limit setting code as a workspace in RooStats is highly desirable.

- **Binned backgrounds**: For analyses using techniques such as sliding windows or an unbinned technique, the Standard Model backgrounds should be given in the form of bins. These backgrounds can then be interpolated.

- **Recast code**: Finally, the collaborations can provide an analysis code directly implemented in one of the public recasting codes detailed above. Such codes can be published via INSPIRE in order to track the versioning and citations.

## *D.2 Simplified model interpretations*

The analyses almost always provide at least one simplified model interpretation along with the search results. These interpretations are simple and can be used in order to take a quick survey of viability of parameter space. Codes such as [KKL$^+$14b, KKL$^+$14a, PSWZ14] can make use of the simplified model results given in the form of 95% Confidence Level (CLs) upper limit or efficiency maps in order to test Beyond the Standard Model parameter space. It will thus be extremely useful if the results are given in a form as easily usable by the theory community.

- **Direct usability of the results**: The results given should be as useful as possible. For example, for a simplified model containing dark matter mass $M_\chi$, mediator mass $M_{med}$ and couplings

$g_\chi, g_q$ it will be extremely useful to have 95% CLs upper limits on the product of couplings $\sqrt{g_\chi g_q}$ or cross section times branching ratio as a function of $M_\chi$, $M_{med}$.

- **Smooth grids**: The usage of simplified model results relies on interpolating between upper limit values. In order to facilitate the interpolation, regions where large variation of upper limits is observed should contain denser grid, if a uniform grid over the entire plane is not possible. For simplified model involving more than three parameters (two masses and product of couplings), slices of upper limits in the additional dimensions will be very useful e.g. for a simplified model involving one step cascade decay, upper limits can be provided for several values of intermediate mass in the plane of mother - daughter masses. Results with only one slice often render invalid to be used in a general model testing.

- **Availability of efficiency maps**: Finally, efficiency maps for all the signal regions involved in the analysis should be made available. These results are not only useful for model testing using simplified models but also to validate implementation of the analysis. Information about the most sensitive signal region as a function of masses is also very useful in order to determine the validity of approximate limit setting procedures being used by theorists (in the absence of any other sophisticated limit setting technique).

# Bibliography


[A+08] J. Alwall et al. Comparative study of various algorithms for the merging of parton showers and matrix elements in hadronic collisions. *Eur.Phys.J.*, C53(2):473–500, 2008.

[A+14a] Georges Aad et al. Search for new particles in events with one lepton and missing transverse momentum in $pp$ collisions at $\sqrt{s}$ = 8 TeV with the ATLAS detector. *JHEP*, 1409:037, 2014.

[A+14b] Jalal Abdallah et al. Simplified Models for Dark Matter and Missing Energy Searches at the LHC. *arXiv:1409.2893*, 2014.

[A+14c] J. Alwall et al. The automated computation of tree-level and next-to-leading order differential cross sections, and their matching to parton shower simulations. *JHEP*, 07(2):079, 2014.

[A+15] Georges Aad et al. Search for new phenomena in final states with an energetic jet and large missing transverse momentum in pp collisions at $\sqrt{s} = 8$ TeV with the ATLAS detector. 2015.

[AAB+14] Jean-Laurent Agram, Jeremy Andrea, Michael Buttignol, Eric Conte, and Benjamin Fuks. Monotop phenomenology at the Large Hadron Collider. *Phys.Rev.*, D89(1):014028, 2014.

[Aad14a] Search for dark matter in events with a hadronically decaying W or Z boson and missing transverse momentum in $pp$ collisions at $\sqrt{s} = 8$ TeV with the ATLAS detector. *Phys.Rev.Lett.*, 112(4):041802, 2014.

[Aad14b] Search for dark matter in events with a Z boson and missing transverse momentum in pp collisions at $\sqrt{s}$=8 TeV with the ATLAS detector. *Phys.Rev.*, D90(1):012004, 2014.

[Aad15] Search for new phenomena in events with a photon and missing transverse momentum in $pp$ collisions at $\sqrt{s} = 8$ TeV with the ATLAS detector. *Phys.Rev.*, D91(1):012008, 2015.

[ABHL14] Prateek Agrawal, Brian Batell, Dan Hooper, and Tongyan Lin. Flavored Dark Matter and the Galactic Center Gamma-Ray Excess. *Phys.Rev.*, D90(6):063512, 2014.

[ADR+14] Mohammad Abdullah, Anthony DiFranzo, Arvind Rajaraman, Tim M.P. Tait, Philip Tanedo, et al. Hidden on-shell mediators for the Galactic Center $\gamma$-ray excess. *Phys.Rev.*, D90(3):035004, 2014.

[AFM11] J. Andrea, B. Fuks, and F. Maltoni. Monotops at the LHC. *Phys.Rev.*, D84:074025, 2011.

[ATL14] Sensitivity to WIMP Dark Matter in the Final States Containing Jets and Missing Transverse Momentum with the ATLAS Detector at 14 TeV LHC. Technical Report ATL-PHYS-PUB-2014-007, CERN, Geneva, Jun 2014.

[AWZ14] Haipeng An, Lian-Tao Wang, and Hao Zhang. Dark matter with $t$-channel mediator: a simple step beyond contact interaction. *Phys. Rev. D*, 89:115014, 2014.

[BB13] Yang Bai and Joshua Berger. Fermion Portal Dark Matter. *JHEP*, 11:171, 2013.

[BCD+15] Nicole F. Bell, Yi Cai, James B. Dent, Rebecca K. Leane, and Thomas J. Weiler. Dark matter at the LHC: EFTs and gauge invariance. 2015.

[BCDF15] Idir Boucheneb, Giacomo Cacciapaglia, Aldo Deandrea, and Benjamin Fuks. Revisiting monotop production at the LHC. *JHEP*, 1501:017, 2015.

[BDSJ+14] Giorgio Busoni, Andrea De Simone, Thomas Jacques, Enrico Morgante, and Antonio Riotto. On the Validity of the Effective Field Theory for Dark Matter Searches at the LHC Part III: Analysis for the $t$-channel. *JCAP*, 1409:022, 2014.

[BDSMR14] Giorgio Busoni, Andrea De Simone, Enrico Morgante, and Antonio Riotto. On the Validity of the Effective Field Theory for Dark Matter Searches at the LHC. *Phys.Lett.*, B728:412–421, 2014.

[BLW14] Asher Berlin, Tongyan Lin, and Lian-Tao Wang. Mono-Higgs Detection of Dark Matter at the LHC. *JHEP*, 1406:078, 2014.

[BT13] Yang Bai and Tim M.P. Tait. Searches with Mono-Leptons. *Phys.Lett.*, B723:384–387, 2013.

[CDFW14] Eric Conte, BÃl'ranger Dumont, Benjamin Fuks, and Chris Wymant. Designing and recasting LHC analyses with MadAnalysis 5. *Eur.Phys.J.*, C74(10):3103, 2014.

[CDM+14] Linda Carpenter, Anthony DiFranzo, Michael Mulhearn, Chase Shimmin, Sean Tulin, et al. Mono-Higgs-boson: A new collider probe of dark matter. *Phys.Rev.*, D89(7):075017, 2014.

[CEHL14] Spencer Chang, Ralph Edezhath, Jeffrey Hutchinson, and Markus Luty. Effective WIMPs. *Phys. Rev. D*, 89:015011, 2014.

[CHH15] Andreas Crivellin, Ulrich Haisch, and Anthony Hibbs. LHC constraints on gauge boson couplings to dark matter. 2015.

[CHLR13] R.C. Cotta, J.L. Hewett, M.P. Le, and T.G. Rizzo. Bounds on Dark Matter Interactions with Electroweak Gauge Bosons. *Phys.Rev.*, D88:116009, 2013.

[CNS+13] Linda M. Carpenter, Andrew Nelson, Chase Shimmin, Tim M.P. Tait, and Daniel Whiteson. Collider searches for dark matter in events with a Z boson and missing energy. *Phys.Rev.*, D87(7):074005, 2013.

[CRTW14] Randel C. Cotta, Arvind Rajaraman, Tim M. P. Tait, and Alexander M. Wijangco. Particle Physics Implications and Constraints on Dark Matter Interpretations of the CDMS Signal. *Phys.Rev.*, D90(1):013020, 2014.

[dF+14] J. de Favereau et al. DELPHES 3, A modular framework for fast simulation of a generic collider experiment. *JHEP*, 1402:057, 2014.

[DFK+15] B. Dumont, B. Fuks, S. Kraml, S. Bein, G. Chalons, et al. Toward a public analysis database for LHC new physics searches using MADANALYSIS 5. *Eur.Phys.J.*, C75(2):56, 2015.

[DNRT13] Anthony DiFranzo, Keiko I. Nagao, Arvind Rajaraman, and Tim M. P. Tait. Simplified Models for Dark Matter Interacting With Quarks. *JHEP*, 1311, 2013.

[For15a] SVN repository for Madgraph inputs for 2HDM model leading to a mono-Higgs signature. `https://svnweb.cern.ch/cern/wsvn/LHCDMF/trunk/models/EW_Higgs_2HDM/`, 2015. [Online; accessed 12-May-2015].

[For15b] SVN repository for Madgraph inputs for dimension-7 EFT models with direct DM-EW boson couplings. `https://svnweb.cern.ch/cern/wsvn/LHCDMF/trunk/models/EW_Fermion_D7/`, 2015. [Online; accessed 24-April-2015].

[For15c] SVN repository for Madgraph inputs for vector and scalar mediator models leading to a mono-Higgs signature. `https://svnweb.cern.ch/cern/wsvn/LHCDMF/`

trunk/models/EW_Higgs_all/, 2015. [Online; accessed 24-April-2015].

[Fuk] Benjamin Fuks. Monotop Effective Theory: MadGraph model. http://feynrules.irmp.ucl.ac.be/wiki/Monotops.

[GIR+10] Jessica Goodman, Masahiro Ibe, Arvind Rajaraman, William Shepherd, Tim M.P. Tait, et al. Constraints on Dark Matter from Colliders. *Phys.Rev.*, D82:116010, 2010.

[HKR13] Ulrich Haisch, Felix Kahlhoefer, and Emanuele Re. QCD effects in mono-jet searches for dark matter. *JHEP*, 1312:007, 2013.

[HKU13] Ulrich Haisch, Felix Kahlhoefer, and James Unwin. The impact of heavy-quark loops on LHC dark matter searches. *JHEP*, 1307:125, 2013.

[HR15] Ulrich Haisch and Emanuele Re. Simplified dark matter top-quark interactions at the LHC. 2015.

[K+14] Vardan Khachatryan et al. Search for physics beyond the standard model in final states with a lepton and missing transverse energy in proton-proton collisions at $\sqrt{s}$ = 8 TeV. 2014.

[Kha14] Search for new phenomena in monophoton final states in proton-proton collisions at $\sqrt{s}$ = 8 TeV. 2014.

[KKL+14a] Sabine Kraml, Suchita Kulkarni, Ursula Laa, Andre Lessa, Veronika Magerl, et al. SModelS v1.0: a short user guide. 2014.

[KKL+14b] Sabine Kraml, Suchita Kulkarni, Ursula Laa, Andre Lessa, Wolfgang Magerl, Doris Proschofsky, and Wolfgang Waltenberger. SModelS: a tool for interpreting simplified-model results from the LHC and its application to supersymmetry. *Eur.Phys.J.*, C74:2868, 2014.

[KSTR15] Jong Soo Kim, Daniel Schmeier, Jamie Tattersall, and Krzysztof Rolbiecki. A framework to create customised LHC analyses within CheckMATE. 2015.

[NCC+14] Andy Nelson, Linda M. Carpenter, Randel Cotta, Adam Johnstone, and Daniel Whiteson. Confronting the Fermi Line with LHC data: an Effective Theory of Dark Matter Interaction with Photons. *Phys.Rev.*, D89(5):056011, 2014.

[PSWZ14] Michele Papucci, Kazuki Sakurai, Andreas Weiler, and Lisa Zeune. Fastlim: a fast LHC limit calculator. *Eur.Phys.J.*, C74(11):3163, 2014.

[PVZ14] Michele Papucci, Alessandro Vichi, and Kathryn M. Zurek. Monojet versus the rest of the world I: $t$-channel models. *JHEP*, 2014.

[RWZ15] Davide Racco, Andrea Wulzer, and Fabio Zwirner. Robust collider limits on heavy-mediator Dark Matter. 2015.

[ZBW13] Ning Zhou, David Berge, and Daniel Whiteson. Mono-everything: combined limits on dark matter production at colliders from multiple final states. *Phys.Rev.*, D87(9):095013, 2013.